



**T.C.**  
**Bursa Uludağ Üniversitesi**  
**Fen Bilimleri Enstitüsü**

**A NOVEL PARAMETRIC PERFORMANCE ANALYSIS  
OF HYBRID REFRIGERATION CYCLES WITH  
MECHANICAL AND ADSORPTION COMPRESSION**

**Mustafa ANJRINI**

**Doktora Tezi**

**A NOVEL PARAMETRIC PERFORMANCE ANALYSIS  
OF HYBRID REFRIGERATION CYCLES WITH  
MECHANICAL AND ADSORPTION COMPRESSION**

**Mustafa ANJRINI**



T.C.  
BURSA ULUDAĞ UNIVERSITY  
GRADUATE SCHOOL OF NATURAL AND APPLIED SCIENCES

**A NOVEL PARAMETRIC PERFORMANCE ANALYSIS OF HYBRID  
REFRIGERATION CYCLES WITH MECHANICAL AND ADSORPTION  
COMPRESSION**

**Mustafa ANJRINI**  
0000-0003-1153-7631

Prof. Dr. Muhsin KILIÇ  
(Supervisor)

PhD THESIS  
DEPARTMENT OF MECHANICAL ENGINEERING

BURSA – 2021  
**All Rights Reserved**

## ÖZET

Doktora Tezi

### MEKANİK VE ADSORPSİYON SIKIŞTIRMALI HİBRİT SOĞUTMA ÇEVİRİMLERİNİN YENİ BİR PARAMETRİK PERFORMANS ANALİZİ

**Mustafa ANJRINI**

Bursa Uludağ Üniversitesi  
Fen Bilimleri Enstitüsü  
Makine Mühendisliği Anabilim Dalı

**Danışman:** Prof. Dr. Muhsin KILIÇ

Çevre sorunları ve büyük enerji tüketimine yol açan önemli teknolojilerden biri, buhar sıkıştırımlı soğutma döngüsünü (VCC) kullanmaktır. Bu nedenle soğutma endüstrilerinde yeni enerji kaynaklarını kullanan yeni teknolojiler düşünülmelidir. Bu yeni teknolojilerden biri adsorpsiyon soğutma çevrimidir (ACC). ACC sisteminin düşük performans değerleri gibi dezavantajlarının üstesinden gelmek için kullanılabilir en umut verici yöntemlerden birisinin VCC sistemleri olduğu kabul edilmektedir. Adsorpsiyonlu soğutma sisteminin etkenliğini artırmak için son zamanlarda birçok iyileştirme ve ilerlemeler yapılmıştır.

Bu araştırmada, buhar sıkıştırımlı soğutma sistemi (VCC) ile adsorpsiyonlu soğutma sistemi (ACC) hibrit bir soğutma sistemi oluşturmak amacıyla birleştirilmiştir. İki soğutma sistemi arasındaki fark sıkıştırma tipidir. ACC sistemi termal sıkıştırma tipini kullanırken, VCC sistemi mekanik sıkıştırma tipini kullanır. Bu çalışmanın ana hedefi olarak, kombine soğutma sisteminin farklı çalışma koşullarındaki performansını araştırmak için bir matematiksel kod yazılmış ve doğrulanmıştır.

Bu çalışmanın ilk bölümünde, VCC ünitesinde farklı soğutucu akışkanlar ve ACC ünitesinde silika jel / su çifti kullanılarak önerilen kombine soğutma sisteminin enerji tasarrufu ve ekserji kavramı dikkate alınarak performansı araştırılmıştır. Ana hedefi, en yüksek performansı ve enerji tasarrufunu sağlayan en iyi soğutucu akışkanı ortaya çıkarmak ve farklı VCC evaporatör sıcaklıklarında adsorban kütlesi ile adsorpsiyon çevrimi süresi arasındaki ilişkiyi araştırmaktır. Bu çalışmanın ikinci kısmında, birkaç ACC evaporatöründe ve ısıtma sıcaklıklarında dört farklı adsorban kullanılarak ACC'nin performans katsayısı (COP) ve spesifik soğutma gücünü (SCP) araştırılmıştır. Üçüncü bölümde ise farklı ACC evaporatör sıcaklıklarında ACC ünitesinde üç farklı adsorban kullanılarak birkaç ortam sıcaklığı ve adsorpsiyon çevrimi süreleri için iki farklı (ACC-VCC) kombine soğutma sistemi konfigürasyonu (seri ve paralel) performans açısından değerlendirilmiştir.

**Anahtar Kelimeler:** Hibrit soğutma sistemi, adsorpsiyon, soğutucular, silika jel, enerji, ekserji, performans analizi

**2021, xi + 122 sayfa.**

## ABSTRACT

PhD Thesis

### A NOVEL PARAMETRIC PERFORMANCE ANALYSIS OF HYBRID REFRIGERATION CYCLES WITH MECHANICAL AND ADSORPTION COMPRESSION

**MUSTAFA ANJRINI**

Bursa Uludağ University  
Graduate School of Natural and Applied Sciences  
Department of Mechanical Engineering

**Supervisor:** Prof. Dr. Muhsin KILIÇ

One of the important technologies that suffer from environmental issues and huge energy consumption is the use of vapor compression cooling cycle (VCC). Therefore, new technologies that use new energy sources should be considered in the cooling industries. One of these new technologies is the adsorption cooling cycle (ACC) which is regarded as one of the most promising methods to overcome the disadvantages of using the VCC systems regardless of ACC low-performance values. Many improvements and progress have recently been applied to increase the effectiveness of the adsorption cooling system.

In this study, the (VCC) is combined with the (ACC) to form one cooling system. The difference between the two cooling systems is the compression type. The VCC system uses mechanical compression, while the ACC system utilizes thermal compression. A mathematical code was written and validated to investigate the combined cooling system performance at different operating conditions as the primary goal of this study.

In the first part of this study, the performance and energy saving of the proposed combined cooling system were investigated considering the exergy concept using different refrigerants in the VCC unit and silica gel/water pair in the ACC unit. The main goal was to reveal the best refrigerant that provides the highest performance and energy-saving and investigate the relationship between the adsorbent mass and the adsorption cycle time at different VCC evaporator temperatures. In the second part, the coefficient of performance (COP) and the specific cooling power (SCP) of the ACC system were investigated using four different adsorbents at several ACC evaporator and heating temperatures. In the third part, the performance of two different (ACC-VCC) combined cooling system configurations (series and parallel) were evaluated utilizing three different adsorbents in the ACC unit at different ACC evaporator temperatures considering several ambient temperatures and the adsorption cycle durations.

**Keywords:** Hybrid refrigeration system, adsorption, refrigerants, silica gel, energy, exergy, performance analysis

**2021, xi + 122 pages.**

## CONTENTS

	<b>Page</b>
ÖZET .....	i
ABSTRACT .....	ii
ACKNOWLEDGEMENT .....	iii
SYMBOLS and ABBREVIATIONS .....	vii
FIGURES .....	ix
TABLES .....	xi
1. INTRODUCTION .....	1
1.1. Motivation .....	1
1.2. Research objectives .....	2
1.3. Research problem statement .....	2
1.4. Thesis outline .....	2
2. THEORETICAL BASICS and LITERATURE REVIEW .....	4
2.1. Adsorption cooling system .....	4
2.1.1. Literature review .....	4
2.1.2. Adsorption concept .....	7
2.1.3. Adsorbents types .....	8
2.1.4. Adsorbent bed characteristics .....	10
2.1.5. Types of adsorbents .....	11
2.1.6. Adsorbate/ Refrigerant .....	13
2.1.7. Adsorption pairs (Adsorbent/adsorbate) .....	14
2.1.8. Adsorption cooling cycle concept .....	15
2.1.9. Adsorption cooling thermodynamic cycle .....	16
2.1.10. Different adsorption cooling system layouts .....	18
2.1.11. The operating modes of the adsorption cooling system .....	24
2.2. Combined (mechanical- thermal) cooling system .....	27
2.2.1. Thermal compression cooling cycles .....	28
2.2.2. Adsorption – vapor compression combined cooling cycles .....	28
2.2.3. Adsorption – vapor compression combined cooling cycles .....	30
2.2.4. (ACC-VCC) combined cooling system configurations .....	40
3. MATERIALS and METHODS .....	44
3.1. Adsorption Cooling Cycle modeling .....	44
3.1.1. Adsorbent/adsorbate adsorption isotherms .....	45
3.1.2. Adsorption kinetics .....	49
3.1.3. Adsorption enthalpy .....	50
3.1.4. Thermal compressor (adsorbent bed) model .....	50
3.1.5. ACC evaporator model .....	56
3.1.6. ACC condenser model .....	57
3.1.7. ACC System performance indicators .....	57
3.2. Vapor compression Cooling Cycle (VCC) modeling .....	58
3.2.1. VCC evaporator model .....	58
3.2.2. Vapor mechanical compressor model .....	59
3.2.3. VCC condenser model .....	60
3.2.4. VCC system performance indicator .....	60
3.3. (VCC-ACC) combined cooling system mathematical model .....	61
3.4. Energy savings .....	62

3.5. Calculations procedure of the mathematical model.....	62
3.6. Validation of the mathematical model .....	64
3.7. Evaluation of different working fluids (refrigerants) in the VCC .....	68
3.8. Evaluation of the working pair in the ACC chiller .....	69
4. RESULTS and DISCUSSION.....	72
4.1. Comparative performance analysis of a combined cooling system with mechanical and adsorption cycles .....	72
4.1.1. Effect of VCC evaporator temperature on VCC performance .....	73
4.1.2. Effect of VCC evaporator temperature on VCC condenser heat in the combined cooling system.....	75
4.1.3. Effect of VCC evaporator temperature on ACC condenser heat.....	76
4.1.4. Effect of VCC evaporator temperature on VCC performance of (VCC-ACC) hybrid cooling system.....	77
4.1.5. Effect of VCC evaporator temperature on the thermal performance of the hybrid cooling system.....	77
4.1.6. Effect of VCC evaporator temperature on the overall performance of the hybrid cooling system.....	78
4.1.7. Effect of VCC evaporator temperature on energy savings amount and VCC performance in the combined cooling system.....	80
4.1.8. Effect of VCC evaporator temperature, inlet hot fluid temperature, cycle time on the amount of adsorbent in the combined cooling system.....	82
4.2. Comparative performance analysis of two-bed adsorption cooling system using water vapor adsorption on different types of silica gel .....	84
4.2.1. Effect of ACC evaporator temperature on the ACC performance indicators.....	85
4.2.2. Effect of different heating inlet temperature on the ACC performance indicators .....	86
4.3. Performance analysis of a mechanical and adsorption combined refrigeration system using two different system configurations .....	88
4.3.1. Effect of ACC evaporator temperature on heat amount in the combined cooling system .....	89
4.3.2. Effect of ACC evaporator temperature on the hybrid system performance with the (series and parallel) configuration .....	91
4.3.3. Effect of ACC evaporator temperature on the overall system performance according to the series connection.....	92
4.3.4. Effect of ACC evaporator temperature on the overall system performance according to the parallel connection .....	93
4.3.5. Effect of ACC evaporator temperature on the ACC system performance according to the series and parallel configurations.....	94
4.3.6. Effect of ACC evaporator temperature on the VCC system performance according to parallel and series configurations .....	95
4.3.7. Effect of ACC evaporator heat transfer rate on the ACC system performance according to the parallel and series configurations.....	97
4.3.8. Effect of ACC evaporator temperature and adsorption cycle time on the overall system performance according to the parallel and series configurations .....	98
4.3.9. Effect of ACC evaporator temperature and ambient temperature on the overall system performance according to the parallel and series configurations .....	99
4.4. General remarks .....	101
5. CONCLUSIONS .....	105

REFERENCES .....	109
APPENDIXES .....	115
RESUME.....	122

## SYMBOLS and ABBREVIATIONS

<b>Symbols</b>	<b>Definition</b>
A	Specific surface area, $m^2/g$
b	Van der Waals volume, $m^3$
$c_p$	Specific heat at constant pressure, $J/kg.K$
D	Diameter of the solid sorbent grains, m
$D_o$	Pre-exponent constant, $m^2/s$
$D_{po}$	Diameter of the adsorbent pore, m
E	Characteristic energy of the pairs considered in the bed, $kJ/kg$
$E_a$	The activation energy of the pairs considered in the bed, $kJ/kg$
$F_o$	A constant characteristic of adsorbent's shape, -
h	Enthalpy, $kJ/kg$
$h_{fg}$	Vaporization enthalpy, $kJ/kg$
$\Delta h_{ads}$	Adsorption heat, $kJ/kg$
m	Mass, kg
M	Molar mass, $kg/kmol$
n	Exponential constant, -
P	Pressure, $kPa$ ;
$P_s$	Pressure at saturation conditions, $kPa$
Q	Heat, $kJ$
$\dot{Q}$	Heat transfer rate, $kW$
R	Universal gas constant, $J/kg.K$
$R_m$	Thermal capacity ratio, -
$r_p$	Average radius of the solid sorbent particle, m
s	Entropy, $kJ/kg.K$
SCP	Specific cooling power; $W/kg$
T	Temperature, $^{\circ}C$
t	Time, s
$v_a$	The specific volume of the adsorbed phase, $m^3/kg$
$v_{bo}$	Specific volume at the boiling temperature, $m^3/kg$
$V_{Po}$	Volume of the pore in the adsorbent, $cc/g$
W	Adsorption space uptake of the solid adsorbent, $m^3/kg$
$W_o$	Limiting adsorption space uptake of the adsorbent, $m^3/kg$
X	Specific adsorbed mass of adsorbate, $kg/kg$
$X_o$	Limiting the specific adsorbed mass of adsorbate $kg/kg$

<b>Subscripts</b>	<b>Definition</b>
ad	Adsorbate
ads	Adsorbent
amb	Ambient air
b	Bed

bm	Bed metallic material
bo	Boiling point
c	Critical point
cf	Cooling fluid
con	Condenser
cyc	cycle
des	Desorption
eva	Evaporator
eq	Equilibrium
elec	Electric
exp	Experimental
f	fluid
H	Hybrid
h	Hot
i	Isentropic
in	Inlet
liq	Liquid
max	Maximum
min	Minimum
out	Outlet
S	Saturation
SF	Second Fluid
T	Total
V	Vapor phase
A,B,..F	Thermodynamic points of the adsorption cooling cycle
1,2,...,9	Thermodynamic points of the ACC-VCC combined cooling system
I,II,..IV	Thermodynamic stats of the second fluid in the ACC-VCC parallel connection

**Abbreviation Definition**

ABC	Absorption cooling cycle
ACC	Adsorption cooling cycle
AC	Activated carbon
COP	Coefficient of performance
De	Deviation ratio
ES	Energy-saving ratio
IR	Increase ratio
SG	Silica gel
SCP	Specific cooling power
VCC	Vapor cooling cycle

## FIGURES

	<b>Page</b>
Figure 2.1. A typical adsorption phenomenon between the gaseous phase and the adsorbed phase when exposed to heat transfer.....	8
Figure 2. 2. Physical adsorbents classifications. ....	9
Figure 2. 3. A basic adsorption cooling system.....	15
Figure 2. 4. Fundamental adsorption thermodynamic cycle for adsorption cooling cycle. ....	16
Figure 2. 5. Schematic of the single-stage adsorption cooling unite modes (a, b, c, d). ....	20
Figure 2. 6. Schematic of the two-stage adsorption cooling unite modes (a, b, c, d). ....	22
Figure 2. 7. Two-stage adsorption thermodynamic cycle. ....	24
Figure 2. 8. The operating modes of the adsorption cooling system. ....	26
Figure 2. 9. Types of sorption refrigeration systems. ....	28
Figure 2. 10. General schematic of (a) absorption cooling system (ABC), (b) vapor compression cooling system (VCC), (c) ABC-VCC combined cooling system. ....	29
Figure 2. 11. General schematic of (a) adsorption cooling system (ACC), (b) vapor compression cooling system (VCC), (c) ACC-VCC combined cooling system. ....	31
Figure 2. 12. Schematic of (ACC-VCC) combined chiller: (a) series connection, (b) parallel connection. ....	43
Figure 3. 1. Schematic design of the thermal compressor basic components. ....	51
Figure 3. 2. Flow chart of calculating the mathematical model. ....	63
Figure 3. 3. Comparisons of $COP_{VCC,H}$ and $COP_{VCC}$ for different ambient air (cooling fluid) temperatures. ....	68
Figure 4. 1. Comparisons of the variation of heat transfer rate in the VCC condenser with respect to VCC evaporator temperature for various refrigerants. ....	73
Figure 4. 2. Comparisons of the variation of $COP_{VCC}$ with respect to VCC evaporator temperature for different refrigerants. ....	74
Figure 4. 3. Comparisons of the variation of heat transfer rates in the intermediate heat exchanger with respect to VCC evaporator temperature for the various refrigerants. ....	75
Figure 4. 4. Comparisons of the variation of heat transfer rate in the ACC condenser with respect to VCC evaporator temperature for different refrigerants. ....	76
Figure 4. 5. Comparisons of the variation of $COP_{VCC,H}$ with respect to VCC evaporator temperature for various refrigerants. ....	77
Figure 4. 6. Comparisons of the variation of $COP_H$ with respect to VCC evaporator temperatures for various refrigerants. ....	78
Figure 4. 7. Comparisons of the variation of $COP_{EXE,H}$ with respect to VCC evaporation temperature for various refrigerants. ....	79
Figure 4. 8. Comparisons of the variation of ES with respect to VCC evaporation temperatures for different refrigerants. ....	80
Figure 4. 9. Comparisons of the variation of IR with respect to VCC evaporator temperatures when VCC system works with ACC and alone for different refrigerants. ....	81
Figure 4. 10. Required amount of mass in a bed with respect to VCC evaporator temperatures, heating temperatures, and two different cycle time values. ...	83

Figure 4. 11. Comparison of the variation of $COP_{ACC}$ with respect to ACC evaporator temperatures for different adsorbents. ....	85
Figure 4. 12. Comparison of the variation of SCP with respect to ACC evaporator temperature for different adsorbents. ....	85
Figure 4. 13. Comparison of the variation of $COP_{ACC}$ with respect to ACC heating temperature for different adsorbents. ....	87
Figure 4. 14. Comparison of the variation of SCP with respect to ACC heating temperature for different adsorbents. ....	87
Figure 4. 15. Comparisons of the variation of $\dot{Q}_{heat,ACC}$ with respect to ACC evaporator temperature for different adsorbents and the two system configurations (a) and (b). ....	90
Figure 4. 16. Comparisons of the variation of $COP_H$ with the respect to ACC evaporator temperature for various adsorbents and the two system configurations (a) and (b). ....	91
Figure 4. 17. Comparisons of the variation of $COP_{EXE,H}$ with respect to ACC evaporator temperature for various adsorbents and the series configuration (a). ....	92
Figure 4. 18. Comparisons of the variation of $COP_{EXE,H}$ with respect to ACC evaporator temperature for various adsorbents and the parallel configuration (b). ....	94
Figure 4. 19. Comparisons of the variation of $COP_{ACC}$ with respect to ACC evaporator temperature for various adsorbents and the two system configurations series and parallel. ....	95
Figure 4. 20. Comparisons of the variation of $COP_{ACC}$ with respect to ACC evaporator temperature for the two system configurations series and parallel. ....	96
Figure 4. 21. Comparisons of the variation of $COP_{ACC}$ with respect to ACC cooling load for different adsorbents and two different adsorbent mass values. ....	98
Figure 4. 22. Comparisons of the variation of $COP_{EXE,H}$ with respect to ACC evaporator temperature for three different cycle times and the two system configurations (a) and (b). ....	99
Figure 4. 23. Comparisons of the variation of $COP_{EXE,H}$ with respect to ACC evaporator temperature for three different ambient temperatures and the configurations (a) and (b). ....	100

## TABLES

	<b>Pages</b>
Table 2. 1. Most common adsorption working pairs traits .....	14
Table 2. 2. Working strategies of single-stage adsorption cooling system.....	21
Table 2. 3. Working strategies of two-stage adsorption cooling system .....	23
Table 2. 4. Operation and valving systems for the adsorption chiller .....	27
Table 3. 1. Comparisons of the present mathematical model results with the experimental data and the deviation ratio.....	65
Table 3. 2. Comparisons of the present mathematical model findings with the experimental data.....	66
Table 3. 3. Parameters and working states utilized in the validation .....	67
Table 3. 4. Properties of refrigerants used in the VCC unit .....	69
Table 3. 5. Parameters and properties of the adsorbate used in this investigation .....	70
Table 3. 6. Parameters utilized in the current research for the four types of adsorbent .	71
Table 4. 1. Operating conditions and parameters used in the present study .....	73
Table 4. 2. Comparisons of VCC performance increase ratio (IR) results when it works with ACC and alone for several refrigerants at various evaporation temperatures .....	81
Table 4. 3. Settings and working conditions are utilized in the current research.....	89

## **1. INTRODUCTION**

In the past decades, it was found that the traditional refrigeration system that uses synthetic refrigerants played an essential role in the ozone layer depletion and in the increase of the global warming effect as well as the energy consumption. Therefore, it is important to search for alternative refrigeration technologies to avoid the conventional refrigeration technology disadvantages.

### **1.1. Motivation**

Energy is one of the essential factors in any community. The relation between energy and society is considered one of the main basics for development in various fields in the country. Recently, energy resources investment is one of the applied sciences for the international countries' social, cultural, and economic prosperity. To keep the progressing continuity in the world, it is important to search for alternative energy methods. It is also essential to consider that the new ways should be environment-being and create a new investment area to overcome the increasing energy demand. Among these proposed technical discoveries is the adsorption cooling system. The suggested new technology is driven by heat sources from renewable energies or waste heat from different thermal fields. To provide thermal comfort to human beings or refrigerate some materials, many cooling applications that deplete the energy sources are obtainable in the market. Therefore, this new cooling technology is considered a promising one to reduce the depletion in the energy sources.

Previous investigations indicated that the present refrigeration technologies consume about 45% of the electrical energy that the residences consume. Thus, plenty of energy is required to be used. This PhD dissertation is undertaken to employ the energy sources rationally by utilizing waste heat or renewable energies to operate the adsorption cooling system. Scientific researchers have been recently making an effort to improve the adsorption refrigeration system by including a multi-bed cycle, multi-stage cycle, thermal wave cycle, mass and heat recovery cycle, integrated cooling systems, etc. Although there are some limits to use the adsorption cooling applications compared to the available

cooling systems, some improved adsorbents and connection methods between the system components have promising adsorption advantages. Employing the new ideas and technologies to the system results in developing the coming adsorption applications' generation. Here in this study, the conventional vapor mechanical compression cooling system brings together with the thermal compression adsorption cooling system. This integration may reduce electrical consumption by 45-87%.

## **1.2. Research objectives**

The research objectives are focused on inclusive theoretical analysis for a two-bed adsorption cooling system integrated with the traditional cooling system to produce 10 kW as a cooling effect. The current study is also concentrated on analyzing the proposed combined cooling system to provide higher results of the specific cooling power (SCP) and coefficient of performance (COP) and investigating the energy-saving ratio. Furthermore, it discusses how to enhance the usage and performance of the proposed combined cooling system by substantial modifications on the system configurations employing different adsorbent materials and working fluids.

## **1.3. Research problem statement**

Even though the traditional vapor compression cooling system and the adsorption cooling system performances with various operating conditions and design configurations were investigated individually, the combination of the two systems still suffers from insufficient studies on the overall combined system performance and the energy-saving amount that this system can conserve. Significant efforts towards improving the combined cooling system performance are required to increase this technology utilization to reduce world energy consumption.

## **1.4. Thesis outline**

The second chapter in this dissertation mainly highlights the theoretical basics of the adsorption cooling cycle, working pairs, different system configurations for various

applications, and a literature review related to the adsorption cooling system. Besides that, cooling systems represented in thermal compression and mechanical compression combination are also investigated. Moreover, a comprehensive literature review of the combined cooling system comprised of the thermal compression (adsorption) and vapor mechanical compression integrated cooling systems is also presented in this chapter. Theoretical information is explained using two different system configurations that link the adsorption and traditional chillers in parallel and series.

The third chapter in this research focuses on the mathematical models in each component of the adsorption/ vapor compression combined cooling system. This section exhibits the necessary materials and their physical and thermophysical properties to compute the system performance indicators. The method used to calculate the mathematical models is also clarified and validated with experimental data from the previous investigations.

The fourth and fifth chapters illustrate the results and their discussions at different working conditions and configurations.

The final chapter also states the further ideas and works that can be investigated and executed to evolve the combined utilization of the adsorption cooling system with the vapor compression cooling system (traditional chiller).

## **2. THEORETICAL BASICS and LITERATURE REVIEW**

These days, improvements and developments are being made on several adsorption systems. An adsorption cooling system is considered an alternative technology to replace the conventional refrigeration systems that consume a considerable amount of energy and utilize harmful refrigerants. However, the adsorption cooling system needs to be improved to overcome the flaw of its low-performance values. The adsorption cooling systems can be developed by using different system configurations, working materials, and heat exchanger designs. Several studies have been implemented on the cooling systems that utilize thermal compressor as the main part (adsorption/absorption) and mechanical compressor (conventional vapor compression) using several layouts and parametric conditions. In the following sections, a literature survey on the adsorption cooling systems, theoretical basics of the adsorption cooling system, a comprehensive literature review on the (thermal and mechanical) compression in the combined cooling systems, theoretical information on two different configurations of adsorption/vapor compression combined cooling systems have been introduced.

### **2.1. Adsorption cooling system**

Theoretical fundamentals and literature review of the adsorption cooling system will be presented in this section.

#### **2.1.1. Literature review**

Lu et al. (2004) executed an experimental test with an adsorption refrigeration system for air conditioning applications under realistic working conditions. The studied system was set in a locomotive and trailed under various operating conditions. The findings demonstrated that the adsorption refrigeration system could supply enough cooling effect to make the driver comfortable. The produced cooling effects could be between 3 to 4.2 kW under normal running conditions.

Wang et al. (2006) designed an adsorption refrigeration system for ice-making applications. The system considered was driven by waste heat from a thermal engine. The

working pair used in the sorption bed was activated carbon/ methanol. They stated that the heat transfer coefficient in the granular bed was lower than in a consolidated bed. However, the performance of the granular bed was superior due to its high permeability. They also indicated that the mass transfer inside the sorption bed was important to guarantee that the adsorption rate would not be affected by the low permeability in the solidified bed. The research stated that using a two-granular sorption bed, the coefficient of performance could be upgraded by 60%. Their results revealed that the optimum cooling power production was 3 kW, and the coefficient of performance was 0.14 at an evaporator temperature of 15°C.

Wang et al. (2006) developed an adsorption refrigeration system for air conditioning applications using zeolite/water as a working pair. The supplied heat was taken from the exhausted gas from the locomotive's engine at 350-450°C. The designed adsorption system consisted of two analogous vacuum chambers. Each one consisted of one evaporator, one sorption bed, and one condenser. According to the experimental findings, the adsorption system was capable of producing a 3.2 kW cooling effect and a 0.152 coefficient of performance at 8°C of evaporating temperature.

Grisel et al. (2010) investigated the design of an adsorption refrigeration system and tested it using a low-grade heat source. The purpose of the innovation was to implement it in a prototype of the trigeneration system. The adsorption system consisted of two-bed linked in parallel together to obtain low cooling water temperature. The working pair used in the sorption bed was silica gel/water. The heat exchanger used in the sorption bed was plate-fin heat exchangers filled with 1.45 kg of the adsorbent. Furthermore, a heat recovery mode between the two-bed was applied to elevate the coefficient of performance. The designed adsorption system could produce cooling power up to 5 kW at the ideal operations. However, the experimental results revealed that the medium performance indicators were 208 W/kg and 0.62 for SCP and COP, respectively, at the realistic conditions.

Vasta et al. (2012) designed and trailed a prototype of an adsorption refrigeration system using zeolite (FAM-ZO2)/ water as a working pair for air conditioning applications in a

truck. The apparatus used the engine refrigerant loop as a waste heat source to provide 2.5 kW of cooling effect. The adsorption system consisted of two beds, a condenser, and an evaporator. Each bed contained a heat exchanger, a finned flat-tube type packed with the adsorbent granules. The weight and size of the prototype were suitable for mobile applications. The prototype was firstly examined at the laboratory under simulated working conditions. Then the prototype was set in a truck cabin and with realistic operating conditions. The laboratory's results demonstrated that the prototype was capable of supplying enough cooling effect ranging from 1 to 2.3 kW. The prototype's performance indicators were 300-600 W/kg and 0.25-0.45 for SCP and COP, respectively. The tests were executed under 90°C and 28°C for heating temperature and condensing temperature, respectively.

Lately, many review articles have been published about the development of adsorption refrigeration systems, including the advantages and disadvantages. However, this type of system still suffers from some drawbacks, such as low specific cooling power (SCP) and coefficient of performance (COP). However, many new layouts as an alternative to the standard adsorption system have been investigated to raise the system's thermal performance.

Sharafian et al. (2014) investigated the heat exchanger types of the adsorption bed for automobile air conditioning and cooling applications. As the adsorption chiller was used in an automobile, the size of the sorption bed was also considered. The research stated that utilizing the heat exchangers in the sorption bed increased the heat transfer surface area between the heat transfer fluids and the adsorbent materials during the thermodynamic processes and reduced the mass transfer resistance between the working pair. They mentioned many types of bed heat exchangers, namely, Spiral plate, Shell and tube, Hairpin, Annulus tube, Plate fin, finned tube, Plate tube, Simple tube, and Plate heat exchangers. The effects of the aforementioned bed types were investigated on the adsorption cooling system performance for vehicles to achieve 350 w/kg as specific cooling power. According to their study, the best performance among the considered adsorber beds was observed for finned tube sorption bed design. They illustrated that the type of sorption bed design depends on the adsorption system application.

Kilic (2018) concerned with silica gel as an adsorbent for adsorption cooling application. He made a comparative performance analysis of an adsorption cooling system with various adsorbates (Water, R404A, R134A, Methanol). His investigation focused on the system performance indicators (specific cooling power SCP and coefficient of performance COP). Among the working pairs investigated in his research, the silica gel/water pair provided the highest performance indicator value (SCP =0.329 kW/kg) and (COP =0.63).

Several studies have presented in the adsorption refrigeration system using advanced cycles such as heat and mass recovery cycles (Maggio et al., 2006; Akahira et al., 2005) (Chekirou et al., 2011), multi-step cycles (Khan et al., 2006), multi-sorption bed cycles (Saha et al., 2006; Miyazaki et al., 2010). These advanced cycles aim to increase the thermal efficiency of the adsorption cooling system and provide high and continuous cooling effects. The achievement of constant cooling effects can be provided by utilizing multiple beds in the system. On the other hand, the improvement in the thermal performance of the adsorption system (COP) can be achieved by recycling the heat between beds, as will explain later in this dissertation. It is possible to increase the cooling power in the system by utilizing a cooling mass recovery among the beds used in the system. This utilization can also increase the adsorption capacity and the system's ability to use low-grade temperature. Finally, the utilization of multi-stage and multi-beds can also enhance the thermal efficiency of an adsorption refrigeration system. These enhancements improve the utilization capability of the waste heat at low temperatures. However, employing these advanced techniques could effect on the production cost as well as the system size.

### **2.1.2. Adsorption concept**

Both adsorption and absorption processes are part of the sorption phenomena, yet they are quite different from each other. The particle dissolution of a substance within another substance to form one solution is called absorption. On the contrary, the physical attraction between a vapor and a solid surface is called adsorption. There are many differences between the two concepts (adsorption/absorption) used in refrigeration

systems related to the heat source, operating considerations, maintenance, and lifetime. Here in this work, we are mainly focusing on the adsorption refrigeration applications only.

The usage of porous materials (adsorbent) to desorb and adsorb vapor molecules (adsorbate) has been investigated in the eighteenth century when the tests and experimental rigs were executed to recognize the purification and separation processes. Indeed, the adsorption principle illustrates that the vapor molecules (adsorbate) are settled in the pores of the sorption surface (adsorbent) due to the electrostatic force between vapor molecules and the atoms in the adsorbent surface. The powerful affinity surface forces also affect the adsorption phenomenon, which is called Van Der Waals forces. The molecular distances within the gaseous phase are much longer than in the pores of the solid adsorbent at the same temperature and pressure conditions. Hence, in the adsorbed phase, the adsorbent density becomes in the liquid form (L. W. Wang et al., 2009). Figure 2.1 depicts the adsorption phenomenon in a part of the adsorbent bed.

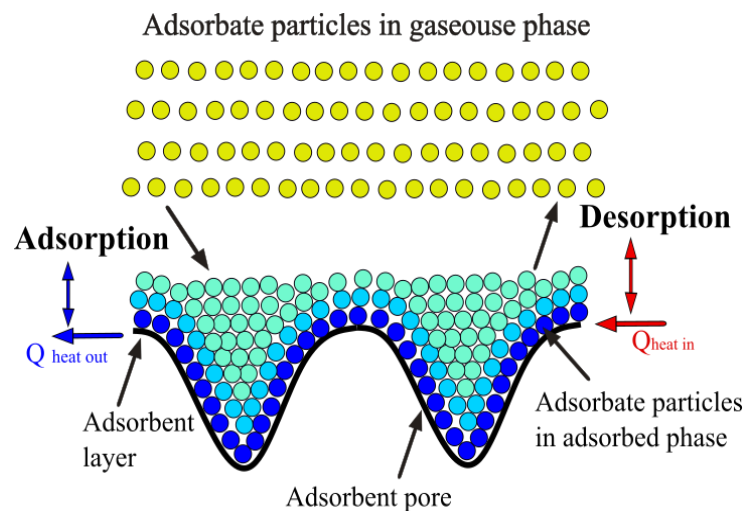


**Figure 2.1.** A typical adsorption phenomenon between the gaseous phase and the adsorbed phase when exposed to heat transfer.

### 2.1.3. Adsorbents types

A successful adsorption process is achieved by using a suitable adsorbent in terms of kinetics and adsorptive capacity. These two requirements can be satisfied using an

adsorbent with a quite large surface area and pore sizes. The adsorbents are categorized depending on the adsorption process.

**Physical adsorbents:**

Physical adsorbents often have porous materials with various pore sizes. The adsorbent's physical process is reversible. It can return to its original state after eliminating the adsorbate by connecting the adsorbent with a heat source (D. C. Wang et al., 2010). The more the amount of cycled adsorbate, the higher performance of the adsorption cooling cycle we get (Maggio et al., 2009). Figure 2.2 illustrates the classification of porous materials.

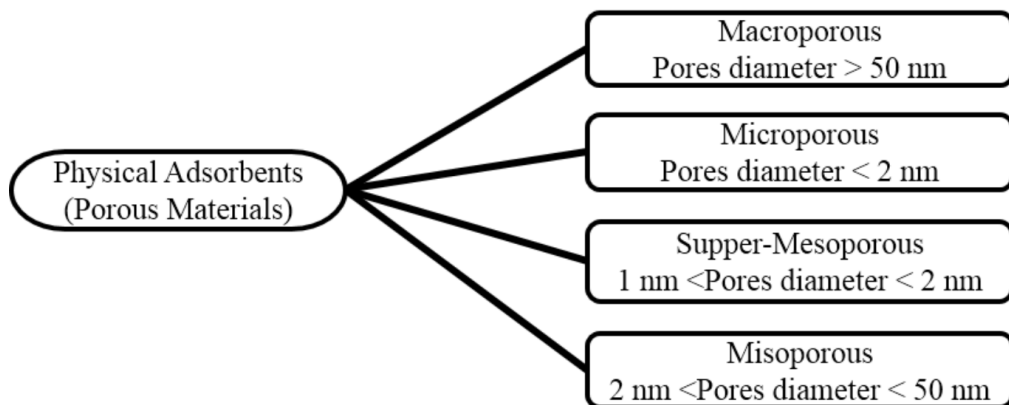


**Figure 2. 2.** Physical adsorbents classifications.

**Chemical adsorbents:**

Chemical adsorbents sorb the refrigerant by the Valence force. The molecules in the adsorbent surface react chemically with the refrigerant. Even though the chemical adsorbent sorbs much more amount of the adsorbate, it has lower stability and does not turn to its first state. As a result, smaller applications can use it. On the negative side, using this type of adsorbent gives low heat and mass transfer performance as it swells and agglomerates, mainly when the cycle operates at low pressure (Li et al., 2009). Besides that, utilizing chemical adsorbent leads to low thermal conductivity and insufficient mass

and heat transfer. Examples of the chemical adsorbents are adsorbents including metal hydrides, metal chloride, and metal oxides (Srivastava & Eames, 1998).

#### **Composite (Physical/Chemical) adsorbents:**

Utilizing composite adsorbents aims to improve the physical adsorbents' performance by increasing the adsorption capacity and avert the previous disadvantages of chemical adsorbents like low conductivity, agglomeration, and swelling. Examples of composite adsorbents are silica gel with inorganic salts (CaCl<sub>2</sub>, MgCl<sub>2</sub>, LiCl, LiBr, etc.) and metal chloride with activated carbon, zeolite, or expanded graphite (Bidyut Baran Saha et al., 2009).

#### **2.1.4. Adsorbent bed characteristics**

This section introduces the parameters that significantly affect the heat and mass transfer rates in the adsorbent materials as well as the adsorption and desorption processes.

##### **Adsorbent porosity:**

This property determines the voids inside the adsorbent granule. It is expressed as the ratio between the volumes of the voids to the total volume. Moreover, this property influences the quality of the heat transfer and the amount of adsorbate in the adsorbent. The adsorption capacity increases by increasing the adsorbent porosity, and the adsorption rate decreases as a result. On the other hand, as the adsorbent property increases, the adsorbent thermal conductivity and the adsorption rate decrease (Demir et al., 2009).

##### **Granular size:**

The size of the adsorbent granule affects the mass and heat transfer processes in the adsorbent. Increasing the size of the granular adsorbent increases the contact heat resistance between the heat exchanger surface and the granules. The continuity of heat

transfer in the adsorbent is related to the granular size. The larger the adsorbent granules, the lower the heat transfer continuity. The mass transfer in the adsorbent is divided into two types; the first one is through the spaces (voids), and the second one is within the granules. The large granules give lower mass transfer than the small ones as the total surface area is lower for a larger size. On the contrary, the adsorbent with small granules size has lower permeability; lower heat transfer performance is achieved (Glaznev & Aristov, 2010).

#### **Pore size:**

The pore size and the adsorbent porosity are linked together. As the pore size increases, the adsorbent porosity decreases, and hence the specific surface area decreases. On the contrary, the bigger the pore size, the lower the isosteric energy is, and as a result, the regeneration energy decreases. Therefore, the compatibility between the selected adsorbate molecule sizes and the adsorbent's pore size is an essential criterion for selecting the appropriate working pair. The adsorption kinetics increases with using adsorbent that has large pore sizes.

#### **2.1.5. Types of adsorbents**

The adsorbate molecules penetrate the solid sorbent or stay at the layer of the highly porous adsorbent. Several types of adsorbents are available in the market. However, the most common sorts of adsorption materials are explained below:

#### **Silica gel:**

Silica gel is a form of silicon dioxide that is made artificially from sodium silicate. The chemical formulation of it is  $\text{SiO}_2$ . Its structure is granular and vitreous. The pore diameter of silica gel is different depending on the silica gel type. For type A, the pore diameter is 2.3 nanometers. For type B, on the other hand, the pore diameter is 0.7 nanometers (Suzuki, 1991). The specific surface area is in a range between 250 to 900  $\text{m}^2/\text{g}$ . Silica gel is originally a mineral substance that is processed into sturdy granular form. It is

generally utilized as a desiccant to avoid damage and disintegration of some products. Silica gel can be employed as a desiccant to control the humidity of the place due to its property of attracting water molecules. Additionally, silica gel holds the effect of the chemical bond of water about 5% and loses its absorptive property when subjected to a temperature above 120°C due to loss of the chemical bond. Silica gel can be used with different refrigerants as a working pair, such as water, methanol, R134A, R404A, etc. However, silica gel has a good affinity against water among the other adsorbates, and using them as a working pair provides reasonable results in adsorption applications (Kılıç, 2018). The physical properties of silica gel will be introduced in the following sections.

### **Zeolites:**

Zeolite was firstly presented in 1756 by Axel Fredrik Cronstedt, who is a Swedish mineralogist. He observed that heating zeolite substance produces considerable amounts of water steam in which the water was already adsorbed in the zeolite. Zeolite is a sort of alumina silicate consisted of alkali soil. The porosity of zeolite is in a range between 0.2 to 0.5 nanometer. There are several types of natural zeolite that reach up to 40. On the contrary, some kinds of zeolite can be artificially manufactured. Indeed, by using different manufacturing methods, we can obtain different granular sizes of the zeolite. Zeolite can be employed for water purification in the industry. It can also be used to increase oxygen content by extracting nitrogen from the air for medical and industrial processes. There are several investigations to utilize zeolites in solar thermal collectors as well as in adsorption refrigeration systems. Many studies in adsorption refrigeration systems that use zeolite/water as a working pair have been presented in the literature (Askalany et al., 2013).

### **Activated Carbon:**

Activated carbon can be manufactured by decompressing the source materials by heating them to high-temperature levels (700 – 800°C) (pyrolyzing) and converting them into carbon (carbonizing). The source material used to produce activated carbon is coal, wood, synthetic polymers, and others. Activated carbon can be found in different forms, such as granulate, powder, and carbon fibers (Srivastava & Eames, 1998). The carbon processed

has a relatively big surface area ( $500 \text{ m}^2/\text{g}$ ), which is essential for chemical reactions and adsorption applications. Additionally, its microporosity is relatively high. Activated carbon can be employed in several applications such as gold purification, water purification, air filters, medicine, metal extraction, gas purification, and many other applications. Activated carbon can be used with different adsorbates as working pairs in different applications such as methanol (El-Sharkawy et al., 2009), ethanol (El-Sharkawy et al., 2008), ammonia (Metcalf et al., 2012), R134a (Saha et al., 2009), R32 (Askalany et al., 2014), and others.

### 2.1.6. Adsorbate/ Refrigerant

Various types of refrigerants can be used in the adsorption cooling systems, yet the suitable adsorbate has to be chosen based on several considerations as in the following:

- **Thermal steadiness:** the adsorbate thermophysical properties in the cycle should not change with respect to operating temperatures.
- **Flammability:** when a high generating temperature is considered in the cycle, this property should be taken into account for choosing the appropriate adsorbate in the adsorption systems.
- **Toxicity and explosion:** one of the factors that should be considered is safety measures. The type of the application and the applied conditions are essential to select a suitable refrigerant.
- **Latent vaporization heat:** Using refrigerant that has higher latent heat leads to better performance values.
- **Compatibility:** some adsorbates have attractive forces to the specific adsorbents while others not. Besides that, some refrigerants have corrosion properties and require special materials to use in the adoption system, which leads to high cost and maintenance.

The suitable adsorbate is the one that satisfies most of the considerations mentioned above. We can find suitable refrigerants in the market that can apply in the adsorption system, such as water, ethanol, methanol, and ammonia. Furthermore, many refrigerants

are understudying to be involved in adsorption applications such as hydrogen, methyl alcohol, R22, R732, oxygen, R134A, etc.

### 2.1.7. Adsorption pairs (Adsorbent/adsorbate)

Evaluation of the adsorbent and the refrigerant separately is not enough for choosing the appropriate one to be employed in the adsorption applications. Adsorption characteristics differ according to the chosen adsorption pairs. The critical features that the adsorbent should have are as the following:

- Low generating temperature.
- Good suitability with the adsorbate.
- Physically and chemically steady at different operating conditions.
- High capacity of the adsorbate in the adsorbent.
- Small pore size and high surface area.
- Low toxicity and non-explosive.

Table.2.1 shows some of the typical working pairs and their essential features. The best working pair is the one that agrees with the basic requirements that vary depending on the application (Askalany et al., 2013; Metcalf et al., 2012; Younes et al., 2017; Freni et al., 2016).

**Table 2. 1.** Most common adsorption working pairs traits

Characteristic Pairs	Operating pressure	$\Delta H_{fg}$ [kJ/kg]	$h_{fg}$ [kJ/kg]	X [kg/kg]	SCP [W/kg]
AC/ Methanol	vacuum	1800-2000	1102	0.45	140-500
AC/Ammonia	positive	1800-2000	1368	0.29	100-200
AC/ 134a	positive	1830-2300	217	0.36	10-50
AC/ Ethanol	vacuum	1200-1400	842	0.19	30-120
Zeolite/Water	vacuum	3200-4200	2258	0.17-0.31	90-250
Silica gel/Water	vacuum	2500-2800	2258	0.3-0.48	190-329

### 2.1.8. Adsorption cooling cycle concept

A primary adsorption cooling system comprises of four major components: an evaporator, a sorption bed, a condenser, an expansion valve. The sorption bed is packed with the adsorbent material. The adsorbent material has the ability of desorbing or adsorbing the refrigerant during the desorption or adsorption processes. In other words, the sorption bed adsorbs the adsorbate when cooled and desorbs the adsorbate when heated. In this regard, the sorption bed works as a thermal compressor to swirl the refrigerant (adsorbate) around the adsorption chiller parts; thus, cooling effects occur in the system's evaporator. Figure 2.3 shows a schematic of a primary adsorption refrigeration system.

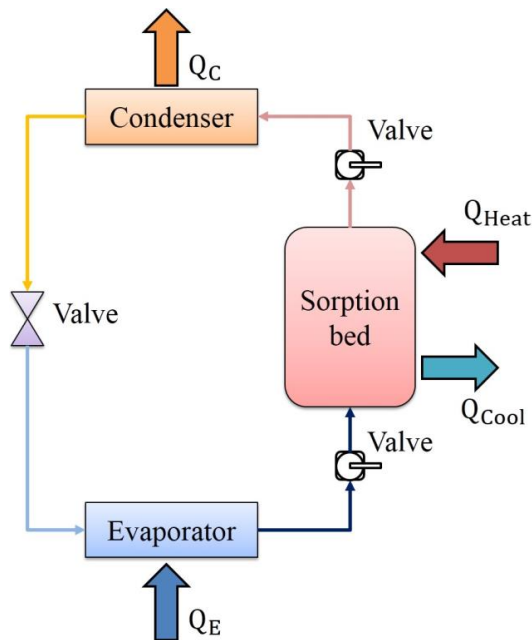


**Figure 2. 3.** A basic adsorption cooling system.

When the sorption bed is subjected to a heat source, the sorption bed temperature increases until it becomes high enough to desorb the adsorbate. Hence, the adsorbate leaves the adsorbent materials. Meanwhile, the pressure in the bed becomes more than the pressure in the condenser. The valve between the condenser and the sorption bed opens to make the adsorbate vapors pass through to the condenser. In the condenser, the refrigerant's vapors leave the latent heat; thus, a phase change occurs from saturated steam to saturated/subcooled liquid to become condensed refrigerant. The refrigerant goes after that through the expansion valve to lower the pressure to the evaporator pressure. The

expansion valve's exit is linked to the evaporator's inlet. The working fluid is vaporized in the evaporator by taking heat from the place to be refrigerated or conditioned. Meanwhile, the sorption bed is connected to a cool sink to decrease its temperature. After applying the adsorption process conditions in the thermal compressor, the adsorbate vapor enters the sorption bed to fulfill the cycle.

### 2.1.9. Adsorption cooling thermodynamic cycle

To comprehend the working principle of the sorption bed, the four major processes have been separated into isosteric cooling and isosteric heating processes (adsorbate concentration changing is not observed). In contrast, the other two processes are the desorption and adsorption processes (adsorbate concentration changing is noticed at constant pressure). The thermodynamic cycle of the thermal compressor processes is shown in the  $\ln P - 1/T$  diagram (Figure 2.4).

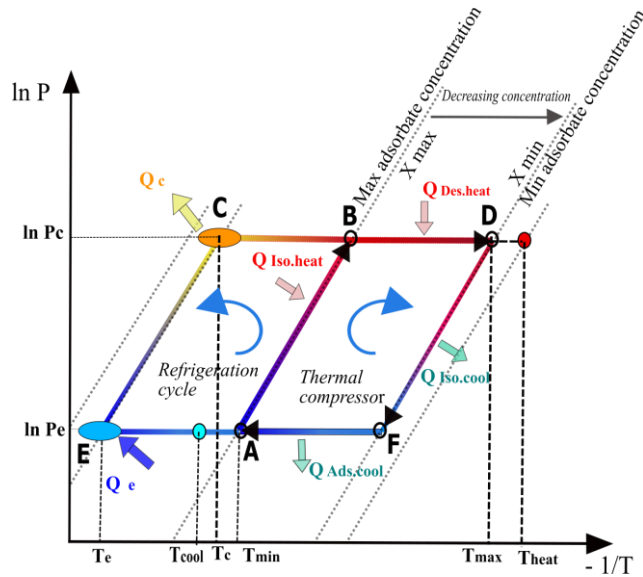


**Figure 2. 4.** Fundamental adsorption thermodynamic cycle for adsorption cooling cycle (Kilic & Anjrini, 2020).

As can be shown (Figure 2.4), there are two cycles in one system. The (ABCE) cycle is the thermodynamic refrigeration cycle, while the (ABDF) cycle is the thermal compressor cycle. The temperature  $T_{heat}$  is the maximum temperature that the sorption bed can reach by the heating source, while the temperature  $T_{cool}$  is the minimum temperature that the

sorption bed can reach by the cooling source. Both the temperatures  $T_{\text{heat}}$  and  $T_{\text{cool}}$  are related to the type of adsorbent material used in the adsorption system. The temperature  $T_E$  is the highest evaporation (saturation) temperature of the refrigerant corresponding to the evaporation pressure  $P_E$ . The temperature  $T_C$  is the minimum condensation (saturation) temperature of the refrigerant corresponding to the condenser pressure  $P_C$ . The temperature  $T_A$  is the minimum temperature corresponding to the cool sink in the adsorption cycle. The temperature  $T_B$  is the minimum temperature that the adsorbent materials start to desorb the adsorbate at the condenser pressure  $P_C$ . The temperature  $T_D$  is the maximum temperature during the desorption process. The temperature  $T_F$  is the maximum temperature that the adsorption process happens at the evaporator pressure  $P_E$ .  $X_{\text{max}}$  is the maximum uptake concentration that appears within the adsorption cycle in the sorption bed at the minimum bed temperature  $T_A$  and the evaporator pressure  $P_E$ . On the contrary,  $X_{\text{min}}$  is the minimum uptake concentration that appears within the adsorption cycle in the sorption bed at the maximum bed temperature  $T_D$  and the condenser pressure  $P_C$ . Both the maximum and minimum uptakes  $X_{\text{max}}$  and  $X_{\text{min}}$  parameters are related to the adsorbent type used in the bed and to the system operating conditions. More details about these parameters are described in the following sections. The main processes in the adsorption cycle are explained as the following (Kılıç, 2018):

- **Isosteric heating (pre-heating) process (A-B):** The working pair temperature increases as the bed materials absorb heat from the outside source heat. Meantime, the valves between the condenser/ evaporator and the thermal compressor (bed) are in closed positions. As a result, the gas pressure increase occurs in the bed until it reaches the pressure in the condenser  $P_C$ .
- **Isobaric heating (desorption) process (B-D):** By increasing the bed temperature through the outside heating source, the adsorbate begins leaving the bed while the pressure in the adsorbent bed is considered constant at the condenser pressure. The working pair temperature is continuously increasing until reaching the maximum value  $T_d$ . The adsorbate vapors go into the condenser to release some of its latent energy and become liquid.

- **Isosteric cooling (pre-cooling) process (D-F):** After accomplishing the isobaric process, the bed connects with the cooling source, and the bed temperature begins to fall down due to losing its heat. Meantime, the condenser and evaporator valves are already closed before starting this process. Thus, the bed pressure drops from the condenser pressure to the evaporation pressure value to start the cycle again.
- **Isobaric cooling (adsorption) process (F-A):** The adsorbate's vapors enter the cooled bed through the opened valve between the evaporator and the thermal compressor. The solid sorbent adsorbs the adsorbate particles; meantime, heat releases from the bed. The process finishes when the bed temperature reduces to the value of  $T_A$  at constant evaporator pressure.

In order to produce uninterrupted cooling effects, more than one adsorption bed (two, four, or six) may be employed in the adsorption chiller. By considering two beds in one thermal compressor, one of the beds is cooled down to adsorb the refrigerant while the other is heated up to desorb the refrigerant. Each bed has an interchanged function in the other cycle. Accordingly, the system can provide a continuous cooling effect.

#### **2.1.10. Different adsorption cooling system layouts**

As mentioned in the previous section, multiple sorption beds should be used in one stage to provide uninterrupted cooling effects. This part of the PhD thesis describes the operating modes of different layouts of the adsorption cooling cycle as the following:

##### **Single-stage adsorption cooling unit:**

The main parts of a single-stage adsorption unit are an evaporator and two sorption beds (thermal compressor) that operate alternatively. The thermal compressor in the adsorption cooling system operates according to four thermodynamic processes: pre-heating, desorption, pre-cooling, and adsorption processes. The adsorption cooling system with a single-stage operates in four modes (a, b, c, and d). In mode (a), bed (1) works in the pre-heating period to heat the adsorbent materials and raise the pressure in the thermal

compressor from the evaporator pressure  $P_e$  to the condenser pressure  $P_c$ . Meanwhile, bed (2) operates in the pre-cooling period to cool down the adsorbent materials and reduce the pressure from the condenser pressure  $P_c$  to the evaporator pressure  $P_e$ . Meantime, all the valves (1, 2, 3, and 4) are closed. In mode (b), the bed (1) operates in the desorption period releasing the adsorbate vapors to the condenser through the valve (4) at the condenser pressure  $P_c$ . Meanwhile, bed (2) works in the adsorption period taking the adsorbate vapors from the evaporator through the valve (2) at evaporator pressure  $P_e$ . Meantime, the valves (1 and 3) are closed. In mode (c), bed (1) operates in the pre-cooling period, while bed (2) runs in the pre-heating period. Meanwhile, valves (1, 2, 3, and 4) are closed as in mode A. In mode (d), the bed (1) operates in the adsorption period taking the adsorbate vapors from the evaporator through the valve (1) at the evaporator pressure  $P_e$ . Meanwhile, bed (2) operates in the desorption period releasing the adsorbate vapors through the valve (3) at the condenser pressure  $P_c$ . In this mode, the valves (2 and 4) are closed. Figure 2.5 shows the schematic of single-stage adsorption cooling unit modes. Table 2.2 describes the working strategies of a single-stage adsorption cooling unit according to the thermodynamic processes in the adsorption cooling cycle (Figure 2.4).

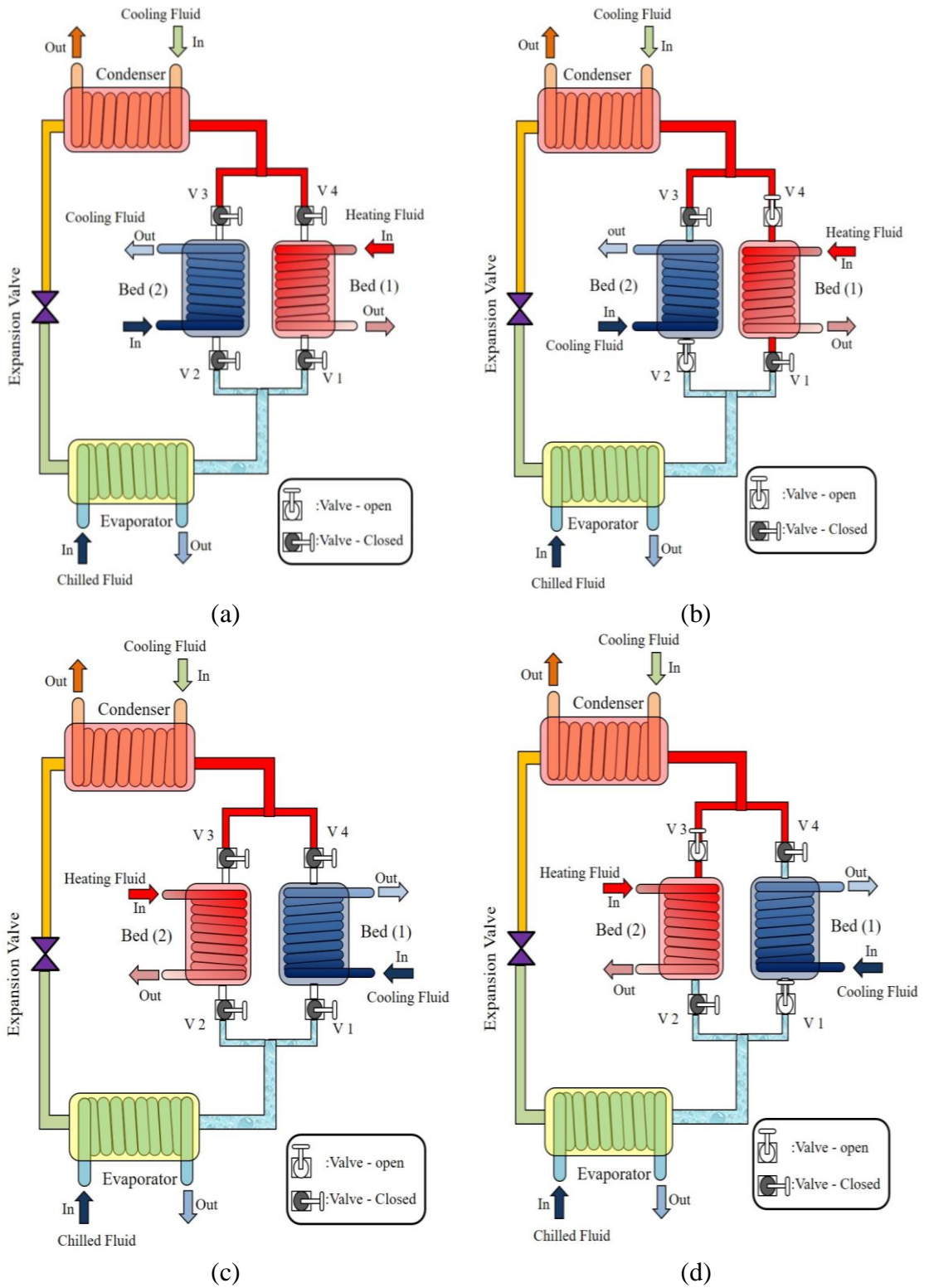


**Figure 2. 5.** Schematic of the single-stage adsorption cooling unite modes (a, b, c, d).

**Table 2. 2.** Working strategies of single-stage adsorption cooling system

Mode	a		b		c		d	
Bed (N)	(1)	(2)	(1)	(2)	(1)	(2)	(1)	(2)
Pre-heating	✓	×	×	×	×	✓	×	×
Desorption	×	×	✓	×	×	×	×	✓
Pre-cooling	×	✓	×	×	✓	×	×	×
Adsorption	×	×	×	✓	×	×	✓	×
Valve (1)	×		×		×		✓	
Valve (2)	×		✓		×		×	
Valve (3)	×		×		×		✓	
Valve (4)	×		✓		×		×	

**Two-stage adsorption cooling unit:**

If the regeneration temperature used to heat the adsorbent materials is low in the range of (50-80°C), using a single-stage adsorption cooling unit might not be practical. Therefore, for efficient usage of lower regeneration temperatures, a two-stage adsorption unit can be presented. In this cycle, the pressure elevation from the evaporator level to the condenser level occurs in two consecutive stages. Thus, an additional two sorption beds will be employed in the adsorption chiller to achieve this task. The four sorption beds will operate according to the four thermodynamic processes: pre-heating, desorption, pre-cooling, adsorption. We assumed at the beginning that all the six valves in the unit are closed. Meanwhile, beds (1 and 3) are in the pre-heating processes, while the other two beds (2 and 4) are in the pre-cooling processes. During these processes, neither desorption nor adsorption occurs. When the adsorbate concentrations in the sorption beds are close to their equilibrium levels, the heating and cooling fluids flow in different positions by switching the unit's six valves. As a result, each sorption bed's task is reversed from adsorption to desorption and vice versa. Figure 2.6 illustrates the operating modes of the two-stage adsorption cooling unit (a, b, c, and d). Table 2.3 describes the working strategies of the two-stage adsorption cooling unit according to the thermodynamic processes of the adsorption cooling cycle (Figure 2.7).

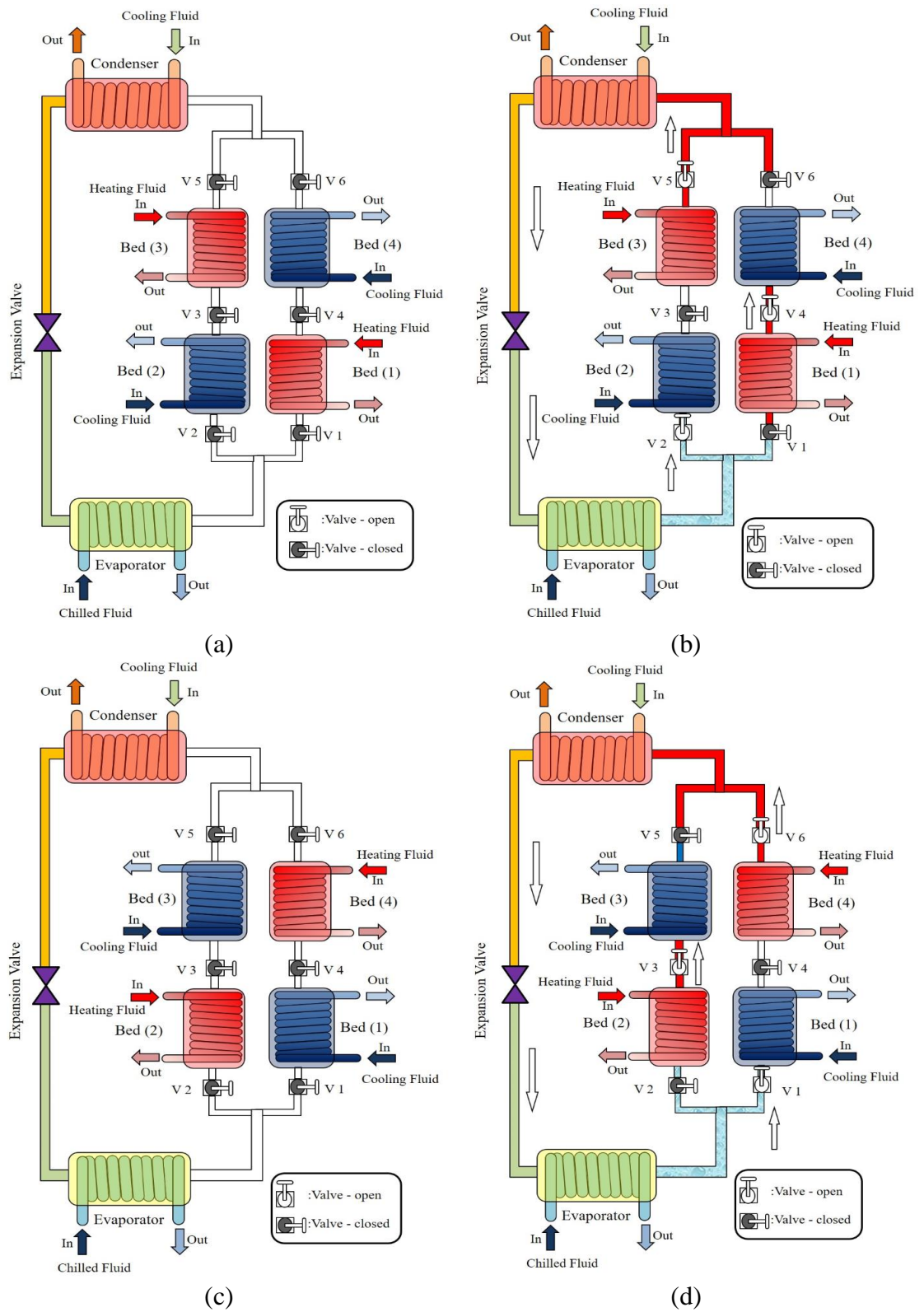
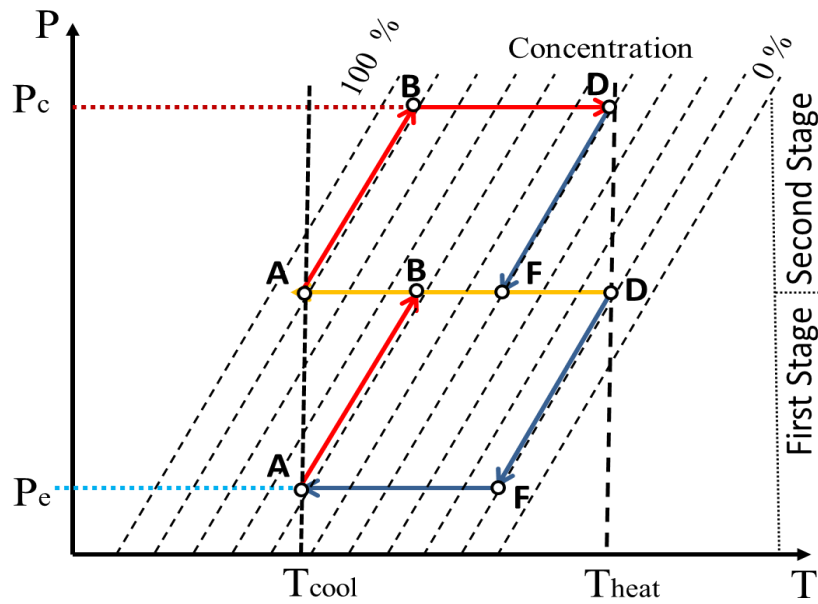


Figure 2. 6. Schematic of the two-stage adsorption cooling unite modes (a, b, c, d).

**Table 2. 3.** Working strategies of two-stage adsorption cooling system

mode	a				b				c				d			
Bed (N)	1	2	3	4	1	2	3	4	1	2	3	4	1	2	3	4
Pre-heating	✓	×	✓	×	×	×	×	×	×	✓	×	✓	×	×	×	×
Desorption	×	×	×	×	×	×	✓	×	×	×	×	×	×	×	×	✓
Pre-cooling	×	✓	×	✓	×	×	×	×	✓	×	✓	×	×	×	×	×
Adsorption	×	×	×	×	×	✓	×	×	×	×	×	×	✓	×	×	×
Re-mass heating	×	×	×	×	✓	×	×	×	×	×	×	×	×	✓	×	×
Re-mass cooling	×	×	×	×	×	×	×	✓	×	×	×	×	×	×	✓	×
Valve (1)	×				×				×				✓			
Valve (2)	×				✓				×				×			
Valve (3)	×				×				×				✓			
Valve (4)	×				✓				×				×			
Valve (5)	×				✓				×				×			
Valve (6)	×				×				×				✓			



**Figure 2. 7.** Two-stage adsorption thermodynamic cycle.

**Three-stage adsorption cooling unit:**

If the regeneration temperature used to heat the adsorbent materials is low in the range of (40-60°C), using single-stage or two-stage adsorption cooling units might not be practical. Therefore, for efficient utilization of lower regeneration temperatures, a three-stage adsorption unit can be employed. In this cycle, the pressure elevation from the evaporator level to the condenser level occurs in three consecutive stages. Thus, an additional four sorption beds and six valves will use for the basic adsorption chiller to achieve this task. The six sorption beds operate according to the four thermodynamic processes: pre-heating, desorption, pre-cooling, adsorption. However, this method requires more equipment to achieve the correct operation; thus, a more complicated system, big size, and high establishing and operating costs (Bidyut B Saha et al., 1995).

**2.1.11. The operating modes of the adsorption cooling system**

As mentioned before, the connection between the evaporator or the condenser and the sorption bed is achieved through four flap valves. These valves operate by the effect of a

pressure difference between the heat exchangers in the whole adsorption system during the desorption and adsorption processes. On the contrary, there are also twelve pneumatic valves that control the flow of heating and cooling fluids to the sorption beds, the flow of the chilled fluid to the evaporator, and the cooling fluid flow to the condenser. Generally, there are three operating modes in the adsorption cooling system:

- The adsorption/desorption mode: In this mode, the sorption bed (1) is heated up by the heating fluid while the cooling fluid cools down the bed (2). Bed (1) is linked to the condenser, bed (2) is connected to the evaporator to provide the cooling effects. Besides that, the cooling fluid flows from the exit of the sorption bed (2) through the tubes in the condenser in order to condense the refrigerant (adsorbate) vapors.
- The mass recovery mode: there is a bypass valve between the two sorption beds that opens to allow the adsorbate vapors to cross from the hot sorption bed (1) to the cold sorption bed (2) according to the pressure swing. However, this operating mode time should be adequate to reach the mechanical equilibrium between the two working beds.
- The heat recovery mode: the cooling fluid flows through the hot bed first, after that flows to the cold one. The same operating mode is applied in the following thermodynamic cycle but by switching the function between bed (1) and bed (2).

The modes in adsorption chiller at adsorption/desorption, mass recovery, and heat recovery are presented during the first cycle (Figure 2.8 a, 2.8 b, and 2.8 c), respectively. In contrast, the modes in adsorption chiller at adsorption/desorption, mass recovery, and heat recovery are presented during the second cycle (Figure 2.8 d, 2.8 e, and 2.8 f), respectively. Table 2.4 illustrates the operation and valving modes of the adsorption chiller.

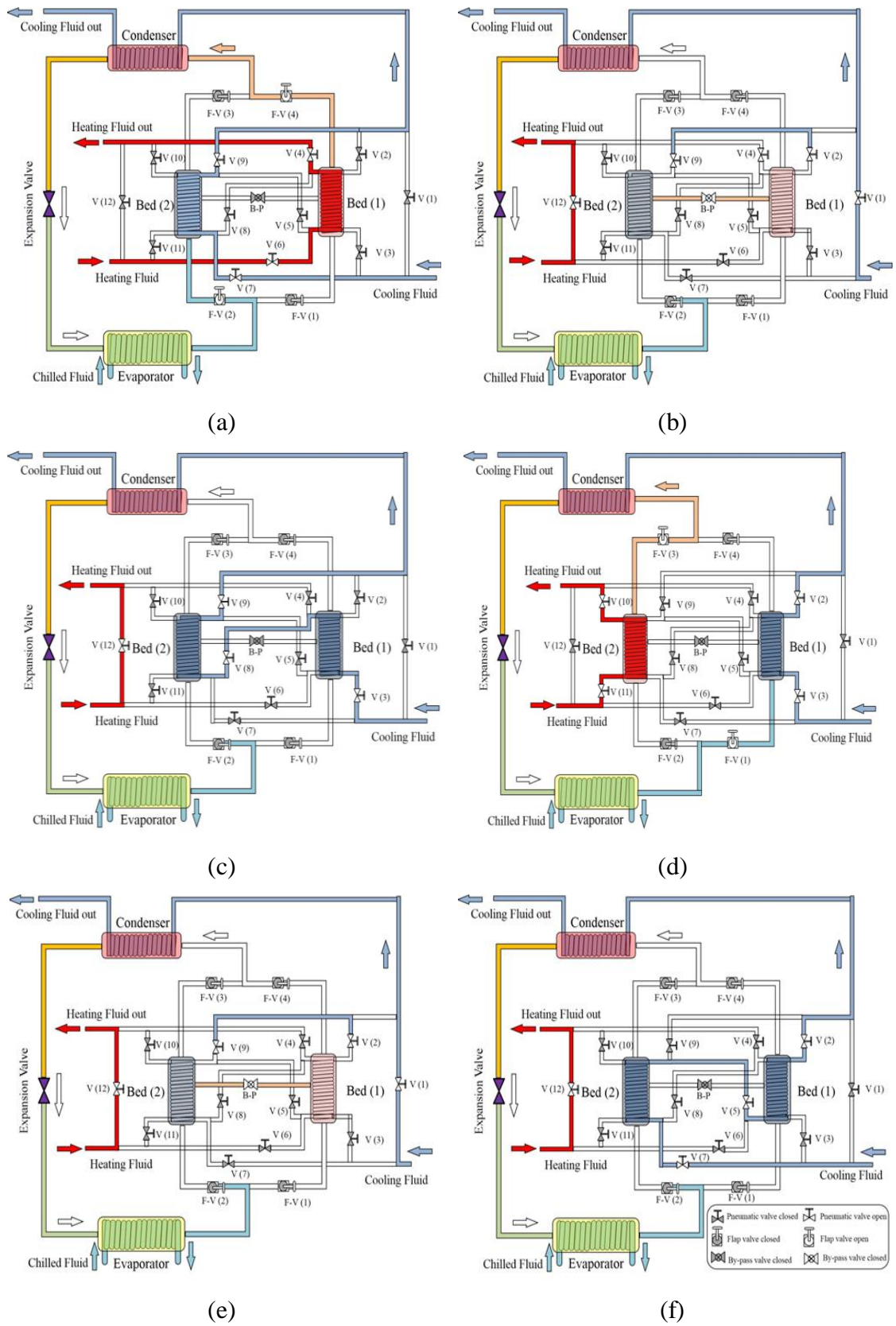


**Figure 2. 8.** The operating modes of the adsorption cooling system.

**Table 2. 4.** Operation and valving systems for the adsorption chiller

Mode	a Des/ads	b Mass recovery	c Heat recovery	d Des/Ads	e Mass recovery	f Heat recovery
Bed (1)	HF	NF	CF	CF	NF	CF
Bed (2)	CF	NF	CF	HF	NF	CF
F-V (1)	x	x	x	✓	x	x
F-V (2)	✓	x	x	x	x	x
F-V (3)	x	x	x	✓	x	x
F-V (4)	✓	x	x	x	x	x
V (1)	x	✓	x	x	✓	x
V (2)	x	✓	x	✓	✓	✓
V (3)	x	x	✓	✓	x	x
V (4)	✓	✓	x	x	x	x
V (5)	x	x	x	x	x	✓
V (6)	✓	x	x	x	x	x
V (7)	✓	x	x	x	x	✓
V (8)	x	x	✓	x	x	x
V (9)	✓	✓	✓	x	✓	x
V (10)	x	x	x	✓	x	x
V (11)	x	x	x	✓	x	x
V (12)	x	✓	✓	x	✓	✓
B-P	x	✓	x	x	✓	x

## 2.2. Combined (mechanical- thermal) cooling system

One of the methods that have been recently used to improve the cooling system performance and to reduce energy consumption is to combine the thermal compression (absorption/desorption) cooling system with the mechanical compression (traditional) cooling system.

### 2.2.1. Thermal compression cooling cycles

The sorption cooling cycle operates by applying the thermodynamic concept with two sinks and two heat sources utilizing three temperature levels. Two of these temperatures are used in the thermal compressor, which replaces the mechanical device (compressor) in a conventional vapor compression cooling cycle. The sorption cooling systems are categorized into two types (adsorption and absorption systems). Figure 2.9 states a brief explanation of both sorption chiller's advantages and disadvantages.

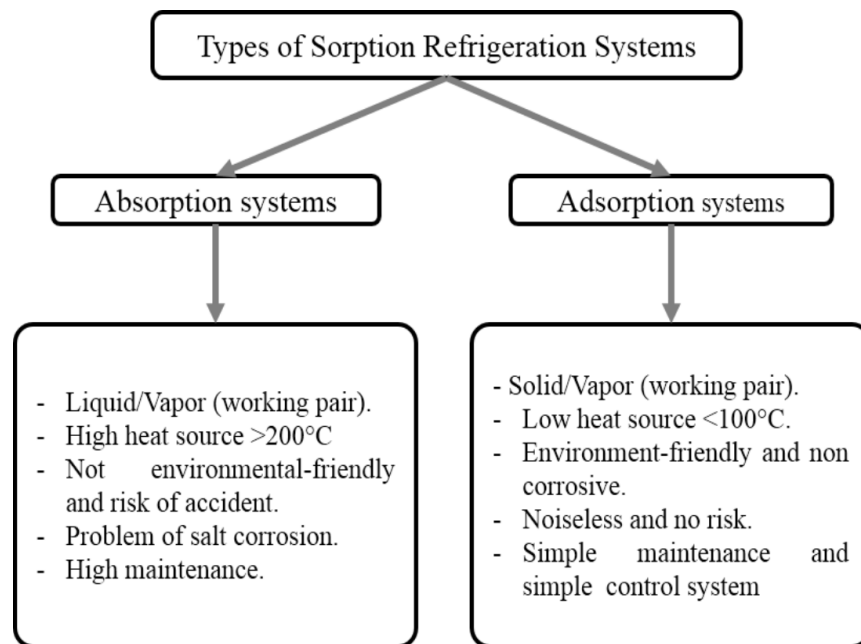


**Figure 2. 9.** Types of sorption refrigeration systems.

### 2.2.2. Absorption – vapor compression combined cooling cycles

The basic vapor compression (mechanical compression) cooling cycle consists of four primary elements: evaporator, mechanical compressor, condenser, and expansion valve. While the fundamental absorption (thermal compression) cooling cycle consists of the following main components: evaporator, absorber, generator, condenser, pump, solution heat exchanger, and expansion valve. Figure 2.10 depicts the general schematic of mechanical and thermal (absorption) compression chillers separately and combined.

The operating principle of the vapor mechanical cooling cycle is to absorb an amount of heat from the place to be refrigerated or conditioned through the evaporator and release that heat through the condenser after adding electrical energy through the mechanical compressor. On the contrary, the operating principle of the absorption cooling system is similar to the conventional vapor cooling system; however, instead of employing the mechanical compressor, the absorption system uses an absorber to raise the weak refrigerant through the pump as the heat is provided to the generator (Nikbakhti et al., 2020).

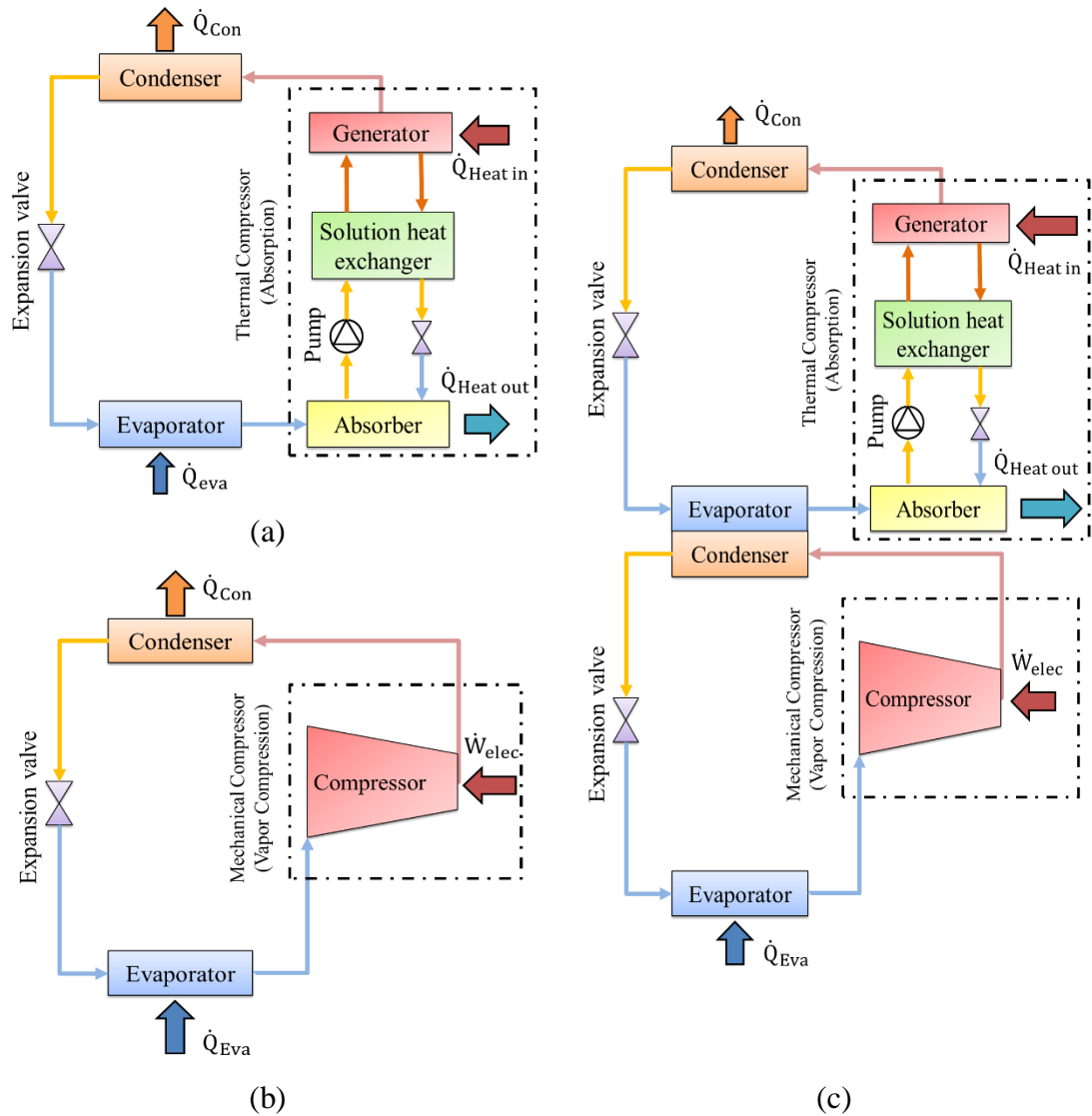


**Figure 2. 10.** General schematic of (a) absorption cooling system (ABC), (b) vapor compression cooling system (VCC), (c) ABC-VCC combined cooling system.

One of the essential benefits of using thermal and mechanical compression in the combined cooling cycle if the systems are combined in a series layout is to fragmentize the pressure ratio between the two heat sinks; the mechanical compressor fulfills part of the pressure whereas the thermal compressor accomplishes the rest. The combination of thermal compression and mechanical compression cycles can be executed in different ways. Many studies concern about the hybridization between the absorption chiller and the traditional chiller. There are studies related to different configurations (Jain et al., 2018; Lijuan et al., 2019; Liu et al., 2019; Ustaoglu, 2020; Babaei et al., 2020), and others related to various heat sources (He et al., 2019; Mousavi & Mehrpooya, 2020; Agarwal et al., 2020; Song et al., 2020).

### **2.2.3. Adsorption – vapor compression combined cooling cycles**

The suggested hybrid cooling system consists of two separated cycles. The first one is Vapor Cooling Cycle (VCC), while the second unit is Adsorption Cooling Cycle (ACC). Each one has its components, as it has previously mentioned, like the following: adsorption cooling cycle has four major components: condenser, evaporator, an expansion valve, and the thermal compressor, which is the vital element in this chiller. The traditional chiller (VCC), on the other hand, also operates through four major elements: evaporator, expansion valve, condenser, and mechanical compressor. A middle heat exchanger physically links the two different cycles (ACC and VCC). Each cycle operates with different refrigerants. Figure 2.11 illustrates the schematic layout of the studied proposed integrated (ACC-VCC) cooling system.

As shown (Figure 2.11 c), the evaporator in the conventional chiller soaks up the heat from the space and transmits it into the upper chiller (adsorption cooling system). The middle heat exchanger (evaporator in the upper cycle and condenser in the bottom cycle) takes this released heat to carry on the adsorption chiller's mission. The evaporated refrigerant then enters the thermal compressor, where the cooled adsorbent adsorbs it. After that, the adsorbent material is heated by a heat source to reject the refrigerant out of the bed. The adsorbate vapors enter the condenser, where it losses its latent heat and condensed it to be liquid. The condensed refrigerant expands through an expansion valve

to the evaporator pressure. The exit of the expansion valve is linked to the evaporator inlet, where the adsorbate is vaporized by taking heat from the (VCC side) in the intermediate heat exchanger. After the adsorption process conditions are prepared in the bed, the refrigerant goes into the bed to complete the cycle. This arrangement's main feature is to fragmentize the total requisite compression ratio into two sections; one is achieved in the thermal compressor using waste heat, while the mechanical compressor accomplishes the required compression ratio consuming less electrical energy.

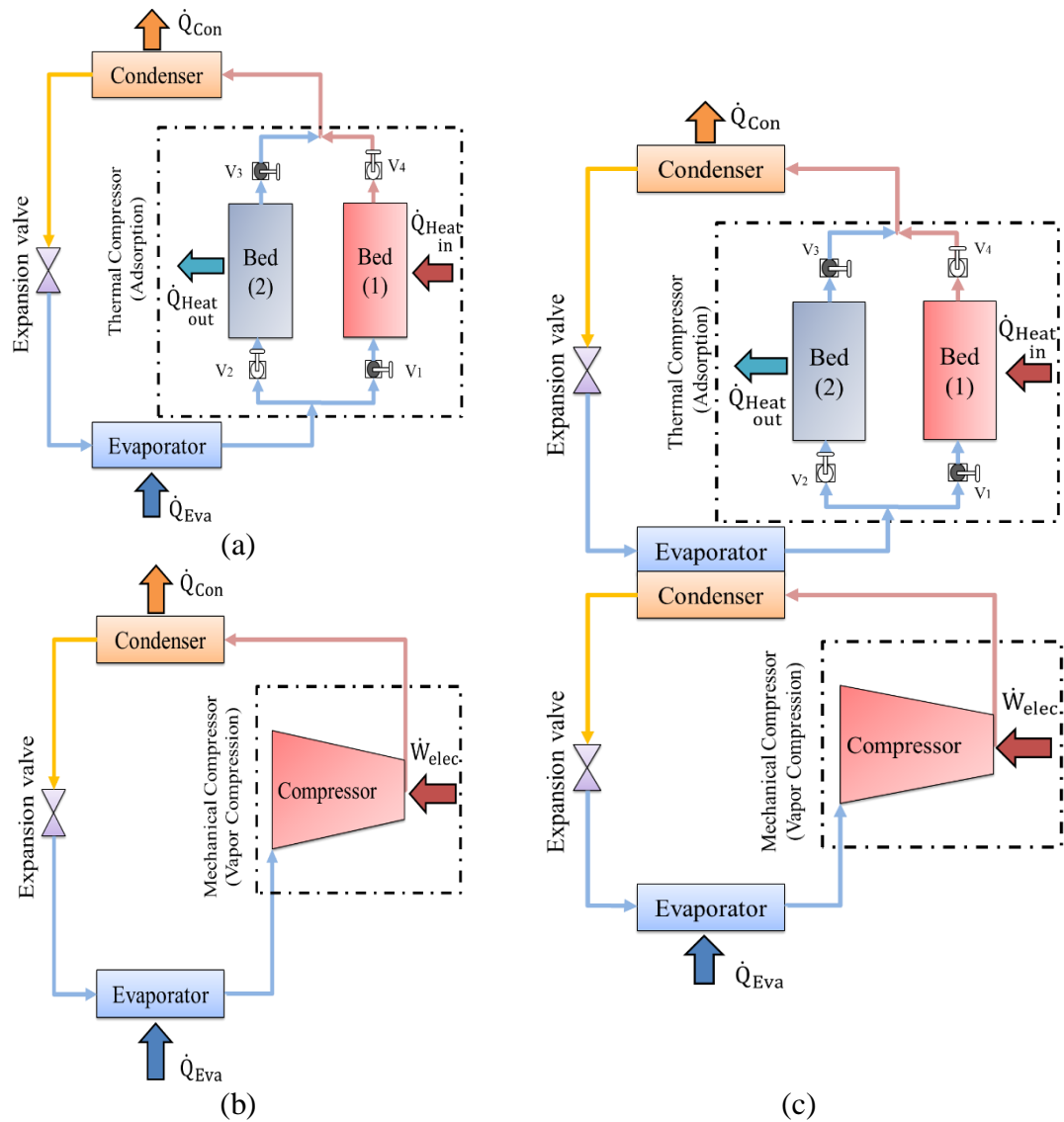


**Figure 2. 11.** General schematic of (a) adsorption cooling system (ACC), (b) vapor compression cooling system (VCC), (c) ACC-VCC combined cooling system.

## **Different configurations and thermal resources of ACC-VCC system – Literature review:**

One of the significant benefits of employing thermal and mechanical compressors in the combined cooling cycle is to fragmentize the pressure ratio between the two heat sinks. Part of the pressure is achieved by the mechanical compressor, and the rest is accomplished by the thermal compressor. This section introduces a detailed review of different connections and layouts of the ACC-VCC combined cooling system.

Banker et al. (2008) investigated the performance of the adsorption-vapor compression combined cooling system. The activated carbon/HFC 134A working pair and HFC 134A refrigerant were used in the adsorption cycle and the vapor compressor, respectively. The investigation was implemented by choosing two configurations: in the first layout, the thermal compressor was supplying the low-grade compression and locating after the evaporator. The refrigerant, after the desorption, enters the vapor compressor. In the second layout, on the contrary, the vapor compressor was providing the low-grade compression where the vapors after the mechanical compressor enter the thermal compressor to complete the cycle. The results indicated that the interchanging between the thermal and mechanical compression systems between low and high-pressure stages provided a lower effect when the thermal compressor operated in the low stage.

Uddin et al. (2013) investigated analytically two different adsorption-vapor compression combined cooling cycle layouts. The first configuration where the two systems shared that same heat exchanger (a condenser in the vapor compression chiller and evaporator in the adsorption chiller) (Figure.2.11 c). In the second configuration, the two chillers shared the same heat exchanger, a sub-cooler in the vapor compression chiller and an evaporator in the adsorption chiller. The activated carbon/ ethanol was chosen as a working pair in the adsorption chiller, while four different refrigerants (R152a, R134a, R1234yf, and R1234ze) were selected in the vapor compression chiller. The results indicated that the R152a refrigerant supplied the highest cooling power among the refrigerant considered. Moreover, changing the refrigerant in the compression chiller had a marginal effect on the coefficient of performance in the adsorption chiller. The cooling capacity and the

coefficient of performance in the traditional compression chiller increased with rising the evaporator temperature and sub-cooler temperature. The first configuration could save energy from 13% to 19%, while the second configuration could save energy from 22% to 30% based on the refrigerants considered in the study. The results also illustrated that the amount of adsorbent mass required to obtain 5.6 kW was 5 kg when the system operated in the second configuration.

Der Pal et al. (2013) evaluated the combined adsorption-compression heat pump system to be used in industrial applications. The primary working fluid used in the proposed cycle was ammonia. The investigation was done on multiple sorbents (salts) in the evaluation study. Two combined system layouts were mentioned in the research related to the position of the mechanical compressor. In the first one, the vapor mechanical compressor was placed in the discharge phase. This benefit of the configuration was in reducing the requisite heat for regeneration and considering a smaller and cheaper compressor. In the second one, a double of the vapor mechanical compressor was needed: one compressor for the discharge phase and another one for the regeneration phase. The results indicated that the payback period was between 2 to 9 years, affected by the energy prices, operating hours, and the compression stage's electrical efficiency.

Kumar et al. (2014) investigated experimentally the performance of the vapor mechanical compressor-adsorption combined cooling system. Activated carbon/ CO<sub>2</sub> as a working pair and CO<sub>2</sub> as a refrigerant were employed in the adsorption cycle and the vapor compressor, respectively. The investigation was done by choosing two configurations: the first configuration where the thermal compressor was supplying the low-grade compression and locating after the evaporator. The refrigerant enters the vapor compressor after starting the desorption. In the second configuration, on the contrary, the vapor compressor was providing the low-grade compression where the vapors after the mechanical compressor enter the thermal compressor to complete the cycle. The results indicated that the compression power of the mechanical compressor was lower when the mechanical compressor was positioned in the low stage. Furthermore, the mass of carbon refrigerant requirement was higher when the mechanical compressor was located in a low

stage position compared to the other position. The authors indicated that the suggested system was appropriate for a few kilowatts loads.

Lychnos et al. (2014) investigated the performance of an adsorption-mechanical compressor hybrid cooling system for air conditioning and ice-making applications. Activated carbon/ammonia was chosen as a working pair in the adsorption cycle, while ammonia was selected as a refrigerant in the mechanical compressor. The thermal compressor and mechanical compressor can work either at the same time or only one of them at one time. The system had a 3-way valve after the evaporator that controls the refrigerant route; the refrigerant either goes to the thermal compressor or mechanical compressor or both of the compressors. The results illustrated that the cooling power ranged from 8 kW to 24 kW when both systems worked together. On the contrary, when only one compressor was operating, the cooling power ranged from 4 kW to 12 kW. Furthermore, the authors mentioned that the bed number depending on the driving temperature. The results stated that the overall coefficient of performance varied in a range between 0.24 to 0.76.

Muztuza Ali et al. (2017) investigated thermodynamically two configurations of adsorption-vapor compression combined cooling system for cooling and desalination applications. Silica gel/water working pair and CO<sub>2</sub> refrigerant were used in the adsorption chiller and vapor compression chiller, respectively. The first layout of the system consisted of a two-stage heat recovery system, where in the first one, heat recovery occurred from the compressed refrigerant to drive the adsorption chiller, while in the second one, the heat recovery occurred inside the heat exchangers between the two pressure levels in the CO<sub>2</sub> cycle. In the second layout, a third stage heat recovery was added where the heat recovery occurred between the gas cooler and the high-pressure evaporator of the adsorption chiller. The results revealed that the first layout enhanced the coefficient of performance for the vapor compression chiller by 28% and supplied 9.86 m<sup>3</sup> freshwater for one ton of adsorbent (silica gel) in a day. On the contrary, the coefficient of performance for the vapor compression chiller in the second proposed layout improved by 61% and supplied 12.66 m<sup>3</sup> freshwater for one ton of adsorbent (silica

gel) in a day. The overall coefficient of performance for layout (1) and layout (2) were 58% and 100% higher than that of the traditional CO<sub>2</sub> cycle.

Palomba et al. (2017) analyzed and tested the adsorption-vapor compression combined cooling system driven by waste heat and electrical sources. Silica gel/water working pair and R410a refrigerant were chosen in the adsorption and vapor compression chillers, respectively. Both chillers shared the same heat exchanger, a condenser in the bottom chiller and an evaporator in the upper chiller, as previously illustrated (Figure 2.11 c). The results indicated that the coefficient of performance of the vapor compression chiller in the combined system could reach up to 8. The electric coefficient of performance of the integrated system could reach up to 6.5. The results also indicated that the seasonal efficiency could be double compared with the traditional electrical chiller performance.

Lychnos et al. (2018) set up and tested a prototype of adsorption-vapor compression combined cooling system. The activated carbon/R723 working pair was used in the adsorption chiller, while R723 refrigerant was chosen in the vapor compression chiller. R723 is an ammonia mixture (60% Ammonia, 40% Dimethylether). The paper explained four configurations of the combined cooling systems using thermal and compression cycles as the following: the first one described in the previous section (Lychnos et al., 2014). In the second configuration, the adsorption and vapor compression chillers were in a parallel connection where both system's evaporators were connected with the same chilling fluid, that entering the adsorption chiller's evaporator first then passing through the vapor compression chiller's evaporator. In the third configuration, both chillers shared the same heat exchanger, evaporation in the adsorption chiller and condenser in the other chiller. In the fourth configuration, the two chillers were operating at the same time, which is similar to the first one but without the 3-way valve that controls the direction of the refrigerant. The experimental results pointed out that the proposed parallel combined system could provide 6 kW of refrigeration capacity with both chillers (2 kW from the adsorption chiller at 80°C driving temperature and 4 kW from the vapor mechanical chiller).

Vasta et al. (2018) investigated experimentally and analytically the adsorption-vapor compression combined cooling system for air conditioning application. Silica gel/water and FAM ZO2/water were chosen separately as a working pair in the adsorption chiller, while five different refrigerants (R410A, R290, R600a, R717, and R744) were selected in the vapor compression chiller. Both chillers shared the same intermediated heat exchanger where the condenser of the vapor compression chiller was connected to the evaporator of the adsorption chiller separately. The results illustrated that this combination could save about 50% in the vapor compression only with respect to the application where the performance of the compression chiller was about 25% lower for all cooling temperatures considered. The results also stated that the FAM ZO2/ water working pair in the adsorption chiller was suitable for hot climates where the coefficient of performance reached 40% in the thermal unit. On the contrary, the results revealed that R600a and R290 were suitable alternatives for R410A in the vapor compression chiller. Moreover, the increase in COP in the vapor compression chiller could reach up to 110% at lower evaporator temperature in the research for R600a, where the coefficient of performance increased from 0.8 to 1.3 at  $-40^{\circ}\text{C}$  (evaporator temperature). In contrast, this value increased from 2 to 33 at  $0^{\circ}\text{C}$  (evaporator temperature) when the condensation temperature is  $25^{\circ}\text{C}$ , while this value increased from 1.4 to 2.6 at  $35^{\circ}\text{C}$  (condensation temperature).

Gibelhaus et al. (2019) investigated the adsorption-vapor compression combined cooling system in terms of optimization, economic analysis, and energy savings. Silica gel 123/water was chosen as a working pair for the adsorption unit while  $\text{CO}_2$  was used as a refrigerant in the vapor compression unit. The proposed system consisted of three steps heat release process of the vapor compression chiller in the combined cycle. The first step at a high temperature, where a heat exchanger was located between the mechanical compressor and condenser to release heat to the heating fluid that drives the adsorption chiller. In the second step, the heat was released in the condenser of the vapor compression chiller to the environment. In the third step, the heat was released to the cooling fluid of the adsorption unit; thus, further cooling of the refrigerant below the ambient temperature. The purpose of the two chillers combination was to increase efficiency as the  $\text{CO}_2$  the compression cycle had low efficiency. An investigation was

also done on the size of the adsorption chiller as it was related to the cycle time. The authors pointed out that the optimal cycle time increased as the size ratio, the ratio between the nominal cooling capacity of the adsorption and compression chillers, increased vice versa. The results illustrated that the energy savings and optimal size ratio depended on the ambient temperature as 15°C, 25°C, and 35°C. The optimal size ratio and energy savings were (0.47 and 15%), (0.84 and 26%), and (1.27 and 35%), respectively. The results declared that the overall energy savings from the model reached up to 35%. The economic and energy savings analyses were also studied in two cities Athena and Cologne. The results of the analysis revealed that the energy-saving and payback period for Athens were 22% and five years, respectively. In comparison, the same quantities for Cologne were 16% and four years, respectively.

Palomba et al. (2020) investigated the efficient exploitation of renewables for adsorption-vapor compression combined cooling system. The study examined three different layouts (parallel connection, series connection, and cascade connection). Silica gel/water was the working pair chosen for the adsorption chiller, whereas four different refrigerants (CO<sub>2</sub>, R134a, R290, and R1270) were employed in the vapor compression chiller. The study analyzed the capacity ratio, which is the ratio between the heat rejected from the vapor compression chiller's condenser and the heat absorbed to the adsorption chiller's evaporator. Researchers found that the optimum value was the one that closes to one. The results concluded that the suitable refrigerant in VCC was the one that affects the volume and size of the overall combined system. The results also indicated that a shorter cycle time could be utilized when higher cooling power was required.

Kiliç and Anjrini. (2020) compared the adsorption-vapor compression combined cooling cycle in terms of performance and adsorbent mass needed for the adsorption cycle. Silica gel/water working pair and different working fluids (R410A, R152A, R1234yf, R32, and R1270) were employed in the adsorption and vapor compression chillers, respectively. The results indicated that the highest performance of the combined system, exergy efficiency, vapor compression chiller reached up to 0.5, 0.334, and 8.8 for R152A, respectively. On the contrary, the lowest performance of the combined system, exergy efficiency, and vapor compression system reached up to 0.32, 0.324, and R1234yf,

respectively. The results also revealed that the highest values of energy savings among the other working fluids considered reached up to 65% for R1234yf. The researchers also investigated the adsorbent mass in the adsorption chiller. They found a relation between the adsorbent mass and the hot fluid temperature, the VCC evaporator temperature, and the adsorption cycle time. The results indicated that by selecting higher hot fluid and evaporator temperatures, a lower amount of adsorbent was required. Additionally, reducing the adsorption cycle time in the adsorption chiller might contribute to using a low amount of adsorbent in the beds of the adsorption chiller.

On the contrary, one of the other essential benefits of using a thermal compressor in the cooling cycle is using different heat resource systems that might come from different ways. The following section introduces a literature review of different heat source systems integrated with the ACC-VCC combined cooling system.

Ma et al. (2006) presented a performance analysis of a combined air conditioning system for green building applications. The proposed system consisted of four systems: the first system was the vapor compression heat pump that provided the cooling effects to cool the air, whereas the condensation heat was utilized to drive the liquid desiccant dehumidification system. The second system was the solar system that consisted of 150 m<sup>2</sup> solar collector, which providing the heat source to drive the adsorption unit. The third system was the two adsorption cooling units that employed silica gel/ water as a working pair and produced 10 kW as a cooling capacity for each. The fourth system was the liquid desiccant dehumidification system that employed a lithium bromide solution as a liquid desiccant, where the purpose of the final system was to recover energy. The results revealed that the proposed system's performance was higher than the traditional vapor compression system by 44.5% at 30% of latent heat, and the enhancement of the performance could reach up to 73.8% at 42% of latent heat.

Cyklis (2014) presented an investigation on sorption (adsorption/absorption) - vapor compression combined systems, but the experimental study was done on the adsorption – vapor compressor combined cooling system. The proposed integrated system consisted of an adsorption chiller, a pumping system, and two compressors. Solar plate collectors

were used to providing the thermal energy to drive the thermal compressor in ACC. Zeolite/water as working pair was chosen for the adsorption chiller while CO<sub>2</sub> was employed as a refrigerant in the vapor compressors. The compression was accomplished by using (CO<sub>2</sub> + R410A) in the two-stage compressor cooling. The results indicated that by implementing (CO<sub>2</sub> + R410A) in the two-stage compressors, a reduction in the total equivalent warming impact and electrical energy reached (60%≤) and 30%, respectively.

Palomba et al. (2018) analyzed experimentally the adsorption-vapor compression combined cooling system driven by a solid oxide fuel cell as a heat source. Silica gel/water working pair and R410a refrigerant were chosen in the adsorption and vapor compression chillers, respectively. Both chillers shared the same heat exchanger, a condenser in the bottom unit and an evaporator in the upper unit. The results revealed that the proposed combined system achieved higher energy savings compared to the adsorption unit alone. The analysis results showed that global energy efficiency reached up to 0.63, and the primary energy savings reached up to 110 MWh/year, whereas the CO<sub>2</sub> emissions avoided reached up to 43 tons annually.

Wittstadt et al. (2018) analyzed the adsorption – vapor compression combined system and compared the results with a conventional vapor compression cooling system. In the combined configuration, the adsorption chiller's evaporator cools down the vapor compression chiller's condenser (Figure 2.11 c). A solar system was connected to the thermal compressor of ACC to provide the thermal energy required to drive the cycle. Water and (propane/R290 mixture) refrigerants were used in the adsorption and vapor compression chillers, respectively. Besides that, a mixture of water-glycol was used as a working fluid in the re-cooling and secondary evaporator cycles. The results indicated that the total power consumption in the combined system was 4.96 kW comparing with 4.6 kW of the conventional cooling system at the same operating conditions. However, the cooling powers were 17.8 kW and 19.3 kW for the traditional and combined systems, respectively, which means a 9% increase in the cooling capacity. Furthermore, the results revealed that the nominal energy efficiency ratio could increase by 24% in the combined system compared with the conventional one.

Palomba et al. (2019) validated the dynamic models of adsorption-vapor compression combined cooling system for designing purposes. The combined system was integrated with a solar system to provide the heat source. The two chillers shared the same heat exchanger, an evaporator in the adsorption chiller and a condenser in the other chiller (Figure 2.11 c). SAPO34/water was chosen as a working pair in the adsorption unit, while the R410A refrigerant was employed in the vapor compression unit. The ACC was connected with a solar system to provide the thermal heat source. In contrast, the VCC was linked with a photovoltaic panel to supply the electrical energy to the mechanical compressor. The results pointed out that the nominal cooling capacity for an adsorption chiller should be at least 50% higher than that of the traditional vapor compression chiller.

Palomba et al. (2019) investigated a daily simulation of adsorption-vapor compression combined cooling system for typical industrial applications. The proposed system was connected with a solar system to provide the heat source to drive the adsorption chiller. Both chillers shared the same heat exchanger, a condenser in the vapor compression unit and an evaporator in the adsorption unit. Silica gel/ water working pair and R290 refrigerant were chosen in the adsorption and vapor compression chillers, respectively. The results of daily simulation (during 24 hours) revealed that the electric chiller of the combined system studied was stable and could provide the desired temperatures at the evaporator. Also, the adsorption chiller could efficiently and reliability cools down the condenser of the traditional chiller.

#### **2.2.4. (ACC-VCC) combined cooling system configurations**

As mentioned before, The proposed hybrid cooling system includes two different cooling units. The first one is the adsorption chiller (ACC), while the second is the vapor compression chiller (VCC). Each cooling cycle has its main components as the following: (ACC) unit has four essential elements: the thermal compressor (solid sorbent), which is the core part of the cycle, condenser, expansion valve, and evaporator. The adsorption phenomenon stated that the adsorbate particles settled down at the adsorbent's superficies between the granular due to the strong attractive and electrostatic energies among the particles. The adsorbate particles leave the solid sorbent when heated and adsorb them as

it is cooled down. Consequently, the thermal compressor operates to drive the refrigerant through the ACC system; the unneeded heat is removed as a result (Vodianitskaia et al., 2017).

The vapor cooling cycle also has four major components: vapor mechanical compressor, evaporator, expansion valve, and condenser. The presented two chillers (ACC and VCC) may physically connect with several types of configurations. Two potential working modes are suggested in this dissertation: series connection and parallel connection. Figure 2.12 shows the two integrated cooling system configurations to be analyzed and compared.

In the series connection (Figure 2.12 a), two units connection happens in the intermediate heat exchanger, which includes an evaporator in the ACC unit and a condenser in the VCC unit. The VCC chiller works between the evaporation temperature that the user needs and the intermediate temperature (VCC condenser temperature side) In this layout. On the contrary, the ACC chiller operates between the ACC evaporator temperature in the intermediate heat exchanger and the ACC condenser temperature. Hence, the ACC evaporator supplies the cooling power to the VCC condenser. In the second layout (Figure 2.12 b), both chillers deliver the cooling effects to the utilizer. Both chillers work between the utilizer side temperature and rejected heat temperature. The total cooling load is divided into two sections in this arrangement according to the operating condition of each unit. Moreover, this sort of integration allows for utilizing the ACC chiller to accomplish the primary load, whereas the vapor compression chiller can be added to cover the peak load, a smaller size in both chillers is presented as a result.

The VCC evaporator absorbs an amount of heat from the cooled place and conveys it into the upper unit. The intermediate heat exchanger takes all the rejected heat to continue the ACC chiller task (Figure 2.12 a). The evaporated working fluid in the adsorption chiller enters the thermal compressor, where the solid adsorbent adsorbs the vapors as its temperature is lowered by outsourcing cooling fluid. After that, solid sorption temperature is heated up via an outside heat source to release the adsorbate vapors out of the thermal compressor component. The vapors are driven to the ACC condenser, where

its temperature is lowered by rejecting its heat to the surroundings and condensed to be in a liquid phase. After that, an expansion valve is employed to expand refrigerant pressure to be in the ACC evaporator pressure level. The inlet of the ACC evaporator is linked to the expansion valve outlet, where the refrigerant is vaporized in the ACC evaporator of the middle heat exchanger by absorbing the rejected heat from the VCC condenser. After the adsorption conditions are equipped in the adsorption beds, the working fluid vapors enter the thermal compressor to do the adsorption cycle again.

In the parallel configuration (Figure 2.12 b), part of the cooling load required is achieved through the adsorption chiller's evaporator. In contrast, the evaporator in the VCC chiller absorbs the remaining cooling load. A secondary fluid cycle that connects the two units enters the ACC chiller's evaporator at the surrounding temperature to leave part of its heat in the evaporator at a temperature level higher than the ACC evaporator temperature. Thereafter, it enters the VCC evaporator to leave the residue of its heat at the temperature level specified by the utilizer, yet higher than the evaporator temperature in the VCC unit. It is important to refer that the temperature values in the ACC evaporator and VCC evaporator are not the same, but they depend on the design specifications of each unit.



### 3. MATERIALS and METHODS

Many simulation tools are available for the design and optimization of mechanical systems in the literature. Modeling is considered the essential technique that can estimate the geometric specifications as well as the operating conditions of the refrigeration systems. There are various modeling techniques that were implemented to simulate the adsorption cooling cycles, such as lumped analytical simulation (Miyazaki et al., 2009; Miyazaki & Akisawa, 2009), dynamic simulation (Bidyut Baran Saha et al., 2009), lumped-parameter simulation (X. Wang & Chua, 2007b), and distributed-parameter simulation (X. Wang & Chua, 2007a). In this study, the modeling technique will be applied for the two chillers (ACC and VCC) separately, and they will be linked together thermodynamically.

#### 3.1. Adsorption Cooling Cycle modeling

To simulate the ACC chiller, many assumptions have been reported in the literature. Sharafian et al. (2015) classified the mathematical model into three groups:

- **Analytical models:** this model is considered a fast and straightforward method in designing and analyzing the performance analytically by using the first law of thermodynamics. However, predicting the cycle time and the status of each process cannot be obtained.
- **Lumped-body models:** they are an integration of mass transfer correlations and the first law of thermodynamics. To raise the accuracy of the model, ordinary differential equations are used; these models allow to predict the cycle time, performance, and status during each process.
- **Geometry – dependent models:** they combined the heat and mass transfer equations with spatial parameters together.

In this PhD study, we focus on lumped–body models, which Barhami et al. have classified this model into three subgroups (quasi-steady state, dynamic modeling with perfect condenser and evaporator, fully dynamic modeling). The fully dynamic thermodynamic

cycle model is proposed because this model can predict the adsorbate uptake rate, COP, SCP, and cycle time with good accuracy despite requiring a large number of inputs. More information about the other types can be found in (Sharafian & Bahrami, 2015). The equations considered in this investigation are obtained from energy and mass balances for each component and thermodynamic relations between these components. The equation type depends on the operating cycle, whether it is cooling or heating, and depends on the linkage state between the sorption beds and the evaporator/condenser that is related to the internal pressure differences between these parts of the adsorption cooling system.

### **3.1.1. Adsorbent/adsorbate adsorption isotherms**

The equilibrium amount of adsorbate particles at specific pressure and temperature can be described by the adsorption isotherm models. The adsorption isotherm model relies on the structure of the solid adsorbent pores. The pore structure contains pore volume, pore size, and surface area. Different adsorption isotherms models can be implemented to specify the equilibrium uptake values. The most common models are the Langmuir model, Toth model, Dubinin-Astakhov model, and Freundlich model.

#### **Langmuir model:**

Langmuir theory is the first concept that was discovered in 1918. The langmuir model is the simplest formulation for a monolayer surface's physical adsorption that describes the adsorption based on the kinetic approach (Do, 1998). The rate of adsorption and desorption from the surface are equal. Several assumptions should be considered in this model as the following:

- The surface of the adsorbents is homogeneous, where the energy of adsorption is deemed to be constant.
- Each place in the adsorbent can host only one molecule of the adsorbate.
- There are no interactions between the adsorbed adsorbate molecules that are close to each other.

The Langmuir model is considered acceptable for low pressures close to a vacuum, where it has restrictions to suit the uptakes for heterogeneous adsorbents at pressures higher than 10 kPa. The following equation expresses the Langmuir model:

$$C = \frac{A.P_v}{1+A.P_v} \quad (3.1)$$

where C is the fractional surface coverage,  $P_v$  is the vapor's pressure, and A is the affinity constant, which gives as:

$$A = A_o. \exp\left(\frac{\Delta H}{R.T_s}\right) \quad (3.2)$$

where  $\Delta H$  is the adsorption heat (kJ/mol),  $T_s$  is the adsorbent temperature (K), R is the universal gas constant,  $A_o$  is the pre-exponential factor (Do, 1998).

### **Brunauer-Emmett-Teller (B-E-T) isotherm model:**

As the Langmuir isotherm model is only valid for monolayer surface adsorbents, the (B-E-T) theory was introduced to extend the previous model to multilayer adsorption. The expression of this model is given as the following (Mohammed, 2019):

$$\frac{P_v}{(P_s - P_v).W} = \frac{1}{W_m.B} + \frac{(B-1).P_v}{W_m.B.P_s} \quad (3.3)$$

where  $B = e^{\frac{\Delta H_1 - \Delta H_L}{R.T_s}}$ ,  $W_m$  is the monolayer capacity. W is the concentration of the adsorbate per unit mass of the adsorbent at specific pressure and temperature.  $\Delta H_1$  and  $\Delta H_L$  are the adsorption heat for the first and higher layers, respectively.  $P_s$  is the saturation pressure.

### **Freundlich isotherm model:**

The relationship between the pressure and the isothermal changes during the adsorption/desorption processes of the adsorbate by a unit of the adsorbent was proposed by Herbert Freundlich in 1909. However, this model is empirical, which means it is only used when the process is linear, and it is given as:

$$X = X_0 \cdot \left( \frac{P_v}{P_s} \right)^{1/n} \quad (3.4)$$

where  $X$  and  $X_0$  are the adsorbate uptake and the maximum adsorbate uptake, respectively.  $1/n$  represents the adsorbent surface heterogeneity, and its values are from 0 to 1.  $P_v$  and  $P_s$  are the vapor and saturation pressures, respectively (Mohammed, 2019).

### **Modified Freundlich isothermal model, (S-B-K) model:**

As the Freundlich isothermal model is not utilized for low and high pressures, Saha, Boelman, and Kashiwagi have introduced a modified version that gives better results corresponding to the experimental data, which is given as (Bidyut B Saha et al., 1995):

$$X = A \cdot \left( \frac{P_v}{P_s} \right)^B \quad (3.5)$$

where  $A = \sum_{i=0}^{i=3} A_i \cdot T^i$  and  $B = \sum_{i=0}^{i=3} B_i \cdot T^i$  where  $A$  and  $B$  coefficients are computed based on the testing data (Bidyut B Saha et al., 1995).

### **Dubinin-Astakhov isothermal model:**

The theory of filling the volume of adsorbent's micropores describes the adsorption equilibrium of solid adsorbents. The theory depends on the temperature stability of the distribution of filling degree ( $W/W_0$ ). Depending on the Polanyi theory that was

developed to investigate the adsorption of adsorbate molecules onto the porous solid adsorbents, the filling degree for the adsorption phenomena can be expressed as:

$$\frac{W}{W_o} = \text{Exp} \left\{ - \left[ \frac{RT}{E} \ln \left( \frac{P_s}{P} \right) \right]^n \right\} \quad (3.6)$$

where:

$$W = X \cdot v_a \text{ and } W_o = X_o \cdot v_o \quad (3.7)$$

$$v_a = v_{bo} \cdot \exp(\Omega (T - T_{bo})) \quad (3.8)$$

$$\Omega = \ln (b/v_{bo}) / (T_c - T_{bo}) \quad (3.9)$$

where  $W$  is the adsorbate concentration at a specific temperature and pressure per adsorbent mass ( $\text{m}^3/\text{kg}$ ),  $W_o$  is the maximum concentration of the adsorbate per unit of adsorbent mass ( $\text{m}^3/\text{kg}$ ),  $E$  is the characteristic energy of the working pair ( $\text{kJ}/\text{kg}$ ).  $X$  is the concentration of adsorbent bed ( $\text{kg}/\text{kg}$ ),  $X_o$  limiting of the adsorbent bed concentration ( $\text{kg}/\text{kg}$ ),  $v_a$  is the adsorbed phase-specific volume ( $\text{m}^3/\text{kg}$ ),  $v_{bo}$  is the specific volume at the temperature of boiling.  $T_c$  and  $T_{bo}$  are the critical and boiling temperatures (K), respectively, and  $b$  is the van der waals volume ( $\text{m}^3$ ) (Kılıç, 2018). Eq (3.6) represents the (D-A) isotherm model for adsorption of vapors onto non-homogeneous adsorbents with a wide pore size distribution, where it has been used in this study.

### **Toth isotherm model:**

The Toth model rectifies the incorrect behavior that the Freundlich and Langmuir models cannot describe precisely at high and low-pressure ends of the adsorbate concentration (Do, 1998). Toth introduces an equation that is relied on the multilayers state equation. It is considered the first option to obtain the isotherm correlation of many heterogeneous solid adsorbents that fitting the experimental data. The Toth model is given as (Wu et al., 2016):

$$X = \frac{b_o \cdot p_v \cdot \exp\left(\frac{\Delta H}{RT_s}\right)}{\left\{1 + \left[\frac{b_o \cdot p_v}{X_o} \exp\left(\frac{\Delta H}{RT_s}\right) t\right]\right\}^{1/t}} \quad (3.10)$$

where  $b_o$  is the equilibrium constant related to the working pair and  $t$  is a parameter related to the structure heterogeneity of the solid adsorbent, which they can be determined by the experimental data.

### 3.1.2. Adsorption kinetics

Several solid adsorbents comprise of a tiny microporous structure. As the adsorption phenomenon is an exothermic process, general variations in adsorbate particle temperatures and the surrounding bulk phase take place when the adsorption occurs. The importance of the temperature difference relies on the relative rates of both mass and heat transfer. Therefore, the better performance of heat transfer, the higher the adsorption rate for the adsorbent material (Rezk, 2012). The linear driving force model (LDF) is commonly used to describe the adsorption rate of adsorbate (refrigerant) onto the adsorbent surface. The LDF model presumes that the temperature of the adsorbent particles is uniform. The thermal conductivity of the adsorbent particles is infinity; the heat transfer effect is ignored as a result. Only the mass balance equation in the fluid stage can be used in the LDF approach resulting in more simplicity of the model to be solved, whether numerically or analytically. Thus, a lower computational time is used (Mohammed et al., 2018). The LDF model is a common approach utilized to simulate the dynamic behavior of the adsorption cooling systems and predict the performance of the chiller. The adsorption kinetics formulation (LDF) model is given as (Mohammed et al., 2018):

$$\begin{aligned} \frac{dX}{dt} &= \frac{15 \cdot D_o}{r_p^2} \exp\left(-\frac{E_a}{R \cdot T}\right) (X_{eq} - X) \\ \rightarrow X(t) / X_{eq} &= 1 - \exp\left(-\left(\frac{15 \cdot D_o}{r_p^2} \exp\left(-\frac{E_a}{R \cdot T}\right) t\right)\right) \end{aligned} \quad (3.11)$$

where  $X_{eq}$  is the balance concentration at a specified temperature and pressure,  $E_a$  is the activation energy of the working pair (kJ/kg),  $D_0$  is the pre-exponent constant ( $m^2/s$ ),  $r_p$  is the average radius of adsorbent particles (m), and  $t$  is the time (s).

### 3.1.3. Adsorption enthalpy

The adsorption enthalpy is considered variable. Indeed, it can be determined by the concentration due to a relatively weaker connection to the temperature. For the adsorption of adsorbates that operate under their thermodynamic critical states, the value of refrigerant vaporization heat is lower than its magnitude; it has a strong temperature dependence as a result (Bidyut B. Saha et al., 2007; Bidyut B. Saha et al., 2009). The variation between adsorption heat and vaporization heat is important in designing the ACC system. During the appraisal process, the isosteric heat can be approximated to the relative working pair's adsorption uptake, which mainly pursues the Dubinin's isotherms (Bidyut B. Saha et al., 2007). The gas stage of the adsorbate is not ideal. Also, the adsorption process is influenced by temperature and pressure variations. Because of that, the adsorption heat can be computed by utilizing the formulation suggested by El-Sharkawy et al. (El-Sharkawy et al., 2006) as:

$$\Delta h_{ads} = h_{fg} + (E) \left[ \ln\left(\frac{W_0}{w}\right) \right]^{1/n} + (E.T.\Omega) \left[ \ln\left(\frac{W_0}{w}\right) \right]^{(1-n)/n} \quad (3.12)$$

### 3.1.4. Thermal compressor (adsorbent bed) model

Since the thermal compressor is the vital component in the adsorption cooling system and there are lots of processes that occur to accomplish its task, there are various mathematical models that describe the processes as the following:

#### **Energy balance for the thermal compressor:**

The thermal compressor (adsorption bed) is considered the predominant of the adsorption cooling cycle that pumps the refrigerant (adsorbate) from the evaporation pressure (low

pressure) to the condenser pressure (high pressure). The adsorption cooling cycle is a heat-driven cycle. The thermal compressor operates in two modes: desorption and adsorption, as it is connected to the condenser and evaporator. To interchange between the two modes, a switching period is required to cool down the hot adsorption bed and heat up the cold bed. This period is two consecutive processes. The first one is the mass recovery process; in this process, the refrigerant (adsorbate) vapors in the high pressure and temperature bed move to the low pressure and temperature bed until the mechanical balance happens. The heat recovery process is the second process, where cold working fluid flows through the pipes in the hot adsorption bed while the heating working fluid flows through the pipes in the low-temperature bed. Figure 3.1 shows a simplified schematic design of a single thermal compressor. Before applying the lumped simulation model, there is a benefit of mentioning the main assumptions that have utilized as the following:

- The thermal compressor materials (bed metal), the adsorbent material, and the adsorbate are momentarily at the same temperature.
- The mass and heat do not transfer to the surroundings; in other words, the thermal compressor is totally isolated (there is no mass and heat losses).

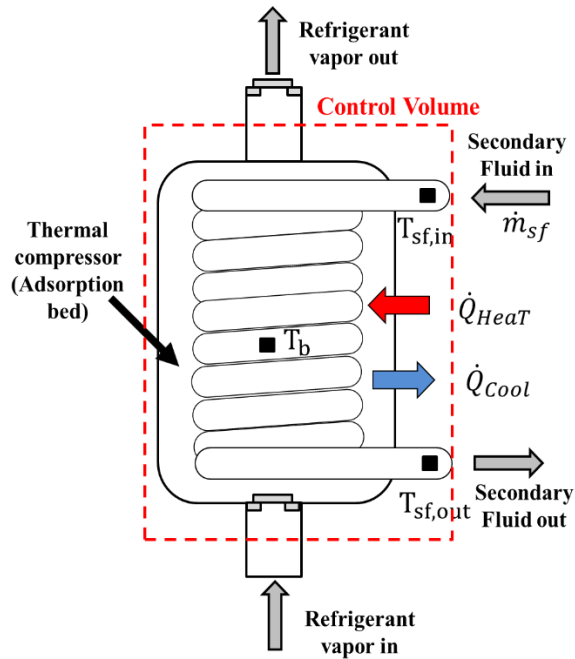


**Figure 3. 1.** Schematic design of the thermal compressor basic components.

Thus, the energy balance equations for the thermal compressor (adsorption bed) consist of the sensible heat of the bed metallic parts, the adsorbate (refrigerant), and the adsorbent materials as the following (Kılıç, 2018):

**For the pre-cooling and adsorption process:**

$$\begin{aligned} & [m_{bm}c_{p,bm} + m_{ads}c_{p,ads}] \frac{dT_b}{dt} + (m_{ads}X_{ad,f}) \frac{dh_{ad,f}}{dt} + (m_{b,v}) \frac{dh_{bed,v}}{dt} = \\ m_{ads} \frac{dX_{ad,f}}{dt} (\Delta h_{ads} + \gamma h_{eva,out} - h_{ad,f}) + \frac{dm_{bed,v}}{dt} (\gamma h_{b,in} - h_{b,v}) - \dot{Q}_{cool} \end{aligned} \quad (3.13)$$

where the value  $\gamma$  is equal to 0 in the pre-cooling process and equal to 1 in the adsorption process.

The first term on the left hand side of thermal compressor energy balance in Eq (3.13) represents the rate of heat needed to cool the thermal compressor metal material and the adsorbent material packed in the adsorption bed. The second and third terms exemplify the rate of heat required to cool the adsorbed refrigerant within the adsorbent pores. On the contrary, the first term on the right hand side symbolizes the amount of heat generated during the adsorption process. The second term represents the rate of heat received with the adsorption/evaporator or mass recovery processes by the adsorbate (refrigerant) vapors from the evaporator. The third term refers to the amount of heat added to the secondary working fluid during the adsorption process.

**For the pre-heating and desorption process:**

$$\begin{aligned} & [m_{bm}c_{p,bm} + m_{ads}c_{p,ads}] \frac{dT_b}{dt} + (m_{ads}X_{ad,f}) \frac{dh_{ad,f}}{dt} + (m_{b,v}) \frac{dh_{b,v}}{dt} = \\ m_{ads} \frac{dX_{ad,f}}{dt} (\Delta h_{ads} + \gamma h_{con,in} - h_{ad,f}) + \frac{dm_{bed,v}}{dt} (\gamma h_{b,out} - h_{b,v}) + \dot{Q}_{heat} \end{aligned} \quad (3.14)$$

where the value  $\gamma$  is equal to 0 in the pre-heating process and equal to 1 in the desorption process.

The first term on the left hand side of thermal compressor energy balance in Eq (3.14) exemplifies the rate of heat required to heat the thermal compressor (metal material and the adsorbent material packed in the adsorption bed). The second and third terms in the left represent the heat transfer rate required to heat the adsorbed refrigerant within the adsorbent pores. On the contrary, the first term in the right hand represents the amount of heat extracted during the desorption process. The second term symbolizes the rate of heat released during the desorption/condenser or mass recovery processes by the adsorbate (refrigerant) vapors moved to the condenser. The third term represents the amount of heat removed from the secondary working fluid during the desorption process.

The amount of heat added or removed from the second working fluid, taking into account the inlet and outlet temperatures, are given as (Sharafian & Bahrami, 2015):

$$\dot{Q}_{heat} = \dot{m}_{sf,heat} \cdot C_{P_{sf}} \cdot (T_{sf,in} - T_{sf,out}) = U_{b,heat} \cdot A_b \cdot \Delta T_{LM b,heat} \quad (3.15)$$

$$\dot{Q}_{cool} = \dot{m}_{sf,cool} \cdot C_{P_{sf}} \cdot (T_{sf,out} - T_{sf,in}) = U_{b,cool} \cdot A_b \cdot \Delta T_{LM b,cool} \quad (3.16)$$

where  $T_{sf,in}$  and  $T_{sf,out}$  are the inlet and outlet temperature of the second fluid that comes from outsource heat into the thermal compressor.  $\dot{m}_{sf,heat}$  and  $\dot{m}_{sf,cool}$  are the mass flow for the heating and cooling second fluid into the thermal compressor, respectively.  $U_{b,heat}$  and  $U_{b,cool}$  are the overall heat transfer coefficient during the desorption and adsorption processes.  $A_b$  is the total heat transfer area of the thermal compressor (adsorption bed).  $\Delta T_{LM b}$  is the log mean temperature difference between the adsorption bed and the second fluid in the thermal compressor that its equation is given as the following, taking into account the process type, whether for heating or cooling the thermal compressor:

$$\Delta T_{LM b} = \frac{T_{sf,in} - T_{sf,out}}{\ln\left(\frac{T_{sf,in} - T_b}{T_{sf,out} - T_b}\right)} \quad (3.17)$$

The overall heat transfer coefficient in the thermal compressor is given as:

$$U_b \cdot A_b = \frac{1}{R_{sf} + R_{bm} + R_{ads}} \quad (3.18)$$

where  $R_{sf}$  is the convection thermal resistance of the second working fluid, taking into account the type of flow regime (laminar or turbulence),  $R_{bm}$  is the conductive thermal resistance of the bed material, including the fins,  $R_{ads}$  represents the heat resistance inside the adsorbent in the radial direction and axial direction. It also includes the contact heat resistance between the adsorbent and the surface of the fin and tubes.  $U_b$ .  $A_b$  term depends on the type and shape of the thermal compressor considered in the adsorption cooling system.

### **Mass balance for the thermal compressor:**

The refrigerant vapors flow between the elements depends on the pressure variation between them. It is important to mention that the assumptions considered in calculating the mass flow through the components, especially in the thermal compressor, are as the following:

- The vapor valves react instantaneously according to the pressure difference, where they are assumed to be fully closed or fully opened.
- The vapor valve between the thermal compressor and the evaporator opens when the pressure in the evaporator is higher than that in the thermal compressor. Otherwise, it stays closed.
- The vapor valve between the thermal compressor and the condenser opens when the pressure in the condenser is lower than that in the thermal compressor. Otherwise, it stays closed.
- The amount of refrigerant (adsorbate) in the sorption bed (adsorbent) could be obtained at any instant from the following equation.

$$m_{b,f} = m_{ads}X_{ad,f} + m_{bed,v} \quad (3.19)$$

The mass transfer rate from the ACC evaporator to the sorption bed (adsorbent) during the adsorption process can be expressed as the following equations.

$$\frac{dm_{b,f}}{dt} = m_{ads} \frac{dX_{ad,f}}{dt} + \frac{dm_{b,v}}{dt} \quad (3.20)$$

$$\frac{dm_{eva,out}}{dt} = \frac{dm_{b,in}}{dt} = \frac{dm_{b,f}}{dt} \quad (3.21)$$

Likewise, the mass transfer rate from the sorption bed (adsorbent) to the condenser during the desorption process can be expressed as the following equations.

$$\frac{dm_{con,in}}{dt} = \frac{dm_{b,out}}{dt} = \frac{dm_{b,f}}{dt} \quad (3.22)$$

The cycling mass of the refrigerant in the adsorption chiller can be obtained from Eq. (3.23) or Eq.(3.24). The non-cycling mass of the refrigerant in the ACC unit can be acquired from Eq. (3.25).

$$M_{cyc,ACC} = \int_{des} \frac{dm_{con,in}}{dt} dt = \int_{ads} \frac{dm_{eva,out}}{dt} dt \quad (3.23)$$

$$M_{cyc,ACC} = m_{ads}(X_{max} - X_{min}) + V_{b,void}(\rho_{v,max} - \rho_{v,min}) \quad (3.24)$$

$$M_{ncyc,ACC} = m_{ads}X_{min} + V_{b,void}\rho_v(P_{con}, T_{max}) \quad (3.25)$$

where  $V_{b,void}$  represents the void volume occupied by the refrigerant (adsorbate) in the vapor stage in the adsorbent bed.  $\rho_{v,max}$  refers to the maximum vapor density at the maximum bed temperature  $T_{max}$  and the condenser pressure  $P_{con}$ .  $\rho_{v,min}$  represents the minimum vapor density at the minimum bed temperature  $T_{min}$  and the evaporator pressure  $P_{eva}$ . Finally, the total adsorbate mass employed in the adsorption chiller can be gained from Eq.(3.26).

$$M_{t,f,ACC} = M_{cyc,ACC} + M_{ncyc,ACC} \quad (3.26)$$

### Pressure in the thermal compressor:

The pressure in the thermal compressor (adsorption bed) relies on the ideal gas equation of state in addition to the mass conversation. The state equation for the refrigerant vapor inside the thermal compressor is given as the following:

$$P_b = \frac{m_{v,b} \cdot R \cdot T_b}{V_{v,b}} \rightarrow dP_b = \frac{R}{V_{v,b}} \cdot d(m_{v,b} \cdot T_b) \quad (3.27)$$

By taking into account the pressure variation during a unit of time, the previous pressure differential equation in the adsorption bed becomes:

$$\begin{aligned} \frac{dP_b}{dt} &= \frac{R}{V_{v,b}} \cdot \frac{d}{dt} (m_{v,b} \cdot T_b) \leftrightarrow \frac{dP_b}{dt} = \frac{R}{V_{v,b}} \cdot (m_{v,b} \cdot \frac{dT_b}{dt} + T_b \frac{dm_{v,b}}{dt}) \\ &\leftrightarrow \frac{dP_b}{dt} = \frac{R}{V_{v,b}} \cdot (m_{v,b} \cdot \frac{T_b}{T_b} \frac{dT_b}{dt} + T_b \cdot \frac{m_{v,b}}{m_{v,b}} \frac{dm_{v,b}}{dt}) \\ &\leftrightarrow \frac{dP_b}{dt} = (P_b \cdot \frac{1}{T_b} \frac{dT_b}{dt} + P_b \cdot \frac{1}{m_{v,b}} \frac{dm_{v,b}}{dt}) \\ &\leftrightarrow \frac{dP_b}{dt} = P_b \cdot (\frac{1}{T_b} \frac{dT_b}{dt} + \frac{1}{m_{v,b}} \frac{dm_{v,b}}{dt}) \end{aligned} \quad (3.28)$$

### 3.1.5. ACC evaporator model

Before determining the analysis model of the ACC evaporator, some assumptions should be taken into account to simplify the mathematical model as the following:

- The ACC refrigerant vapors are assumed to be ideal gases.
- The pressure value relies on the amounts of vapors at the top of the evaporator.
- Refrigerant parameters are considered according to saturation conditions.
- The evaporator temperature is corresponding to the instantaneous pressure in the evaporator. It is noteworthy to mention that the amount of refrigerant in the evaporator is higher than that in the condenser as there is a time delay between the adsorption and desorption process in the thermal compressor (adsorption bed).

- The whole refrigerant flow rate that comes from the condenser through the expansion valve is instantly evaporated.

The energy balance equation for the refrigerant is given as:

$$Q_{eva,ACC} = \oint_0^{t_{cycle}} \frac{dm_{eva,out}}{dt} \cdot \Delta h_{fg}(T_{eva}) dt \quad (3.29)$$

### 3.1.6. ACC condenser model

Before determining the analysis model of the ACC condenser, some assumptions should be considered to simplify the mathematical model as the following:

- The ACC refrigerant vapors are assumed to be ideal gases.
- The pressure value relies on the amounts of vapors at the top of the condenser.
- Refrigerant parameters are considered according to saturation conditions.
- The temperature of the refrigerant in the condenser is the same as the condensation temperature and corresponds to the instantaneous pressure in the condenser.

The energy balance equation for the refrigerant is given as:

$$Q_{con,ACC} = \oint_0^{t_{cycle}} \frac{dm_{con,in}}{dt} \cdot [\Delta h_{fg}(T_{con}) + C_{Pv}(T_{con,in} - T_{con})] dt \quad (3.30)$$

### 3.1.7. ACC System performance indicators

ACC system performance indicators can be determined by the coefficient of performance ( $COP_{ACC}$ ) and the specific cooling power (SCP) in kW/kg<sub>ads</sub>. These two performance indicators are important values for the technical specifications of the adsorption chiller.  $COP_{ACC}$  and SCP can be computed by Eq. (3.31) and Eq. (3.32), respectively.

$$COP_{ACC} = \frac{Q_{eva,ACC}}{Q_{heat}} \quad (3.31)$$

$$SCP = \frac{Q_{eva,ACC}}{t_{cycle} \cdot m_{ads}} \quad (3.32)$$

The heat load  $Q_{heat}$  and the cooling capacity  $Q_{eva,ACC}$  of the ACC system in a cycle can be computed by Eq.(3.14) and Eq.(3.29), respectively.

### 3.2. Vapor compression Cooling Cycle (VCC) modeling

As mentioned in the previous section, the basic vapor compression (mechanical compression) cooling cycle consists of four primary elements: the evaporator, the mechanical compressor, the condenser, and the expansion valve. The vapor compression cooling cycle's operating principle is to absorb an amount of heat from the place to be refrigerated or conditioned through the evaporator and release that amount of heat through the condenser after adding electrical energy through the mechanical compressor.

In this research, the thermodynamic model of the VCC system depends on a basic cycle. The main components of the cycle are formerly shown (Figure 2.11 b). However, before the modeling, many assumptions should be considered during the computations as the following:

- The VCC system runs under steady-state conditions.
- The differences in kinetic and potential energy are neglected.
- The expansion valve works under the isenthalpic process.
- There are neither pressure drops nor heat losses in the VCC system.
- Mass flow within the VCC unit is constant.

#### 3.2.1. VCC evaporator model

VCC evaporator is the component that meets the user requests in terms of cooling effects changes. It absorbs the heat removed from the place to be conditioned or materials to be refrigerated. During the heat-absorbing process, the refrigerant phase changes from the liquid-vapor mixture to saturated vapor at the end of the evaporation process. The

thermodynamic model of the VCC evaporator depends on some assumptions as the following (Figure 2.12 a):

- The refrigerant temperature outlet from the VCC evaporator is as same as the evaporation temperature  $T_1 = T_{eva}$ .
- The pressure in the VCC evaporator is considered constant according to the evaporation temperature  $P_1 = f(T_1 = T_{eva}, x = 1)$ .
- Both the enthalpy and entropy at the evaporator outlet values are taken in vapor saturation state as  $h_1 = f(T_1 = T_{eva}, x = 1)$  and  $S_1 = f(T_1 = T_{eva}, x = 1)$ , respectively.

The amount of heat absorbed from the place to be cooled can be computed as:

$$\dot{Q}_{eva,VCC} = \dot{m} (h_1 - h_5) \quad (3.33)$$

### 3.2.2. Vapor mechanical compressor model

The mechanical compressor in the VCC chiller is the component that drives the refrigerant inside the cooling cycle by converting the electrical energy into mechanical energy. The thermodynamic model of the mechanical compressor depends on some assumptions as the following (Figure 2.12 a):

- The refrigerant leaves the mechanical compressor at the VCC condenser pressure  $P_2 = P_{con}$ .
- The process in the mechanical compressor is not ideal. There are some losses, such as (thermal and frictional pressure losses). Thus, the isentropic efficiency is considered during the calculations as  $\eta_i = 0.85$ . Hence, the enthalpy at the compressor outlet is calculated as  $h_2 = (h_{2s} - h_1)/\eta_i + h_1$ . Where  $h_{2s}$  is the enthalpy of the refrigerant at the compressor outlet if the process is isentropic ( $S_2 = S_1$ )
- The mechanical energy in the compressor is lower than the electrical energy provided by the electrical efficiency  $\eta_{elec} = 0.90$ .

The amount of electrical power input to the mechanical compressor can be computed as:

$$\dot{W}_{elec} = \frac{\dot{m} (h_2 - h_1)}{\eta_{elec}} \quad (3.34)$$

### 3.2.3. VCC condenser model

VCC condenser is the component that releases the amount of heat absorbed by the VCC evaporator  $\dot{Q}_{eva,VCC}$  and the energy added to the refrigerant through the mechanical compressor to the surroundings, either to the ambient or other equipment similar to our case study. During the heat rejection, the refrigerant phase changes from super-heated steam into the subcooled liquid phase at the end of the condensation process. The thermodynamic model of the VCC condenser relies on some assumptions as the following (Figure 2.12 a):

- The refrigerant temperature at the outlet of the VCC condenser is the same as the condensation temperature  $T_3 = f(P_3, x=0)$ .
- The pressure in the VCC condenser is considered constant according to the condenser temperature  $P_2 = P_3 = P_4$
- Both the enthalpy and entropy at the condenser outlet values are taken in liquid saturation state as  $h_3 = f(P_3, x=0)$  and  $S_3 = f(P_3, x=0)$ , respectively.

The amount of heat rejected from the VCC condenser can be computed as:

$$\dot{Q}_{con} = \dot{m} (h_2 - h_3) \quad (3.35)$$

### 3.2.4. VCC system performance indicator

It is widely known that the refrigerator's efficiency is specified in terms of COP. The aim of the vapor mechanical refrigeration system, as we know, is to absorb some heat  $\dot{Q}_{eva}$  from the conditioned place by consuming electrical power  $\dot{W}_{ele}$ . The COP of VCC system can be expressed by:

$$COP_{VCC} = \dot{Q}_{eva,VCC} / \dot{W}_{elec} \quad (3.36)$$

### 3.3. (VCC-ACC) combined cooling system mathematical model

In this system, the heat absorbed in the ACC evaporator from the VCC condenser (series configuration situation) should be considered carefully. The heat amount that is absorbed in the ACC evaporator must be the same as that rejected from the VCC condenser. Thus, while designing the (ACC-VCC) combined cooling system, energy equilibrium must be satisfied as:

$$\dot{Q}_{eva,ACC} = \dot{Q}_{con,VCC} \quad (3.37)$$

To estimate the combined cooling system performance, it is acceptable to apply the thermal coefficient of performance  $COP_H$  of the whole system, which is the ratio between the cooling capacity provided by the VCC unit and the utilized total energy rate to the hybrid system:

$$COP_H = \dot{Q}_{eva,VCC} / (\dot{Q}_{heat,ACC} + \dot{W}_{elec}) \quad (3.38)$$

The denominator includes the combination of the VCC power and the rate of ACC heat input quantities, which gives an incorrect measure. For that reason, it is acceptable to utilize the exergy concept to overcome this issue by changing the heat quantities in the VCC evaporator and ACC heat input to their exergy components. The surrounding temperature is the reference temperature used in the exergy equation. Thus, the (VCC-ACC) combined cooling system performance can be calculated as:

$$COP_{EXE,H} = [\dot{Q}_{eva,VCC} (1 - \frac{T_{eva,VCC}}{T_{amb}})] / [\dot{W}_{elec} + \dot{Q}_{heat,ACC} (1 - \frac{T_{amb}}{T_{h,ACC}})] \quad (3.39)$$

The cooling load in the parallel linkage (Figure 2.12 b) is sectioned according to the working conditions in every chiller. Some hypotheses have considered computing the

cooling load as the following:  $T_I = T_{SF}$ ,  $T_{II} = T_{eva,ACC} + 2^\circ\text{C}$ ,  $T_{III} = T_{II}$ ,  $T_{IV} = T_I + 3^\circ\text{C}$ . Hence, the total cooling load in the parallel linkage can be calculated by:

$$\dot{Q}_T = \dot{Q}_{eva,ACC} + \dot{Q}_{eva,VCC} = \dot{m}_{SF} \cdot CP_{SF} (T_{II} - T_I) + \dot{m}_{SF} \cdot CP_{SF} (T_{IV} - T_{III}) \quad (3.40)$$

The second fluid utilized in the tubes that link both evaporators is water.

The performance of the parallel configuration can be calculated using the following equation (Figure 2.12 b):

$$COP_{EXE,H} = \frac{\left[ \dot{Q}_{eva,VCC} \left( 1 - \frac{T_{eva,VCC}}{T_{amb}} \right) + \dot{Q}_{eva,ACC} \left( 1 - \frac{T_{eva,ACC}}{T_{amb}} \right) \right]}{\left[ \dot{W}_{elec} + \dot{Q}_{heat,ACC} \left( 1 - \frac{T_{amb}}{T_{h,ACC}} \right) \right]} \quad (3.41)$$

### 3.4. Energy savings

Here in this thesis, the energy-saving amount by applying our (VCC-ACC) combined cooling system against the conventional chiller under the same boundary working conditions is also computed. Furthermore, the increase ratio (IR) in the performance of the traditional cooling system for both the integrated and non-integrated systems is calculated. The temperature at the VCC condenser for the non-integrated system is assumed to be the same situation as the ACC-VCC combined cooling system. The electric energy saving ratio (ES) and the  $COP_{VCC}$  increase ratio (IR) can be calculated as:

$$ES = \left[ \frac{(\dot{W}_{elec,VCC} - \dot{W}_{elec,H})}{\dot{W}_{elec,VCC}} \right] \times 100 \quad (3.42)$$

$$IR = \left[ \frac{[COP_{VCC,H} - COP_{VCC}]}{COP_{VCC}} \right] \times 100 \quad (3.43)$$

### 3.5. Calculations procedure of the mathematical model

The ACC mathematical codes are written in the RAD studio ten environment utilizing Delphi 10 program language. The thermo-physical fluid properties considered in the mathematical model are used as real fluid properties by utilizing the CoolProp library written in the C++ programming platform, which can compute properties for more than 100 various fluids with pretty good accuracy. More details about the CoolProp library

might be found in (Bell et al., 2014). Besides that, the amount of adsorption heat is computed as a function of temperature, concentration, and pressure. The above-mentioned equations are solved by an iterative method. In contrast, the VCC mathematical codes are written in the engineering equation solver (EES). Figure 3.2 clarifies the flow chart of the mathematical calculations made in the (VCC-ACC) combined cooling system.

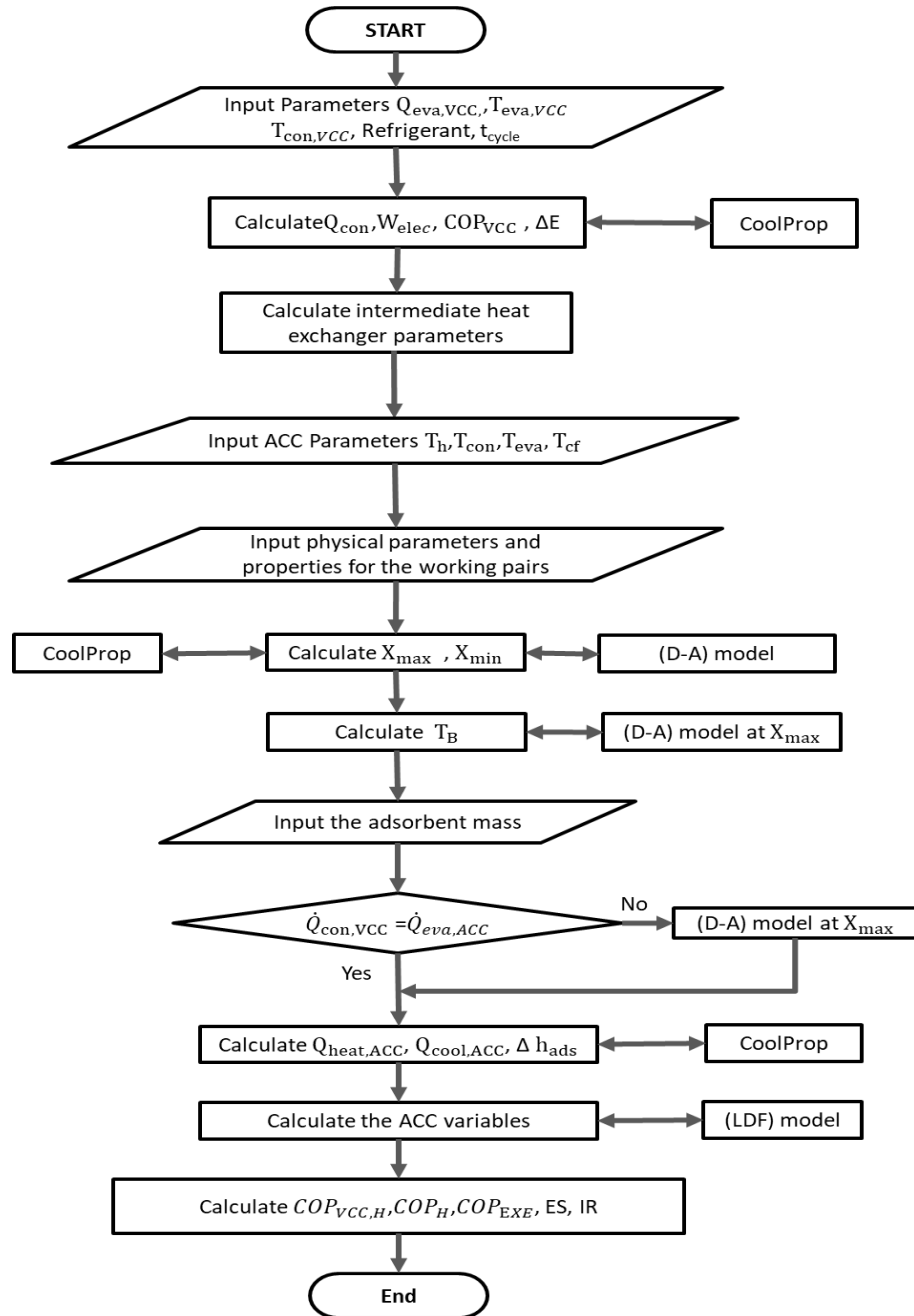


**Figure 3. 2.** Flow chart of calculating the mathematical model (Kilic & Anjrini, 2020)

### 3.6. Validation of the mathematical model

Several papers have already been published dealing with the adsorption refrigeration systems for the usage of water-silica gel as a working pair. Di et al. (2007) and Vodianitskaia et al. (2017) executed an experimental investigation by the usage of the silica gel/water pair. The published results are utilized to prove the validity of the current mathematical model for adsorption chiller. The calculations are performed according to the measurable factors and operating conditions specified in these reference papers.

Di et al. (2007) stated that the thermal capacity of the adsorption cooling unit materials remarkably affects the coefficient of performance. Therefore, they proposed a thermal capacity ratio as:

$$R_m = (mc_p)_{bm} / (mc_p)_{ads} \quad (3.44)$$

When  $R_m$  increases, more cooling and heating are needed for the bed, including the adsorbent and the metal materials, which leads to lower COP values. This ratio is considered as ( $R_m = 3$ ) as in their study. Table 3.1 states the results convergence between the current results and the measurements of (Di et al., 2007) for various heating temperatures as 65, 75, and 85°C at  $T_{cool, in} = 30^\circ\text{C}$ ,  $T_{chill, in} = 20^\circ\text{C}$ . It is discernible that the estimated coefficient of performance and specific cooling power values have good agreement with the experiential results of (Di et al., 2007). As the inlet temperature rises from 65 to 85°C, there is a slight rise in the coefficient of performance values. In contrast, specific cooling power and  $\dot{Q}_{eva,ACC}$  increase clearly with increasing this fluid inlet temperature.

**Table 3. 1.** Comparisons of the present mathematical model results with the experimental data (Di et al., 2007) and the deviation ratio

$T_h$	$\dot{Q}_{eva,ACC}$ (kW)			SCP (W/kg)			COP		
	Present	Exp	De <sup>1</sup> (%)	present	Exp	De <sup>2</sup> (%)	present	Exp	De <sup>3</sup> (%)
65	5.9	6.0	1.7	64.6	63.9	1.1	0.39	0.37	5.4
75	7.9	7.5	5.3	79.9	80.2	0.4	0.40	0.37	8.1
85	10.1	9.4	7.4	100.4	99.8	0.6	0.42	0.43	2.3

$$De^1 = \frac{|\dot{Q}_{eva,ACC,exp} - \dot{Q}_{eva,ACC,pre}|}{\dot{Q}_{eva,ACC,exp}}, De^2 = \frac{|SCP_{exp} - SCP_{pre}|}{SCP_{exp}}, De^3 = \frac{|COP_{exp} - COP_{pre}|}{COP_{exp}}$$

Vodianitskaia et al. (2017) recently conducted an experimental investigation on the adsorption cooling system using silica gel/water pair as a working pair. In their study, pressure, adsorbate flow, and temperature measurements through the thermodynamic cycle were implemented for two different choices of adsorbent granular sizes to estimate the resulting performance and dynamics. The measurable factors and the working conditions explained in their research are considered. According to their study, 2.1 kg of adsorbent granular beads with 2.0 mm as the diameter is considered in this investigation. The total cycle time is considered as 80 minutes. Table 3.2 reports the comparative analysis between the currently estimated results and the experimental data of (Vodianitskaia et al., 2017) for the various inlet hot fluid temperatures from 65 to 95°C at  $T_{cool} = 30^\circ\text{C}$ ,  $T_{eva} = 15^\circ\text{C}$ . It is noticeable that the estimated coefficient of performance and specific cooling power values also have a good agreement with the experimental results considered. When the temperature rises, there is a tenuous increase in the coefficient of performance values. In contrast, the SCP value increases sharply with increasing the heating temperature. The largest deviations are 6.9% and 3.8% for SCP and COP, respectively.

**Table 3. 2.** Comparisons of the present mathematical model findings with the experimental data (Vodianitskaia et al., 2017)

T <sub>h</sub> (°C)	SCP (W/kg)			COP		
	Present	Exp	De <sup>2</sup> %	Present	Exp	De <sup>3</sup> %
65	43	40	7.5	0.54	0.52	3.8
70	52	50	4.0	0.55	0.53	3.8
75	62	60	3.3	0.55	0.53	3.8
80	69	69	0.0	0.55	0.53	3.8
85	74	74	0.0	0.54	0.52	3.8
90	79	79	0.0	0.53	0.52	1.9
95	81	84	3.6	0.52	0.51	1.9

$$De^2 = \frac{|SCP_{exp} - SCP_{pre}|}{SCP_{exp}}; De^3 = \frac{|COP_{exp} - COP_{pre}|}{COP_{exp}}$$

In the present literature, a few papers have been published on the (VCC- ACC) combined cooling system. Vasta et al. (2018) carried out an experimental investigation of thermal-compression cascade cooling cycles using silica gel-water by changing the heat source and the ambient temperatures. A traditional chiller using R410A working fluid was utilized in their testing system. In their experimental study, the evaporation temperature and cooling load in the evaporator of the vapor compression chiller were fixed at 7°C and 10 kW, respectively. Besides that, they used an electric chiller to compensate for the lower capacity of the adsorption chiller. The middle heat exchanger consists of the VCC condenser and the ACC evaporator. Hence, the rejected heat from the VCC working fluid and the evaporation heat of the ACC must be equal. To fulfill this condition and execute the comparative analysis with the experimental investigation, it is presumed that the working conditions were varied with the surrounding temperature, which is similar to the temperature of cooling fluid utilized in cooling the adsorbent beds and ACC condenser. Figure 3.3 illustrates the results between the current computations and the testing data of (Vasta et al., 2018) for various cooling temperatures. The same working conditions and parameters specified in the testing investigations are employed in the existing calculations. Some thermodynamical and physical parameters have been used from other

studies (Kılıç, 2018; Askalany et al., 2013) to notice the performance behavior. Table 3.3 clarifies the operating conditions and settings utilized in the validation of the mathematical model with the paper of (Vasta et al., 2018).

**Table 3. 3.** Parameters and working states utilized in the validation

Condensing temperature	$T_{\text{cond,VCC}} = T_{\text{cf}} + 15 \text{ [}^\circ\text{C]}$
Evaporation temperature	$T_{\text{eva,VCC}} = 7 \text{ [}^\circ\text{C]}$
Heating temperature	$T_{\text{h}} = 95 \text{ [}^\circ\text{C]}$
Refrigerant in the VCC chiller	R410A
Cooling fluid temperature	$T_{\text{cf}} = 25 \text{ to } 40 \text{ [}^\circ\text{C]}$
ACC Condensing temperature	$T_{\text{con,ACC}} = 45 \text{ [}^\circ\text{C]}$
VCC Cooling heat capacity	$\dot{Q}_{\text{eva,VCC}} = 10 \text{ [kW]}$
Adsorbent mass in a bed	$m_{\text{ads}} = 16 \text{ [kg]}$
Thermal capacity ratio	$R_{\text{m}} = 1.5$
The highest temperature in the adsorbent bed	$T_{\text{D}} = T_{\text{h}} - 5^\circ\text{C}$
The lowest temperature in the adsorbent bed	$T_{\text{A}} = T_{\text{cf}} + 2^\circ\text{C}$

Figure 3.3 states the comparisons between the experimental result of (Vasta et al., 2018) and the current thesis according to various cooling fluid temperatures. It is obvious that both  $\text{COP}_{\text{VCC}}$  and  $\text{COP}_{\text{VCC,H}}$  values reduce as the cooling fluid temperature increases. Meantime, the coefficient of performance of the hybrid cooling system is always better than the vapor compression chiller alone. It can be noticed that the estimated coefficient of performance values of the (ACC-VCC) hybrid system are in good agreement with the testing results considered (Vasta et al., 2018). Additionally, COP values for vapor compression chiller are also in excellent agreement with the computed data when the cooling fluid temperature is lower than  $33^\circ\text{C}$ . It is also noticeable that there is an increasing deviation between the  $\text{COP}_{\text{VCC}}$  values with increasing the cooling fluid temperature. However, the variations are within the range of testing uncertainties. Thus, the agreement of the results can be acceptable.

To sum it up, the current model is validated appropriately. The present simulation results are reliable and robust. Therefore, the mathematical model can be utilized in the following studies with confidence.

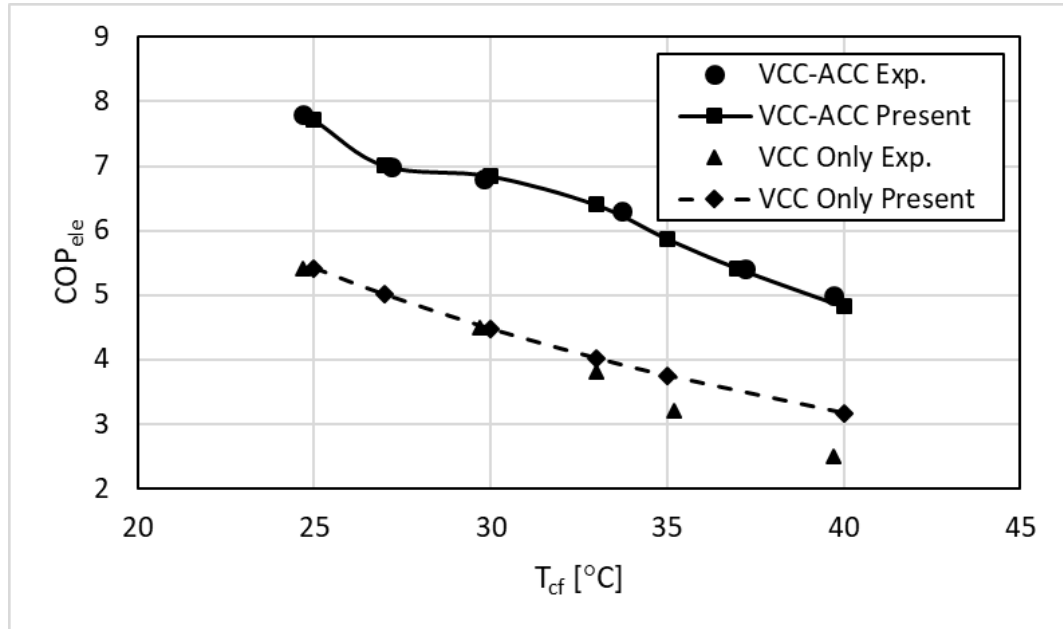


**Figure 3. 3.** Comparisons of  $COP_{VCC,H}$  and  $COP_{VCC}$  for different ambient air (cooling fluid) temperatures (Kilic & Anjrini, 2020).

### 3.7. Evaluation of different working fluids (refrigerants) in the VCC

Choosing the correct refrigerant to apply in the VCC chiller is considered an important element in noticing the system performance and electric energy consumption. Besides that, the ecological impact of the working fluid should also be taken into account. There are several working fluids in the market that act differently in the cooling system. However, a suitable refrigerant is the one that ensures the best system performance and less or zero ecological impact. The different kinds of working fluids can be grouped into generations as well as chemical groups. The mutual factors that could be considered are toxicity, flammability, ODP, and GWP. More details about the kinds of working fluids and their classifications can be found in the references (Freni et al., 2016; Bolaji & Huan, 2013; Younes et al., 2017).

In the current work, we have used different working fluids in the VCC chiller. Table 3.4 states the characteristics of the five different working fluids considered, which are namely R152A (difluoroethane), R410A (pentafluoroethane), R1234yf (tetrafluoropropene), R32 (difluoromethane), and R1270 (propylene) with the same working conditions in vapor compression chiller (Kilic & Anjrini, 2020). It is discernible that all the working fluids have minimal potential for global warming and zero ODP other than the refrigerant R410A. The working fluids considered are chosen to be used in refrigeration and air conditioning systems.

**Table 3. 4.** Properties of refrigerants used in the VCC unit (Kilic & Anjrini, 2020)

Refrigerant/working fluid	R152A	R1270	R410A	R32	R1234yf
Type	HFC	Natural	HFC	HFC	HFO
Critical temperature [°C]	113.3	92.4	71.3	78.1	94.7
Boiling temperature [°C]	-24.1	-47.7	-51.5	-51.7	-29.5
Molecular mass [kg/kmol]	66	42.1	72.6	52	114
Specific gas constant, [kJ/kg.K]	0.1259	0.1976	0.1145	0.1598	0.07291
Vaporization enthalpy at 0°C [kJ/kg]	306.6	377.8	221.4	315.3	163.3
Critical pressure, [kPa]	4520	4665	4901	5784	3382
GWP	138	2	2088	677	4
ODP	0	0	0	0	0
Flammability	Low	Yes	No	Low	High
Toxicity	No	No	No	Low	No

### 3.8. Evaluation of the working pair in the ACC chiller

Choosing the right working pair in the adsorption chiller also plays an important factor in determining the adsorption cooling system performance and the (VCC-ACC) combined cooling system. Plenty of studies and researches have been published using different types of working pairs in the ACC system. However, it is noteworthy to indicate that the

suitable working pair is the one that gratifies the essential requirement that varies according to the application. Here in this work, water has been chosen as an adsorbate, whereas silica gel is considered as the main component to be utilized as an adsorbent. Table 3.5 and Table 3.6 state the essential parameters and properties for the adsorbate and adsorbents considered in this PhD dissertation (Gong et al., 2011; Mohammed et al., 2018; Kilic & Anjrini, 2020).

**Table 3. 5.** Parameters and properties of the adsorbate used in this investigation (Kilic & Anjrini, 2020)

Parameter	Water
Boiling temperature, $T_{bo}$ , [K]	373.15
Critical temperature, $T_c$ , [K]	347.25
Specific gas constant, $R$ , [kJ/kg.K]	0.4615
Critical pressure, $P_c$ , [kPa]	22064
Critical density, $p_c$ , [kg/m <sup>3</sup> ]	322
The van der waals volume, $b$ , [m <sup>3</sup> ]	0.001692
Saturated liquid specific volume at boiling temperature, $v_b$ , [m <sup>3</sup> / kg]	0.001043
Saturated liquid specific volume at $T = 273.15$ K, $v_o$ , [m <sup>3</sup> / kg]	0.000875
$\Omega$	0.001764

**Table 3. 6.** Parameters utilized in the current research for the four types of adsorbent (Gong et al., 2011; Mohammed et al., 2018; Kilic & Anjrini, 2020)

Property	RD Silica gel	RD Silica gel 2060	Silica gel- LiCl	Silica gel- CaCl <sub>2</sub>
Chemical formula	SiO <sub>2</sub> .n(H <sub>2</sub> O)	SiO <sub>2</sub> .n(H <sub>2</sub> O)	SiO <sub>2</sub> .n(H <sub>2</sub> O) + LiCl	SiO <sub>2</sub> .n(H <sub>2</sub> O) + CaCl <sub>2</sub>
D (mm)	0.8-0.89	0.5-0.59	0.5-1	0.25-0.5
A (m <sup>2</sup> /g)	827.5	686.3	300	350
V <sub>Po</sub> (cc/g)	0.462	0.335	1	1
D <sub>Po</sub> (nm)	3.24	3.19	15	15
Inorganic salt content %	0	0	20	33.7
C <sub>p</sub> (kJ/kg.K)	0.92	0.92	0.85	0.85
E (kJ/kg)	192.29	242.79	270.4	
n	1.35	1.35	1.604	1.1
D <sub>O</sub> (m <sup>2</sup> /s)	2.8 E <sup>-4</sup>	2.8 E <sup>-4</sup>	2.54 E <sup>-4</sup>	2.54 E <sup>-4</sup>
E <sub>a</sub> (kJ/kg)	2247.5	2247.5	2020	2330.7
r <sub>p</sub> (m)	4E <sup>-4</sup>	2.9 E <sup>-4</sup>	4.75 E <sup>-4</sup>	1.74 E <sup>-4</sup>
X <sub>o</sub> (kg <sub>ref</sub> /kg <sub>ads</sub> )	0.48	0.38	0.489	0.8

## **4. RESULTS and DISCUSSION**

In this PhD dissertation, we investigated and discussed the (ACC-VCC) combined cooling system mainly in terms of system performance indicators and the energy saving amount at three different cases as the following:

### **4.1. Comparative performance analysis of a combined cooling system with mechanical and adsorption cycles**

The current study investigates the energy-saving and performance of the ACC-VCC combined system instead of the vapor mechanical chiller alone. The analyzing study is executed by employing a silica gel /water pair in the adsorption chiller and several refrigerants in the vapor compression chiller: (R410A, R1234yf, R152a, R32, and R1270). The investigation is considering the typical limits of air conditioning and refrigeration applications. The evaporator temperatures at the bottom chiller (vapor compression cooling system) are ranged between -40 to 0°C. It is important to indicate that the setting of evaporator temperature relies on the type of application. The cooling fluid cools the ACC condenser and the sorption beds through the adsorption and pre-cooling processes. It is supposed that the surrounding air temperature is utilized as the cooling fluid temperature through the isobaric cooling process (adsorption) of the adsorption cycle and in the ACC condenser. Table 4.1 states the conditions used in this part of the PhD thesis.

**Table 4. 1.** Operating conditions and parameters used in the present study

Description	Symbol	Value	unit
Adsorbent mass in one bed	$m_{ads}$	44	kg
Heating temperature	$T_h$	95	°C
Evaporation temperature	$T_{eva,ACC}$	17	°C
VCC condensing temperature	$T_{con,VCC}$	22	°C
ACC condensing temperature	$T_{con,ACC}$	45	°C
Ambient air temperature	$T_{amb} = T_{cool}$	40	°C
Thermal capacity ratio	$R_m$	1.5	-
VCC cooling heat capacity	$\dot{Q}_{eva,VCC}$	10	kW
Adsorption/Desorption time	$t$	500	s
Adsorption cycle time	$t_{cyc}$	1100	s

#### 4.1.1. Effect of VCC evaporator temperature on VCC performance

Figure 4.1 and Figure 4.2 clarify the rejected heat transfer rates from the VCC condenser and  $COP_{VCC}$  results for the vapor mechanical only at the ambient temperature ( $T_{amb} = 40^\circ\text{C}$ ), respectively.

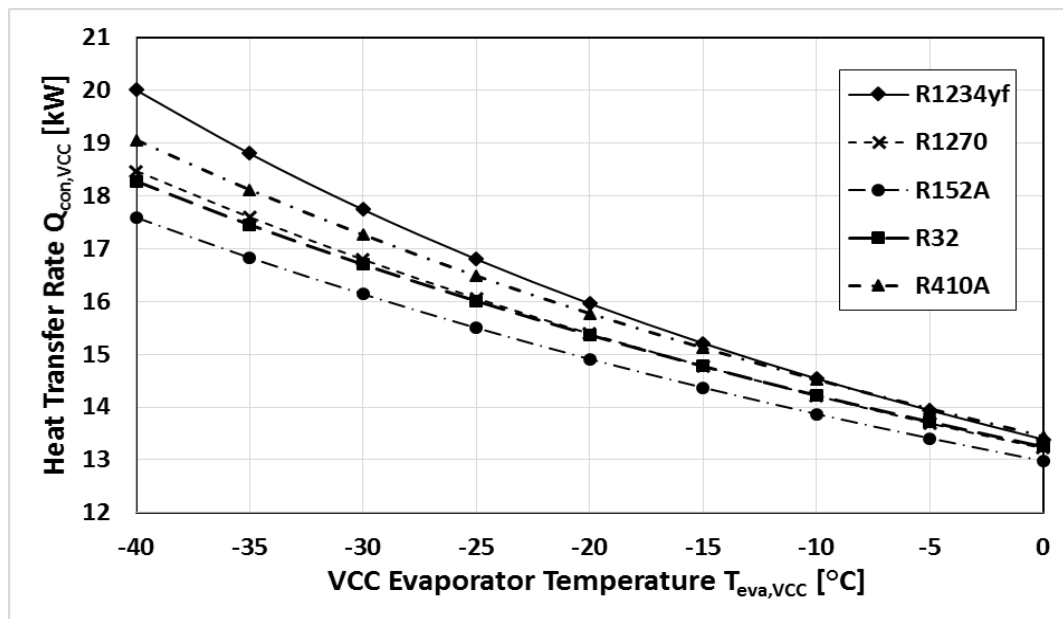


**Figure 4. 1.** Comparisons of the variation of heat transfer rate in the VCC condenser with respect to VCC evaporator temperature for various refrigerants.

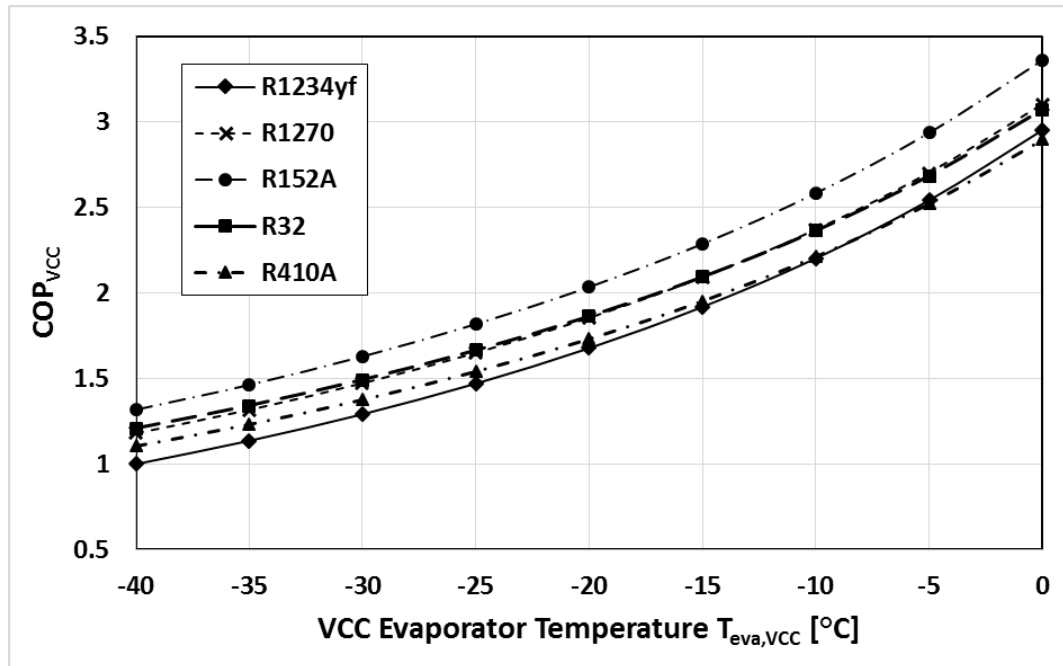


**Figure 4. 2.** Comparisons of the variation of  $COP_{VCC}$  with respect to VCC evaporator temperature for different refrigerants.

Figure 4.1 shows the results between the aforementioned refrigerants in the vapor mechanical chiller according to various evaporator temperatures. It is discernible that the released heat transfer rate values decrease noticeably by raising the evaporator temperature for all the working fluids considered in this study. It can also be seen that the higher values of the rejected heat in the VCC condenser have gotten when employing (R410A and R1234yf) refrigerants. In contrast, the lowest values of the rejected heat transfer rate in the VCC condenser are obtained by employing (R152A) refrigerant. Figure 4.2 states the results of the coefficient of performance  $COP_{VCC}$  in the vapor mechanical chiller for all refrigerants according to different evaporator temperatures between -40 to 0°C. It is evident that the coefficient of performance value in the VCC unit elevates by increasing the value of the evaporator temperature. When the evaporator temperature increases, the pressure difference between the condenser and the evaporator in the vapor mechanical chiller decreases; as a result, lower power input in the mechanical compressor and higher values of the  $COP_{VCC}$  are obtained. Additionally, it can be noticed that the lowest and highest VCC performance values are obtained by employing R1234yf and R152A, respectively.

#### 4.1.2. Effect of VCC evaporator temperature on VCC condenser heat in the combined cooling system

Figure 4.3 illustrates the results of heat transfer rates in the intermediate heat exchanger of the VCC-ACC combined cooling system for various working fluids according to different VCC evaporator temperatures. Obviously, at high evaporator temperature values, a significant reduction happens in the heat transfer rates within the intermediate heat exchanger. Indeed, the input power required in vapor mechanical chiller decreases as the evaporator temperature rises; consequently, a lower amount of heat in the VCC condenser releases. Furthermore, more heat transfer rates are provided at low VCC evaporator temperatures when utilizing various working fluids in the vapor mechanical chiller. The higher values of the heat transfer rate are attained by employing R1234yf refrigerant in the vapor mechanical chiller. It is important to indicate that the rejected heat from the VCC condenser must be equal to that absorbed in the ACC evaporator. Therefore, Figure 4.3 is important to specify the proper working fluid in the vapor mechanical chiller that meets the evaporation heat of the adsorption chiller during the design.

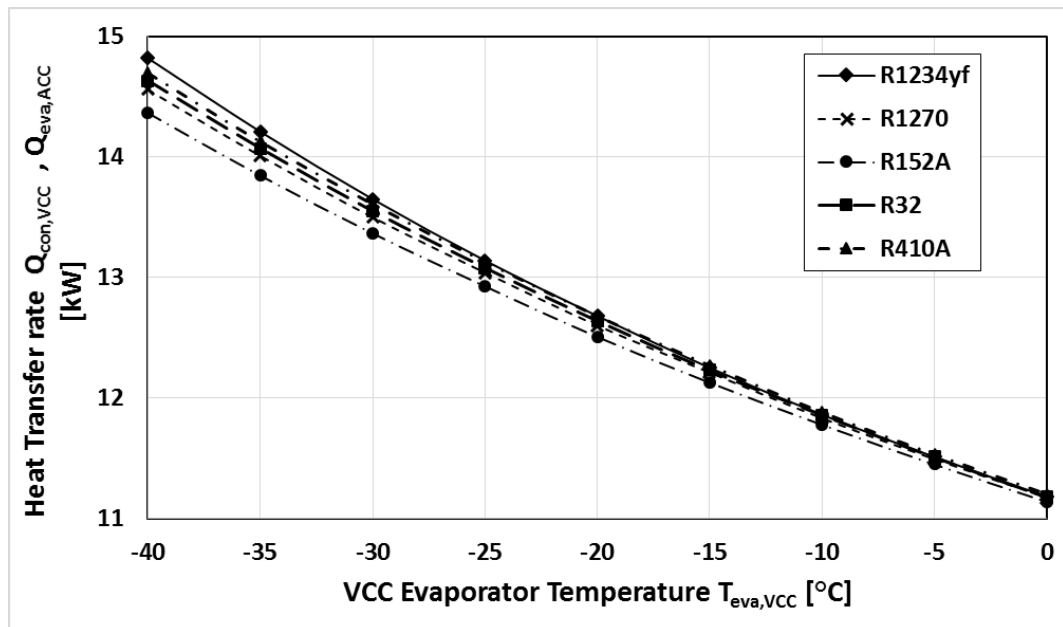


**Figure 4. 3.** Comparisons of the variation of heat transfer rates in the intermediate heat exchanger with respect to VCC evaporator temperature for the various refrigerants.

### 4.1.3. Effect of VCC evaporator temperature on ACC condenser heat

Figure 4.4 shows the computed results of the released heat transfer rate in the condenser of an adsorption chiller, which is the upper part of the proposed combined cooling system when employing different working fluids in the vapor mechanical chiller at various evaporator temperatures within the range of -40 to 0°C. The results are relatively close to each other, taking into account the working fluids considered in the current calculations. Figure 4.4 also highlights that increasing the value of VCC evaporator temperature leads to a reduction in the released heat values by the adsorption chiller's condenser. The commentary of this behavior that at low VCC evaporator temperatures, the ACC evaporator takes more amount of heat from the VCC condenser (Figure 4.3). Hence, higher released heat transfer rates are obtained, which reached up to 26.46 kW when employing R1234yf refrigerant in the vapor mechanical chiller. On the contrary, the lowest released heat transfer rate was attained for the R152A refrigerant.

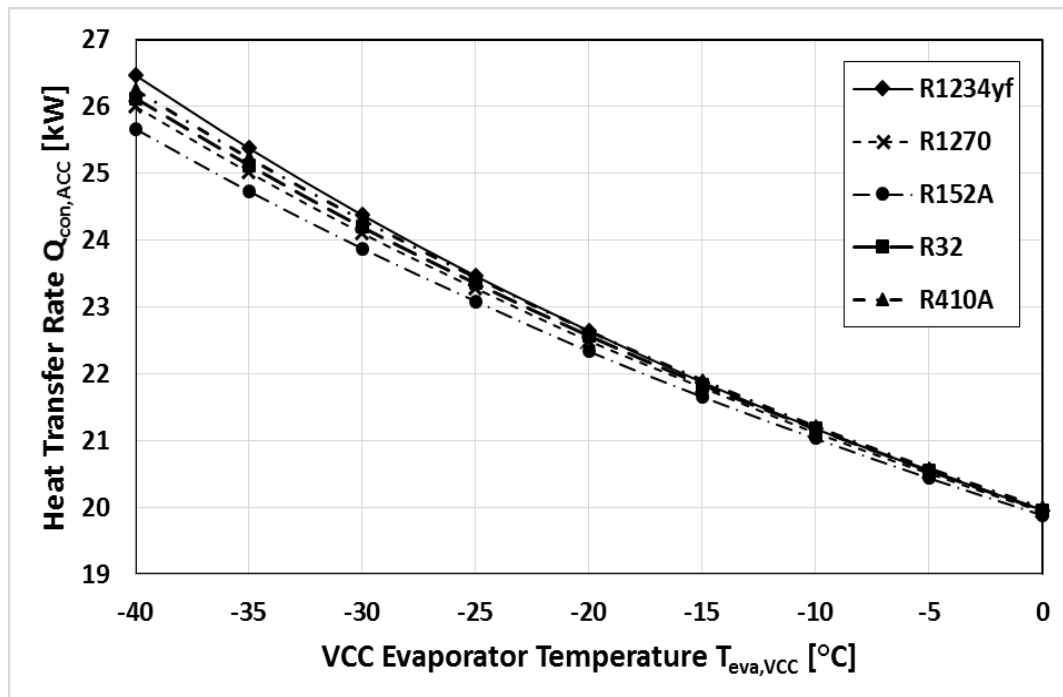


**Figure 4. 4.** Comparisons of the variation of heat transfer rate in the ACC condenser with respect to VCC evaporator temperature for different refrigerants.

#### 4.1.4. Effect of VCC evaporator temperature on VCC performance of (VCC-ACC) hybrid cooling system

Figure 4.5 presents the performance of the vapor compression chiller when combined with the adsorption chiller for different working fluids according to the several VCC evaporator temperatures. The VCC system performance increases obviously by raising the VCC evaporator temperatures. The VCC system performance increases obviously by raising the VCC evaporator temperature, where it reaches up to 8.8 for R152A refrigerant at the highest VCC evaporator temperature considered in the current investigation. The clarification for this rise in the system performance is that as the evaporator temperature moves to a higher value, the pressure difference between the condenser and the evaporator in the vapor compression chiller decreases, requiring lower power input to the compressor. As a result, higher  $COP_{VCC,H}$  values were achieved.

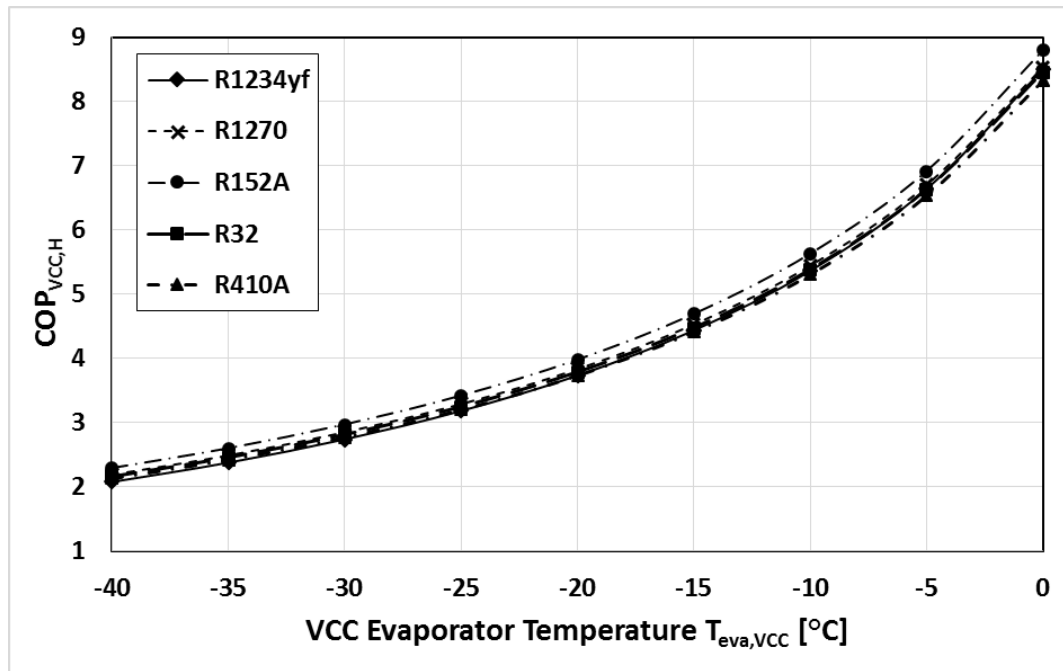


**Figure 4. 5.** Comparisons of the variation of  $COP_{VCC,H}$  with respect to VCC evaporator temperature for various refrigerants.

#### 4.1.5. Effect of VCC evaporator temperature on the thermal performance of the hybrid cooling system

Figure 4.6 illustrates the results of the coefficient of performance for the VCC-ACC combined system considering different VCC evaporator temperatures when employing different working fluids in the vapor compression chiller. It is clear that rising the VCC

evaporator temperature causes an increase in system performance values. The interpretation of this behavior is that at high evaporator temperatures, the power input in the vapor compression chiller will be less, higher performance values can be obtained as a result. In addition to that, all the working fluids employed in this investigation act in the same way. The lowest system performance is achieved through employing R1234yf refrigerant in the vapor compression chiller ( $COP_H = 0.32$ ) at the lowest evaporator temperature considered. on the other hand, The highest performance is attained via utilizing R152A in the vapor compression chiller ( $COP_H = 0.476$ ) at the highest evaporation temperature considered in this part of the study.

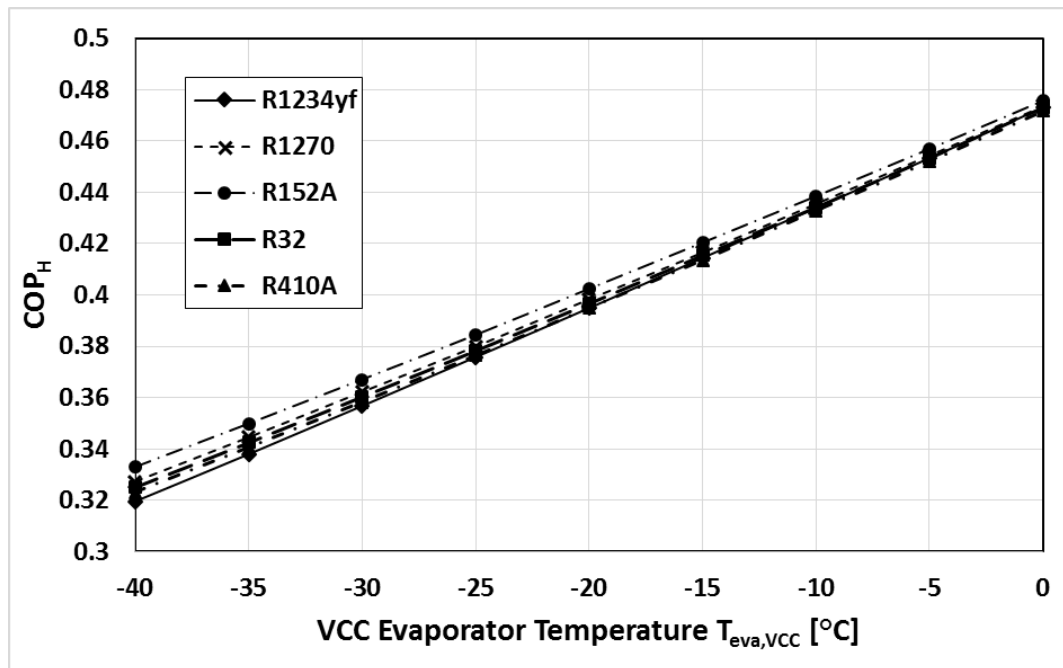


**Figure 4. 6.** Comparisons of the variation of  $COP_H$  with respect to VCC evaporator temperatures for various refrigerants.

#### 4.1.6. Effect of VCC evaporator temperature on the overall performance of the hybrid cooling system

Figure 4.7 indicates the results of the VCC-ACC combined system performance utilizing the exergy concept by varying the VCC evaporator temperature for several working fluids considered in this research.

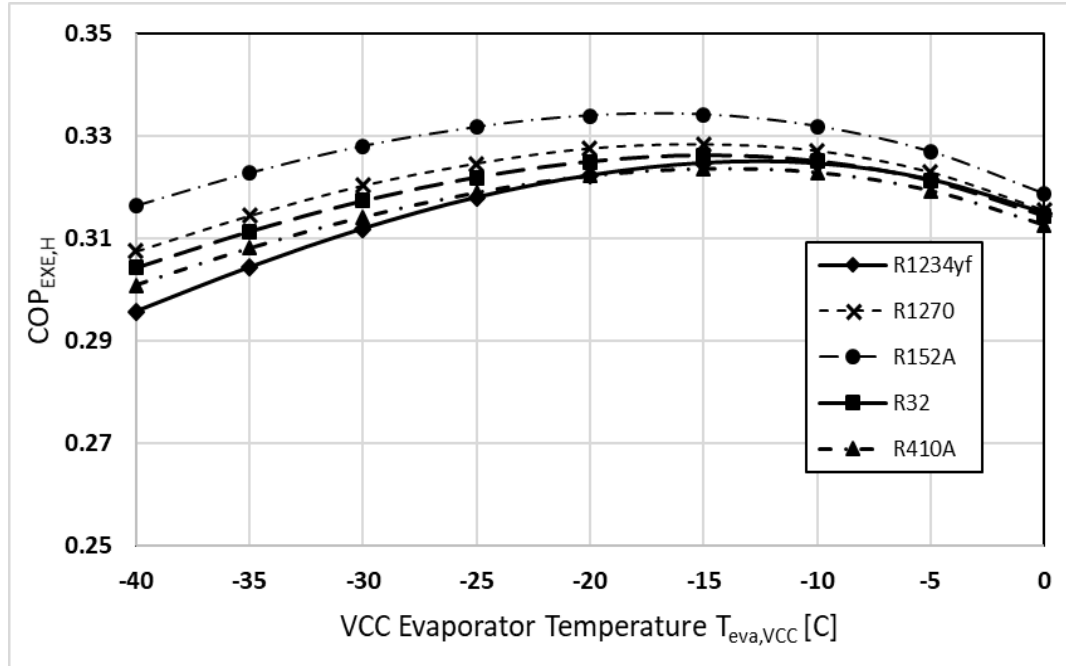


**Figure 4. 7.** Comparisons of the variation of  $COP_{EXE,H}$  with respect to VCC evaporation temperature for various refrigerants.

It can be noticed from the results that the  $COP_{EXE,H}$  values for all working fluids increase clearly until about the VCC evaporator temperature of  $-15^{\circ}C$ , then they decrease slowly, where the maximum point takes place at about  $-15^{\circ}C$ . The interpretation for this act is that at high VCC evaporator temperatures ( $-15$  to  $0^{\circ}C$ ), the requisite power inputs to drive the vapor compression chiller reduce and the VCC system performance  $COP_{VCC,H}$  values noticeably increase at high VCC evaporator temperature (Figure 4.5). Consequently, the evaporation heat transfer rate absorbed in the intermediate heat exchanger is lower; the heat transfer rate inputs and the exergy rates in the ACC unit are also lower as a result. Furthermore, the VCC compressor power and the exergy rate also decrease by increasing the VCC evaporator temperature. Hence, all these together would finally make a difference in the  $COP_{EXE,H}$  by obtaining significant effects when the VCC evaporator temperature values are high within the range considered in this study.

#### 4.1.7. Effect of VCC evaporator temperature on energy savings amount and VCC performance in the combined cooling system

Figure 4.8 shows the results of the energy savings at different evaporation temperatures of VCC for various working fluids. It is obvious that the energy-saving values elevate gradually while the VCC evaporator temperature increases for all working fluids. However, at higher evaporator temperatures, the rise in energy-saving values becomes more remarkable, where the vapor compression chiller operates more productively, as previously explained (Figure 4.5). It is also noticeable from the results that the highest energy savings values are obtained for R1234yf working fluid, among the others, reached up to 65.29% at the highest VCC evaporator temperature considered in this research. While the lowest energy saving values achieved for R152A working fluid reached up to 42.38% at the lowest VCC evaporator temperature considered (-40°C).

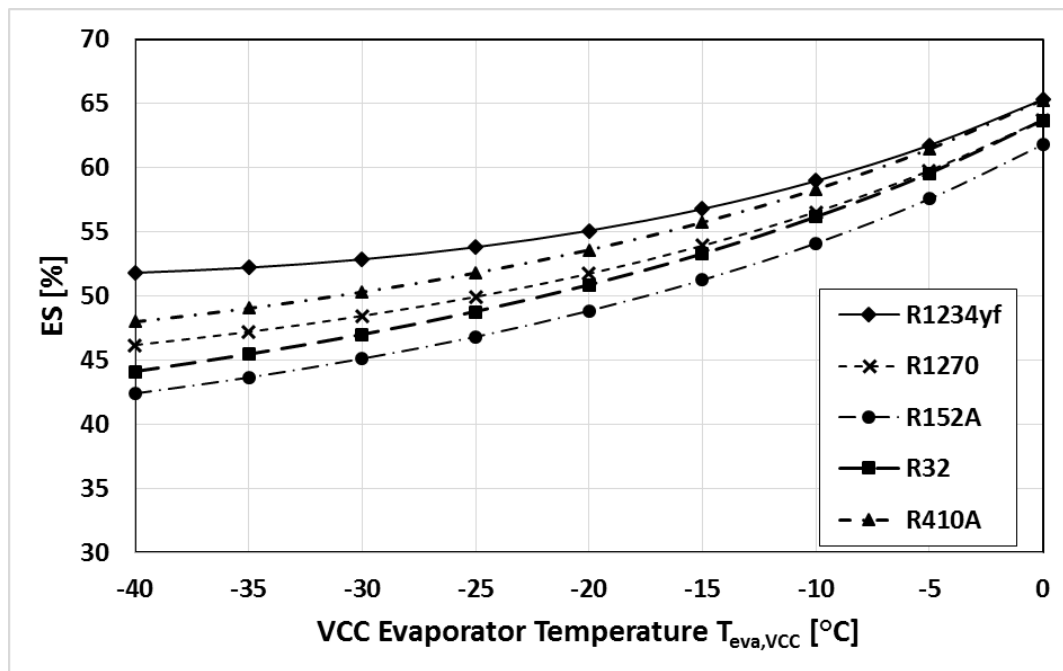


**Figure 4. 8.** Comparisons of the variation of ES with respect to VCC evaporation temperatures for different refrigerants.

Figure 4.9 presents the significance of employing the combined system against utilizing the vapor compression chiller alone in terms of  $COP_{VCC}$ . All the refrigerants provide an increase in the performance of the vapor compression chiller when it is combined with

the adsorption chiller. Table 4.2 shows the VCC performance when it operates alone and when combined with the adsorption cooling system in addition to the increasing ratio between the two situations at the highest and lowest VCC evaporator temperatures considered in this investigation.

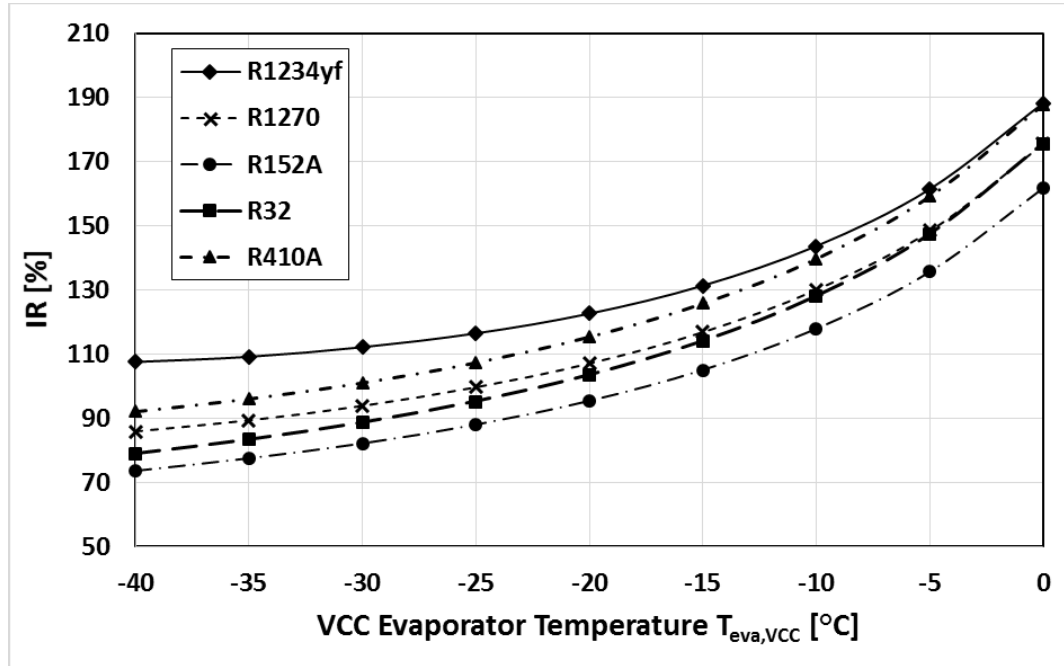


**Figure 4. 9.** Comparisons of the variation of IR with respect to VCC evaporator temperatures when VCC system works with ACC and alone for different refrigerants.

**Table 4. 2.** Comparisons of VCC performance increase ratio (IR) results when it works with ACC and alone for several refrigerants at various evaporation temperatures

Working fluid	COP <sub>VCC,H</sub>		COP <sub>VCC</sub>		IR %	
	-40°C	0°C	-40°C	0°C	-40°C	0°C
R152A	2.287	8.797	1.32	3.36	73.52	161.82
R410A	2.126	8.383	1.106	2.895	92.22	187.668
R1270	2.195	8.54	1.181	3.1	85.86	175.6
R1234yf	2.075	8.505	0.99	2.95	107.54	188.207
R32	2.161	8.456	1.208	3.07	78.9	175.44

The results demonstrate that the highest increase ratios were achieved for R1234y refrigerant. The highest IR values are 188.207 and 187.668 for R1234yf and R410A, respectively, at the highest VCC evaporator temperature considered in the current investigation. These results reveal that the vapor compression chiller works more constructively when it is merged with the adsorption chiller, particularly at higher evaporator temperatures in the VCC unit.

#### **4.1.8. Effect of VCC evaporator temperature, inlet hot fluid temperature, cycle time on the amount of adsorbent in the combined cooling system**

It has been previously discussed in the validation part that by rising cooling fluid temperature, the cooling capacity of the adsorption chiller noticeably reduces. Indeed, this is a result of increasing the ACC evaporator and the VCC condenser temperatures. Thus, the ACC-VCC combined chiller performance reduces with increasing the surrounding temperature. This issue can be fixed by altering the adsorbent mass for the highest cooling fluid temperature during the adsorption chiller design. However, this leads to a larger size of the sorption beds and the adsorption system. Another way to solve this problem is by decreasing the cycle time of the adsorption cycle. However, it should be mentioned that the reduction in the cycle time may lead to less adsorption of the adsorbate in the adsorption beds as a result of the lower time to accomplish the adsorption process and the heat and mass transfer rates in the adsorption beds. Therefore, In order to observe the impact of the suggested two-way solutions on the adsorbent mass in a bed, a study has executed by taking into account two different cycle times as 1100 s, where 50 s for pre-cooling/ pre-heating and 500 s for desorption/ adsorption, and 660 s, where 30 s for pre-cooling/ pre-heating and 300 s for desorption/ adsorption. The surrounding temperature is considered as 40°C. Thus, the system can work in a wide surrounding temperature up to 40°C. The requisite amount of adsorbent mass in a bed is computed for several VCC evaporation temperatures. Besides that, during the analysis, three different hot fluid temperatures are considered as 85, 90, and 95°C.

Figure 4.10 illustrates the effects of varying the evaporator temperatures in the vapor compression chiller, inlet heat temperatures in the adsorption chiller, and two different cycle times on the amount of adsorbent.

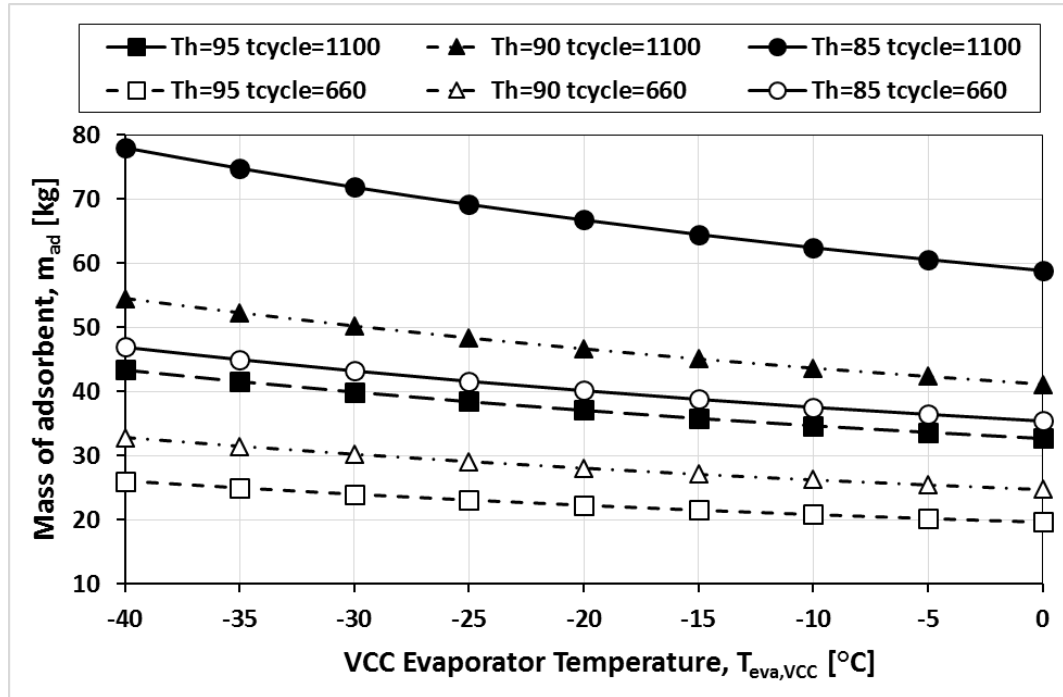


**Figure 4. 10.** Required amount of mass in a bed with respect to VCC evaporator temperatures, heating temperatures, and two different cycle time values.

The results reveal that raising the value of VCC evaporator temperature requires a lower mass of adsorbent. The higher values of VCC evaporator temperature, the lower amount of released heat in the VCC condenser; thus, less heat is required to complete the adsorption cycle. Figure 4.10 also illustrates the link between the hot fluid temperature that enters the beds and the adsorbent mass in the adsorption chiller. Utilizing high hot fluid temperature results in an elevation in the adsorbate uptake rate and the amount of inlet heat to the bed as a result. Thus, a lower adsorbent mass is needed to reduce the necessary heat amount to operate the adsorption chiller while the adsorption chiller performance is constant. Increasing the hot fluid temperature value from 85 to 90°C and 90 to 95°C leads to a decrease in the requisite adsorbent mass in a bed by 30% and 20%, respectively. When the VCC evaporation temperature increases within the range considered in this study, the adsorbent mass in a bed reduces by 25% for all cases.

Furthermore, decreasing the entire cycle time from 1100 s to 660 s leads to lowering the adsorbent mass for all hot fluid temperatures considered by approximately 40%. It can be summarized that the shortest cycle time, the highest hot fluid temperature. The operating VCC evaporation temperature must be considered for specifying the adsorbent mass amount in the adsorption chiller design. This will lead to a smaller size of the adsorption chiller. It is noteworthy to mention that the adsorbent mass amount required to adsorption chiller is associated with the adsorption bed design and the adsorbent characteristics.

#### **4.2. Comparative performance analysis of two-bed adsorption cooling system using water vapor adsorption on different types of silica gel**

This section of the PhD thesis aims to investigate the performance of an adsorption cooling system employing various types of adsorbents, yet the widely utilized working pair is the silica gel/water pair. There are also several sorts of silica gel as well as many types of composite adsorbents that use silica gel as the main component. In this part of the investigation, the analysis was executed for the ACC performance using water as adsorbate and four kinds of solid adsorbents, namely RD silica gel 2060, RD silica gel, silica gel-LiCl, and silica gel-CaCl<sub>2</sub>. The calculations in this part of the study were implemented in MATLAB platform using CoolProp library. The solid adsorbents' mass for all types considered in this part of the study is considered as  $m_{ads.} = 47$  kg. The thermal capacity, on the other side, is taken as  $m_{bm} \cdot C_{bm} = 78$  kJ/K (Kılıç, 2018). Two study cases have been considered in this part of the calculations. The first case is done by employing different evaporator temperatures between 5°C and 20°C. The heating and cooling inlet temperatures utilized are kept constant at 90°C and 30°C, respectively. The second one is done by considering different heating inlet temperatures between 65°C and 95°C, while the evaporator and cooling inlet temperatures are kept constant at 10°C and 30°C, respectively. The desorption/adsorption time has been computed through the linear driving force equation, assuming that adsorption time and desorption time are the same. Pre-heating/cooling period time is kept constant at 50 seconds. The same working conditions for the four different silica gels are performed through the computations.

#### 4.2.1. Effect of ACC evaporator temperature on the ACC performance indicators

Figure 4.11 and Figure 4.12 show the results for COP and SCP indicators for the different adsorbents considered at various ACC evaporation temperatures.

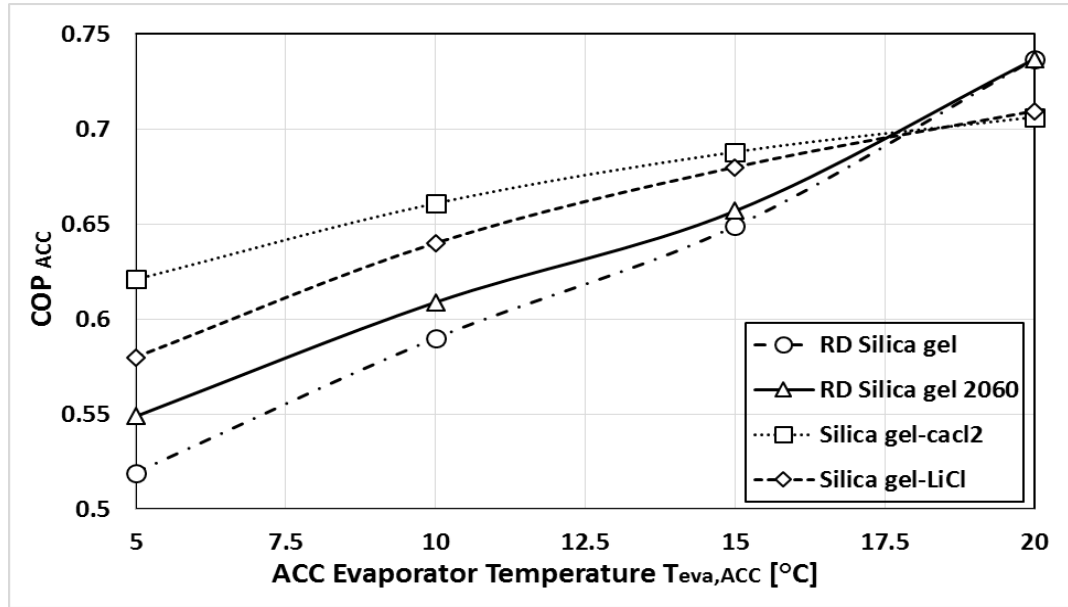


**Figure 4. 11.** Comparison of the variation of COP<sub>ACC</sub> with respect to ACC evaporator temperatures for different adsorbents.

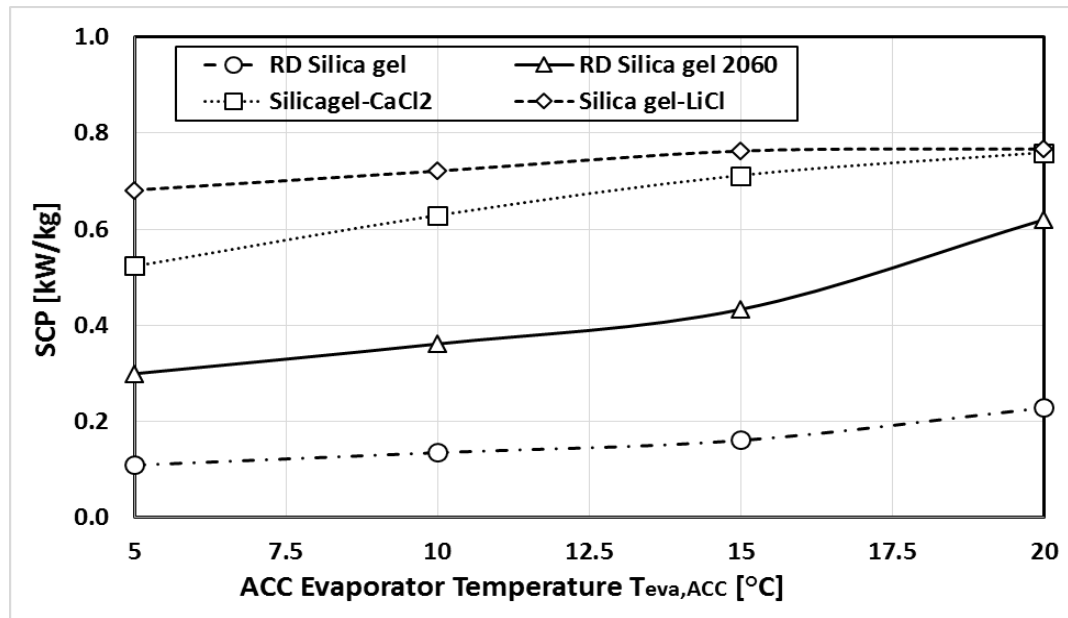


**Figure 4. 12.** Comparison of the variation of SCP with respect to ACC evaporator temperature for different adsorbents.

It is clear that all the performance curves gradually increase with the rise in the  $T_{\text{eva,ACC}}$  (Figure 4.11). The commentary of this behavior is that elevating the  $T_{\text{eva,ACC}}$  leads to an increase in the maximum adsorbate concentration into the solid adsorbent  $X_{\text{max}}$ ; thus, an increase in the evaporation heat and  $\text{COP}_{\text{ACC}}$  occur. Additionally, the composite adsorbents give better  $\text{COP}_{\text{ACC}}$  values than the standard adsorbents. Indeed, composite adsorbents provide higher maximum concentration values of the water into their structure. Figure 4.12 shows that the SCP curves slightly increase with the rise in the  $T_{\text{eva,ACC}}$  values. Although the evaporation heat values increase as the  $T_{\text{eva,ACC}}$  increases, the requisite time to desorb the adsorbate increases too; thus, a slight elevation in SCP values is observed. After the comparison, it can be seen that the composite materials (silica gel-CaCl<sub>2</sub> and silica gel-LiCl) have the highest performance indicators values at different  $T_{\text{eva,ACC}}$ .

#### **4.2.2. Effect of different heating inlet temperature on the ACC performance indicators**

Figure 4.13 and Figure 4.14 present the calculated results of SCP and  $\text{COP}_{\text{ACC}}$  for the adsorbents considered in this part of this dissertation at various heating temperatures. The results demonstrate that there is an increase in both performance indicators by increasing heating inlet temperature  $T_h$ . As the heating inlet temperature value increases, the difference between  $X_{\text{max}}$  and  $X_{\text{min}}$  of adsorbate into adsorbent increases; this elevation affects the desorption heat and the evaporation heat. Consequently, an increase in both performance indicator values occurs. The composite adsorbents provide higher performance values than the standard adsorbents considered in this study reach up to 0.64 and 0.66 for silica gel-LiCl, and silica gel- CaCl<sub>2</sub>, respectively. On the contrary, the results also illustrate a slight increase in the specific cooling power values for standard adsorbents (RD silica gel and RD silica gel 2060). However, the increase in the specific cooling power values for composite adsorbents reaches up to 0.54 and 0.73 kW/kg for silica gel-LiCl and silica gel- CaCl<sub>2</sub>, respectively. The specific cooling power values are related to the cycle time, which changes according to both the adsorption uptake rate and heating inlet temperature.

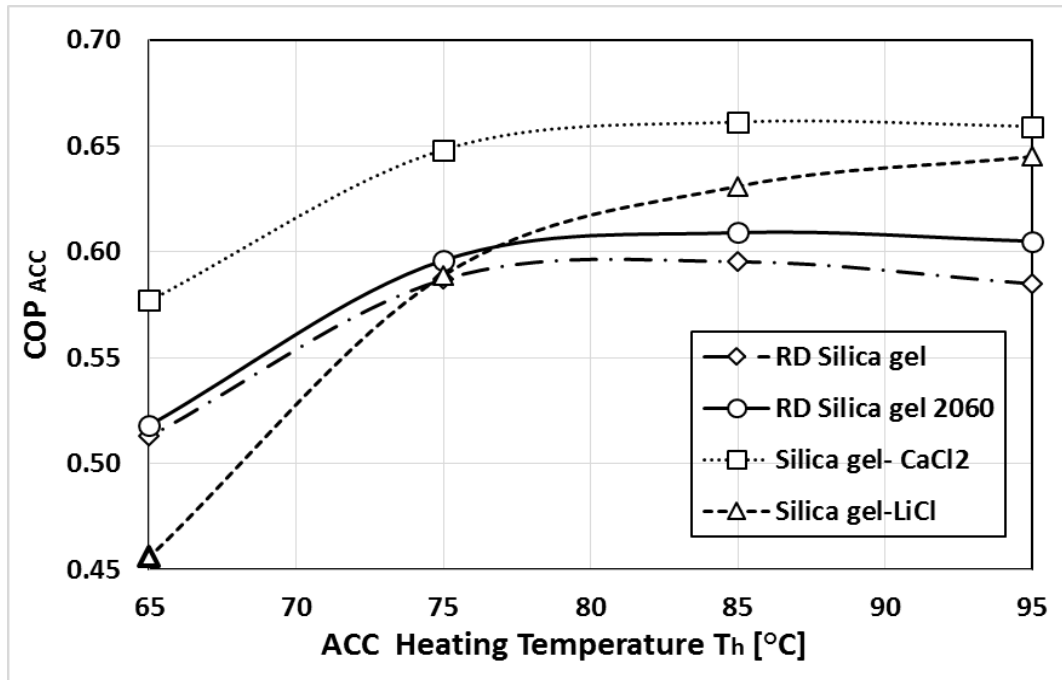


**Figure 4. 13.** Comparison of the variation of COP<sub>ACC</sub> with respect to ACC heating temperature for different adsorbents.

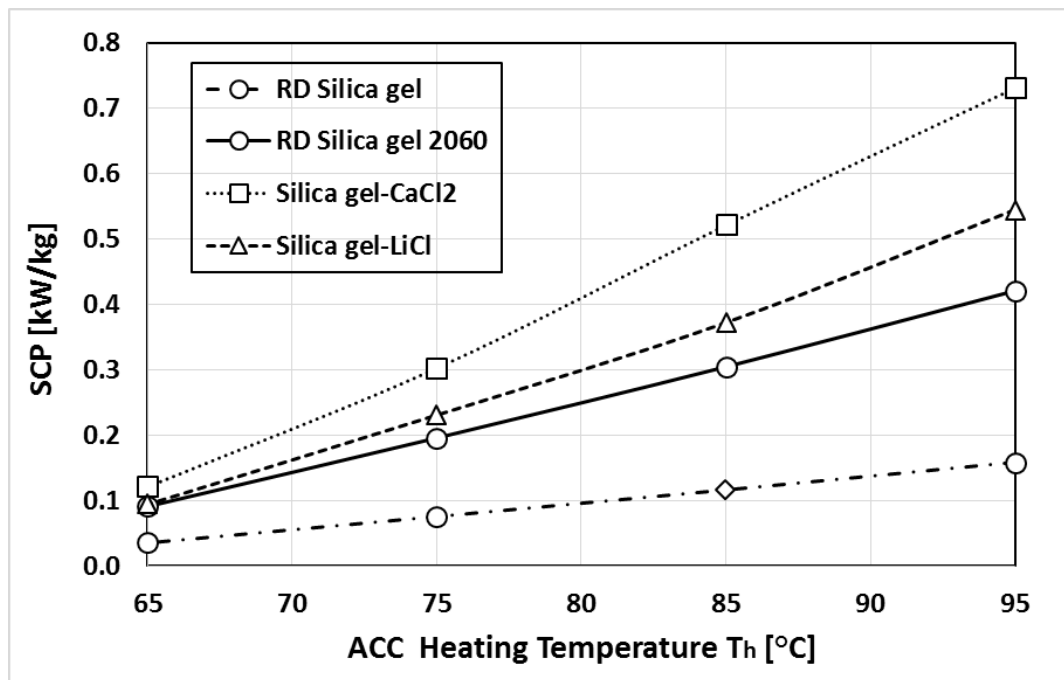


**Figure 4. 14.** Comparison of the variation of SCP with respect to ACC heating temperature for different adsorbents.

In this section of the study, the desorption time values are related to the heating temperature. The lower the heating temperature, the longer the required desorption time; thus, lower SCP values are obtained at lower heating temperatures at the same operating conditions.

#### **4.3. Performance analysis of a mechanical and adsorption combined refrigeration system using two different system configurations**

This section of the PhD dissertation aims to make a comparative performance analysis of the ACC-VCC combined cooling system using two different layouts (parallel and series) (Figure 2.12). Moreover, three kinds of adsorbents are employed: (RD silica gel, RD silica gel 2060, and Silica gel–LiCl) in addition to water as a refrigerant in the adsorption chiller. In contrast, the refrigerant employed in the vapor compression chiller is R152A as it provides a higher system performance not only for the vapor compression chiller but also for the overall combined cooling system performance. The condensing temperatures in the vapor compression chiller range from 15 to 25°C in the series configurations (Figure 2.12 a). The difference between the VCC condenser temperature and the ACC evaporator temperature is kept constant ( $\Delta T = 5^\circ\text{C}$ ). The setting of VCC condenser temperature depends on the design boundaries in the adsorption chiller. The surrounding atmosphere (named as cooling fluid) is also used to cool down the ACC condenser and the thermal compressor. The surrounding temperature and the heating inlet temperature are considered to be constant at 30°C and 95°C, respectively. It is essential to mention that the adsorption chiller's cycle time varies according to the adsorbent material type employed in the beds. However, in this investigation, the cycle time is assumed to be constant for all materials considered in the beds. Table 4.3 presents the parameters and thermal quantities utilized in this part of the research.

**Table 4. 3.** Settings and working conditions are utilized in the current research

Mass of solid sorbent (adsorbent)	$m_{ads} = 44$ [kg]
Heating temperature	$T_h = 95$ [°C]
ACC evaporation temperature	$T_{eva,ACC} = 10$ to $20$ [°C]
ACC condensing temperature	$T_{con,ACC} = 45$ [°C]
Ambient temperature	$T_{amb} = 40$ [°C] $T_{amb} = 28-40$ [°C]
Cooling temperature	$T_{cool} = 30$ [°C]
VCC condenser temperature	$T_{con,VCC} = 15$ to $25$ [°C]
VCC evaporation temperature	$T_{eva,VCC} = -5$ [°C]
Second fluid temperature (Parallel)	$T_{SF} = 25$ [°C]
VCC cooling capacity	$\dot{Q}_{eva,VCC} = 10$ [kW]
Thermal capacity ratio	$R_m = 1.5$
Adsorption /desorption time	$t_{ads} = 500$ [s] $t_{ads} = (300, 400, 500)$ [s]
Pre-heating/pre-cooling time	$50$ [s]
Cycle time	$t_{cyc} = 1100$ [s] $t_{cyc} = (700, 900, 1100)$ [s]

#### 4.3.1. Effect of ACC evaporator temperature on heat amount in the combined cooling system

Figure 4.15 illustrates the heat that the ACC system needed to complete the adsorption cycle at various ACC evaporator temperatures according to two different arrangements considered (series (a) and parallel (b)). Additionally, it presents different heat transfer rates by employing the three types of adsorbents due to the different thermophysical and physical traits among the adsorbents utilized in this investigation (Table 3.6).

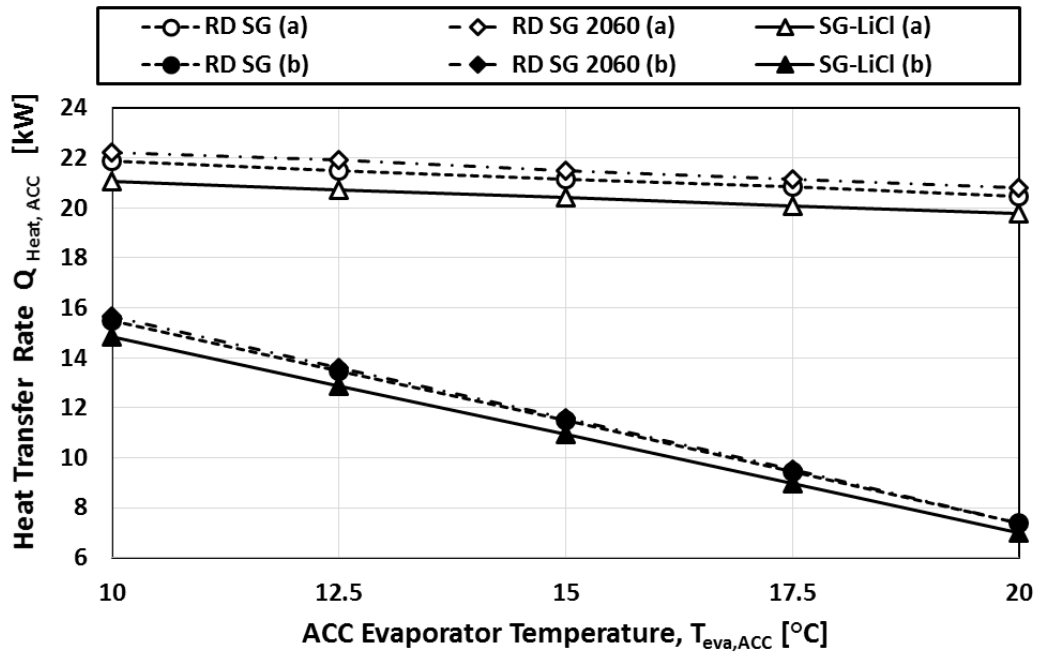


**Figure 4. 15.** Comparisons of the variation of  $\dot{Q}_{heat,ACC}$  with respect to ACC evaporator temperature for different adsorbents and the two system configurations (a) and (b).

Figure 4.15 illustrates that silica gel-LiCl (the composite adsorbent) requires lower heat transfer rate values than the others utilized in the adsorption chiller. The results also emphasize that as the value of  $T_{eva,ACC}$  increases the  $\dot{Q}_{heat,ACC}$  gradually reduces. This is due to a smaller temperature difference between the condenser and the evaporator in the ACC unit as the ACC evaporator temperature increases. On the contrary, it is also noticeable that the heat  $\dot{Q}_{heat,ACC}$  required to the ACC chiller in series linkage (Figure 2.12 a) is higher than that in the parallel linkage. In fact, in the parallel linkage, as the ACC evaporator temperature  $T_{eva,ACC}$  value increases, the cooling load  $\dot{Q}_{eva,ACC}$  dramatically reduces; thus, the heat needed to the adsorption chiller remarkably reduces. The highest  $\dot{Q}_{heat,ACC}$  provided is 22.2 kW at the lowest ACC evaporator temperature considered ( $T_{eva,ACC} = 10^{\circ}C$ ) for RD silica gel 2060 according to the series linkage, while the lowest heat transfer rate value  $\dot{Q}_{heat,ACC}$  obtained is 7 kW for silica gel-LiCl at  $T_{eva,ACC} = 20^{\circ}C$  within the same running conditions according to the parallel linkage. It is visible from the results that RD silica gel 2060 requires more amount of heat among the adsorbents utilized for both system configurations proposed in this section of the study.

### 4.3.2. Effect of ACC evaporator temperature on the hybrid system performance with the (series and parallel) configuration

Figure 4.16 presents the performance results of the hybrid cooling system (series (a) and parallel (b)) considering the different adsorbents used in this study at several ACC evaporator temperatures.

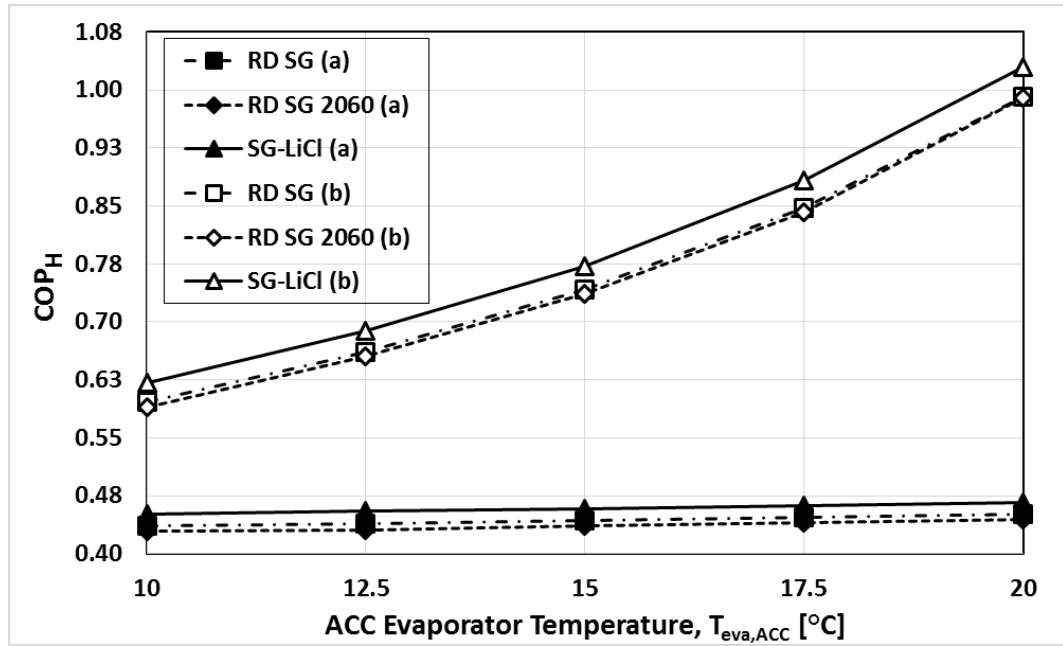


**Figure 4. 16.** Comparisons of the variation of  $COP_H$  with the respect to ACC evaporator temperature for various adsorbents and the two system configurations (a) and (b).

It is evident from the results that rising the ACC evaporator temperature  $T_{eva,ACC}$  results in a small increase in the hybrid (ACC-VCC) cooling system's coefficient of performance. Rising the ACC evaporator temperature  $T_{eva,ACC}$  drives to a reduction in the heat transfer rate  $\dot{Q}_{heat,ACC}$ . However, as we previously indicated that the temperature difference between VCC condenser and ACC evaporator remains constant at  $\Delta T = 5^\circ C$ ; as a result, rising the ACC evaporator and the VCC condenser temperature values lead to an elevation in the electrical power input to the mechanical compressor  $\dot{W}_{elec}$ , which drives to a small increase in the performance for series linkage (Figure 2.12 a). On the contrary, it is clear from the results, according to the parallel connection, that rising the ACC evaporator temperature  $T_{eva,ACC}$  leads to remarkable enhancements in the hybrid cooling system's

coefficient of performance values  $COP_H$ . Moreover, rising the adsorption chiller's evaporator temperature drives to a remarkable decrease in the requisite heat inputs  $\dot{Q}_{heat,ACC}$ . Hence, the improvements in the hybrid system performance values appear as shown in the results' figure (Figure 4.16). The results demonstrated that the composite adsorbent supplies the better hybrid system performance values  $COP_H$  as the composite adsorbent (silica gel-LiCl) needs smaller thermal energy inputs  $\dot{Q}_{heat,ACC}$  than the others considered in this study.

#### 4.3.3. Effect of ACC evaporator temperature on the overall system performance according to the series connection

Figure 4.17 illustrates the performance results considering the exergy concept for various ACC evaporator temperatures and different adsorbents in the adsorption section of the (VCC-ACC) combined cooling system with the series connection.

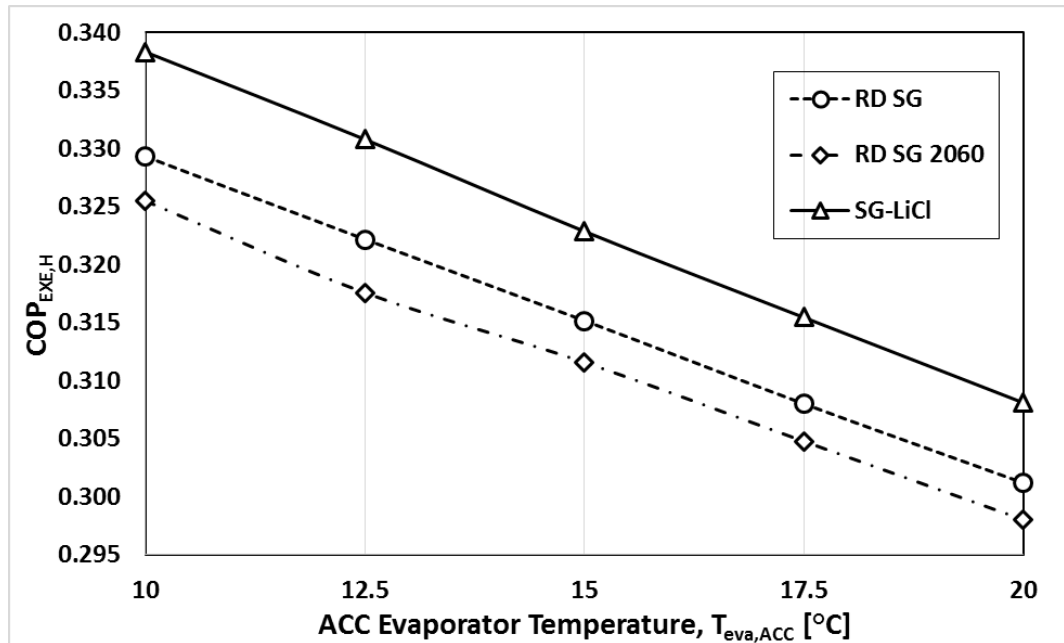


**Figure 4. 17.** Comparisons of the variation of  $COP_{EXE,H}$  with respect to ACC evaporator temperature for various adsorbents and the series configuration (a).

It is important to mention that the difference between the evaporation temperature in ACC and condensation temperature in VCC stays constant ( $\Delta T= 5^{\circ}C$ ) for the series linkage.

The results demonstrate that using the composite adsorbent (silica gel-LiCl) in the adsorption chiller provides better performance values than the others. The composite adsorbent needs smaller heat inputs to complete the desorption process than the others used, as previously illustrated (Figure 4.15); thus, higher system performance values are provided. It is clear from the results (Figure 4.17) that the performance of the combined system reduces as the  $T_{\text{eva,ACC}}$  value increases. In fact, as the ACC evaporator temperature and VCC condenser temperature increase, the power needed for the mechanical compressor also elevates; thus, smaller performance values are provided. The lowest and highest performance values are 0.298 and 0.338 for RD silica gel 2060 and silica gel-LiCl at the highest and lowest evaporator temperature in the ACC unit considered in this part of this research, respectively.

#### **4.3.4. Effect of ACC evaporator temperature on the overall system performance according to the parallel connection**

Figure 4.18 presents the relationship between the combined cooling system performance and the ACC evaporator temperature according to the parallel configuration (Figure 2.12 b). The entire load is divided into two sections; the ACC chiller absorbs the first one while the VCC unit accomplishes the second part, respectively. As the ACC evaporation temperature changes, the evaporator heat in the ACC unit also modifies; thus, the VCC evaporator heat load also changes. Some assumptions have considered through the computations as the following:  $T_I = T_{\text{SF}}$ ,  $T_{II} = T_{\text{eva,ACC}} + 2^\circ\text{C}$ ,  $T_{III} = T_{II}$ ,  $T_{IV} = T_1 + 3^\circ\text{C}$ . Eq.(3.41) is utilized to calculate the  $\text{COP}_{\text{EXE,H}}$  in the parallel connection. The results present an elevation in the performance values by increasing the ACC evaporator temperature. The interpretation of these results is that as the ACC evaporator temperature rises, the ACC evaporator heat reduces, and smaller heat inputs are needed for the thermal compressor. On the other hand, as the evaporator heat reduces in the ACC chiller, the evaporator heat increases in the VCC chiller (the overall heat load remains constant at 10 kW for both chillers); as a result, more electrical power is needed to drive the vapor compression chiller. By implementing these quantities in Eq. (3.41), the results appear as shown (Figure 4.18). The best performance value reaches 0.354 for silica gel-LiCl at  $T_{\text{eva,ACC}} = 20^\circ\text{C}$ . On the contrary, the lowest performance values reached by employing

RD silica gel 2060 as it needs higher heat transfer rates  $\dot{Q}_{\text{heat,ACC}}$  as previously illustrated (Figure 4.15).

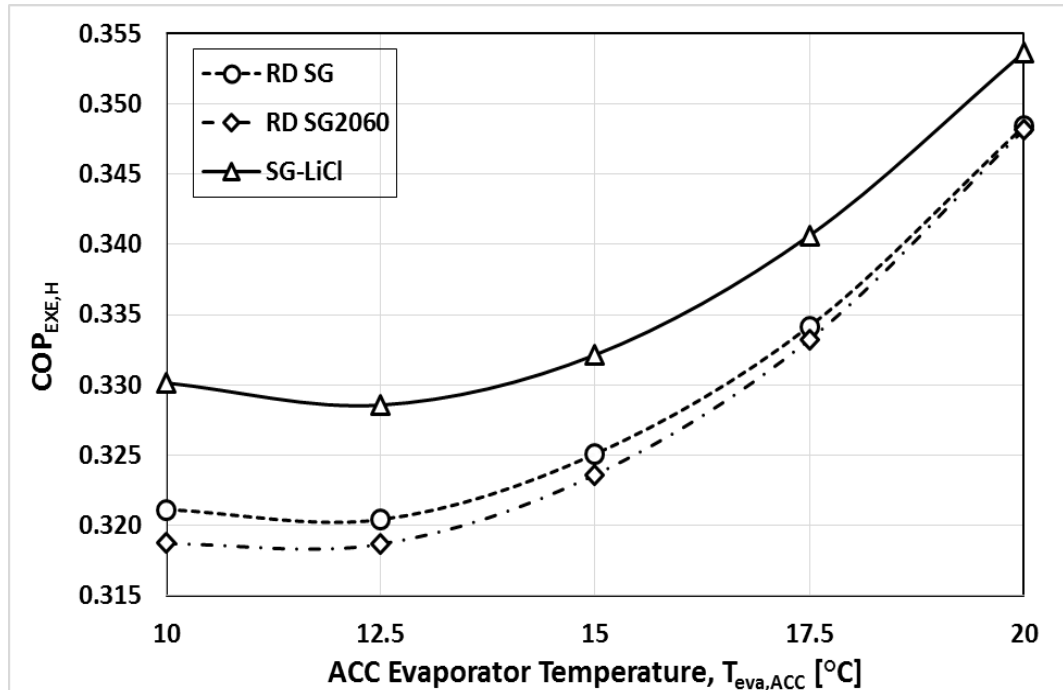


**Figure 4. 18.** Comparisons of the variation of  $\text{COP}_{\text{EXE,H}}$  with respect to ACC evaporator temperature for various adsorbents and the parallel configuration (b).

#### 4.3.5. Effect of ACC evaporator temperature on the ACC system performance according to the series and parallel configurations

Figure 4.19 shows the ACC system performance results of the introduced combined cooling system when employing the various adsorbents for series (a) and parallel (b) configurations.

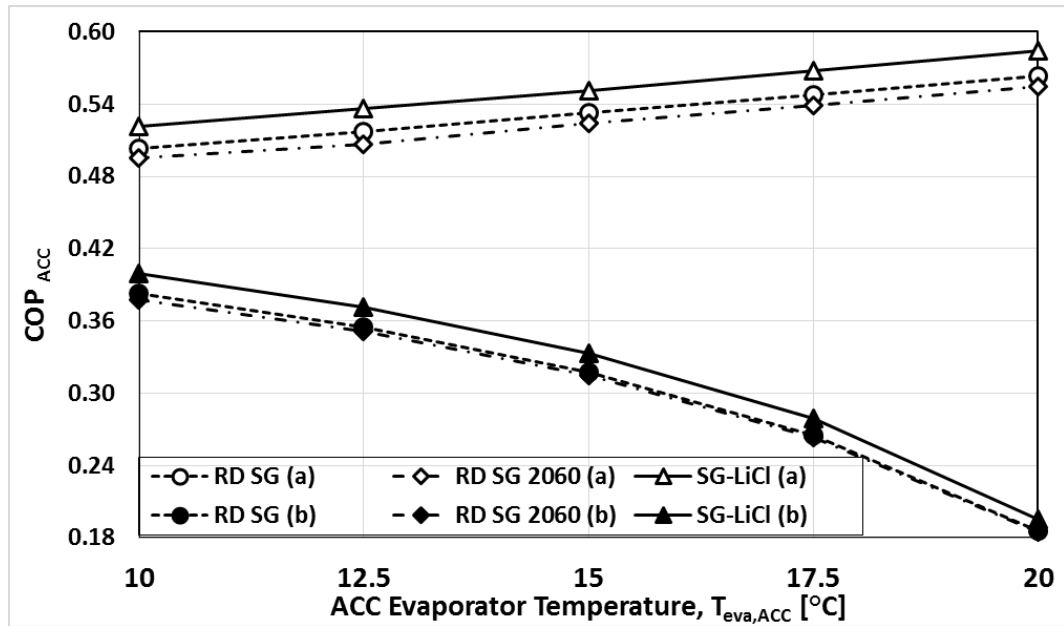


**Figure 4. 19.** Comparisons of the variation of  $COP_{ACC}$  with respect to ACC evaporator temperature for various adsorbents and the two system configurations series and parallel.

The evaluation takes into account using different evaporator temperatures in the adsorption section from 10 to 20°C. Figure 4.19 shows a slight increase in the ACC performance as the  $T_{eva,ACC}$  elevates for series linkage reached up to 0.584 using silica gel-LiCl (composite adsorbent) in the adsorbent beds. In fact, as the ACC evaporator and the VCC condenser temperature increase, the ACC evaporator heat also increases; thus, slight increases appear in the  $COP_{ACC}$  values. On the contrary, as the ACC evaporator temperature in the parallel linkage increases, the secondary working fluid's outlet temperature increases ( $T_{II} = T_{eva,ACC} + 2^{\circ}C$ ), which drives to smaller heat taken through the ACC evaporator. consequently, a smaller  $COP_{ACC}$  values were obtained. The computed results reveal that silica gel-LiCl (composite adsorbent) supplies better performance numbers for series and parallel connections considered in this investigation.

#### 4.3.6. Effect of ACC evaporator temperature on the VCC system performance according to parallel and series configurations

Figure 4.20 shows the relations between the coefficient of performance for the vapor compression cooling unit combined with the adsorption cooling unit using two different connections (series and parallel).

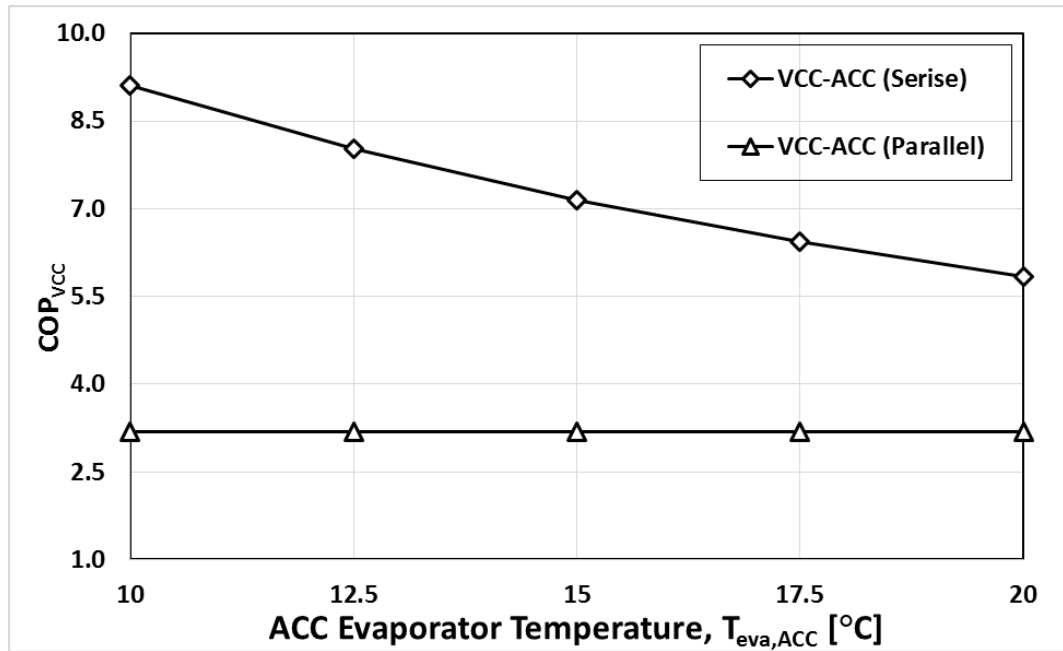


**Figure 4. 20.** Comparisons of the variation of  $COP_{ACC}$  with respect to ACC evaporator temperature for the two system configurations series and parallel.

It should be mentioned that the temperature difference between the ACC evaporator and the VCC condenser remains at the same value ( $\Delta T = 5^{\circ}C$ ) for series linkage. Figure 4.20 illustrates that as the ACC evaporator temperature  $T_{eva,ACC}$  elevates the coefficient of performance of vapor compression chiller  $COP_{VCC}$  reduces. In fact, Increasing the adsorption unit's evaporator temperature leads to an increase in the vapor compression unit's condenser temperature; so, more electrical energy is required for the VCC system; consequently, smaller VCC performance values at stationary cooling load value (10 kW). In contrast, the coefficient of performance values of VCC unit connected with ACC unit in parallel nearly stay constant by elevating the adsorption chiller's evaporator temperature  $T_{eva,ACC}$ . As it has formerly indicated, the linkage between the two proposed chillers happens in the chilling fluid that links the ACC evaporator with the VCC evaporator. Thus, elevating the ACC evaporator temperature drives to smaller ACC cooling load  $\dot{Q}_{eva,ACC}$  taken through the ACC evaporator and higher VCC cooling load  $\dot{Q}_{eva,VCC}$  taken through the vapor compression chiller. However, the evaporation and condensation temperatures remain constant in the VCC chiller, whereas the cooling load only changes at several evaporator temperatures in the ACC unit; thus, raising the VCC

cooling loads  $\dot{Q}_{\text{eva,VCC}}$ . Because the elevation in the ACC evaporator temperatures results in a rise in the electrical power that the mechanical compressor needs in the vapor compression chiller, the VCC performance stays approximately constant in the parallel linkage and smaller than that in the series linkage. The best coefficient of performance  $\text{COP}_{\text{VCC}}$  reached to 9.1 at  $T_{\text{eva,ACC}} = 10^\circ\text{C}$ . The results also demonstrated that if the VCC chiller works alone (without ACC chiller) at the same working conditions ( $T_{\text{eva,VCC}} = -5^\circ\text{C}$ ,  $T_{\text{cond,VCC}} = 45^\circ\text{C}$ ,  $\dot{Q}_{\text{eva,VCC}} = 10 \text{ kW}$ ) the coefficient of performance  $\text{COP}_{\text{VCC}}$  reaches 3.18 using R152A, and the requisite electrical power is larger than the two configurations considered in this part of the investigation. Consequently, the VCC chiller runs more effectively with smaller system dimensions if it is integrated with the ACC chiller at the same operating conditions.

#### **4.3.7. Effect of ACC evaporator heat transfer rate on the ACC system performance according to the parallel and series configurations.**

Figure 4.21 shows the effect of the type of adsorbents and the amount of adsorbent employed in this study at various evaporator heat in the ACC chiller ranging from 5 kW to 15 kW. It is essential to mention that the ACC evaporator temperature remains constant in this assessment at  $15^\circ\text{C}$ . It can be seen from the calculated outcomes that as the evaporation heat increases, the adsorption system performance also increases. Although rising the  $\dot{Q}_{\text{eva,ACC}}$  leads to an increase in the requisite heat to the thermal compressor; increasing the evaporator heat provides more effect on raising the adsorption system performance than increasing the thermal input. The computed results also clarify that using smaller values of the adsorbent mass supplies better ACC system performance. However, the adsorbent amount should be carefully specified as it influences the adsorbate (refrigerant) amount in the adsorption chiller, which should also be adequated to fulfill the evaporation desired in the adsorption chiller's evaporator. Figure 4.21 also demonstrates that the best and smallest values of the adsorption system performance were achieved when employing 20 kg of the silica gel-LiCl and 40 kg of RD silica gel 2060, respectively. The smallest adsorption system value reaches up to 0.39 at  $\dot{Q}_{\text{eva,ACC}} = 5 \text{ kW}$ . In contrast, The best adsorption system value reaches up to 0.71 at  $\dot{Q}_{\text{eva,ACC}} = 15 \text{ kW}$ .

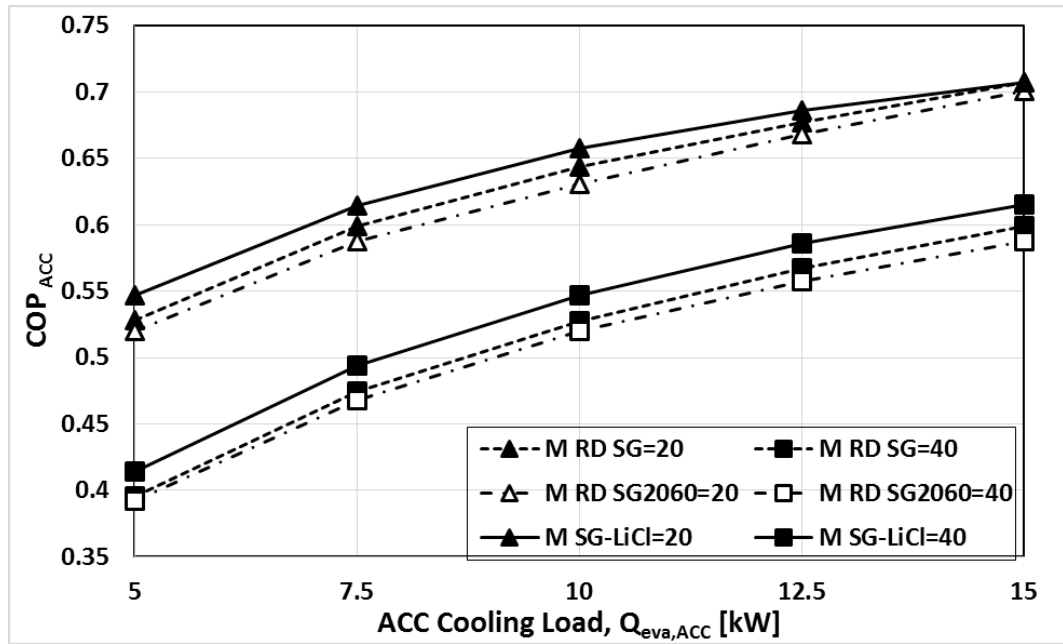


**Figure 4. 21.** Comparisons of the variation of  $COP_{ACC}$  with respect to ACC cooling load for different adsorbents and two different adsorbent mass values.

#### 4.3.8. Effect of ACC evaporator temperature and adsorption cycle time on the overall system performance according to the parallel and series configurations

Figure 4.22 presents the performance of the proposed combined cooling system according to the series and parallel connection layouts (Figure 2.12) at three different adsorption cycle times and several evaporator temperatures  $T_{eva,ACC}$ . The results were computed by employing RD silica gel/water in the ACC unit and R152A refrigerant in the VCC unit. The computed results reveal that using a smaller cycle time value leads to a reduction in the system performance in the series and parallel layouts. Indeed, reducing the adsorption cycle time drives to more thermal energy  $\dot{Q}_{heat,ACC}$  required to the ACC chiller; hence, smaller performance in the entire cooling system, where reducing the adsorption cycle time from the 1100 s to 700 s leads to a lowering in the  $COP_{EXE,H}$  from 0.33 to 0.284 for series linkage at  $T_{eva,ACC} = 10^{\circ}C$ . The best system performances were achieved when employing the higher adsorption time considered in this study 1100 s. Whereas the smallest system performances were obtained at the smallest adsorption cycle time considered. It is important to refer to that specifying the adsorption cycle time is indispensable as it should be adequate to effectively complete the desorption and

adsorption procedures. Figure 4.22 also shows that the effect of using various evaporator temperatures within the range considered in this evaluation was previously discussed (Figure 4.17). In contrast, in the parallel system connection, the best system performance values were reaches up to 0.35 at  $T_{\text{eva,ACC}} = 20^{\circ}\text{C}$  and 1100 s as a cycle time, while the smallest overall system performance value  $\text{COP}_{\text{EXE,H}}$  reached 0.27 at  $T_{\text{eva,ACC}} = 10^{\circ}\text{C}$  and 700 s as adsorption cycle time. It is also obvious from the calculated results that elevating the evaporator temperature in the adsorption chiller drives to an increase in the overall performance values  $\text{COP}_{\text{EXE,H}}$ , as previously discussed (Figure 4.18).

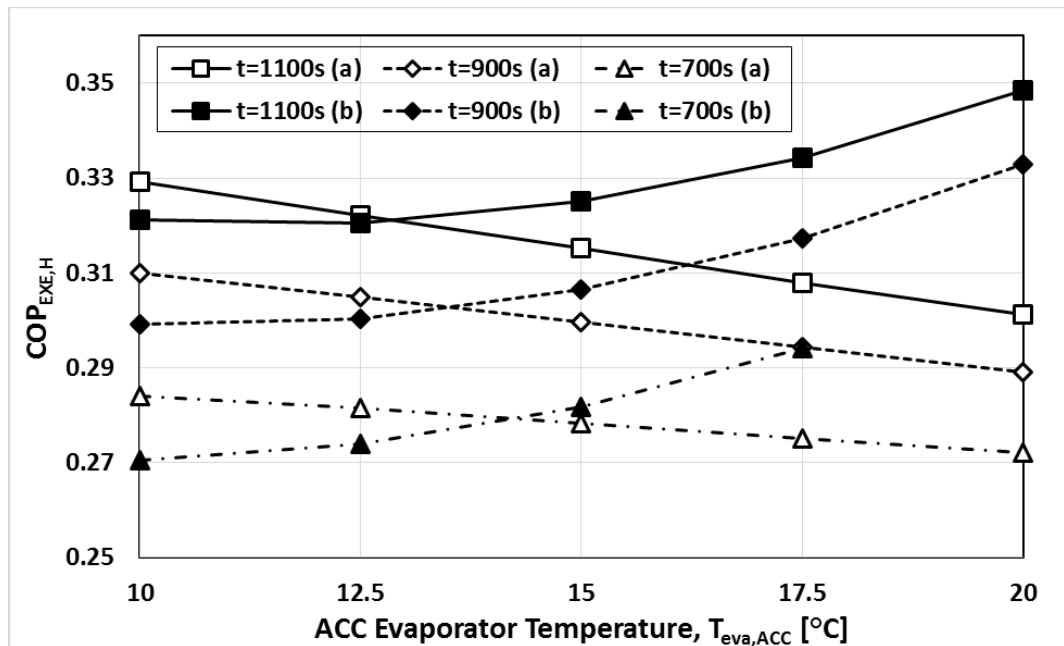


**Figure 4. 22.** Comparisons of the variation of  $\text{COP}_{\text{EXE,H}}$  with respect to ACC evaporator temperature for three different cycle times and the two system configurations (a) and (b).

#### 4.3.9. Effect of ACC evaporator temperature and ambient temperature on the overall system performance according to the parallel and series configurations

Figure 4.23 shows the results of the overall system performance  $\text{COP}_{\text{EXE,H}}$  at various ACC temperatures  $T_{\text{eva,ACC}}$  and different ambient temperatures  $T_{\text{amb}}$  for the two suggested connections (series and parallel).

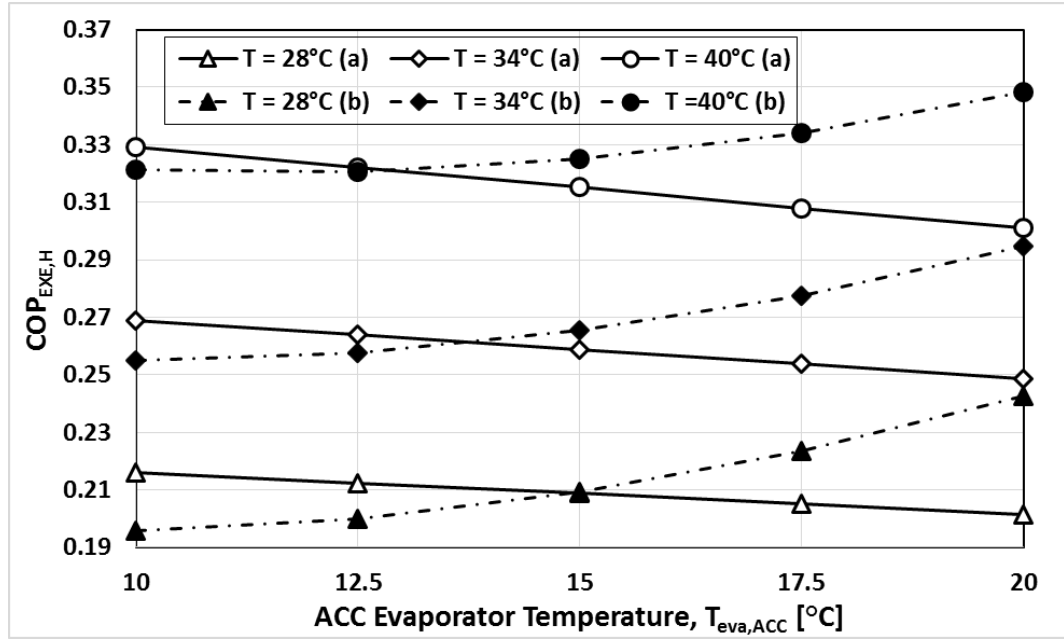


**Figure 4. 23.** Comparisons of the variation of  $COP_{EXE,H}$  with respect to ACC evaporator temperature for three different ambient temperatures and the configurations (a) and (b).

The results in this section were computed by using RD silica gel/water as a working pair in the ACC chiller and R152A as a refrigerant in the VCC chiller. The results clarify that elevating the surrounding temperature drives to an increase in the overall system performance  $COP_{EXE,H}$  where it reached 0.35 at the ambient temperature ( $T_{amb} = 40^\circ\text{C}$ ). Changing the surrounding temperature value, where the combined cooling system works, will only impact the overall system performance  $COP_{EXE,H}$  according to Eq.(3.39) and Eq (3.41), as the exergy concepts of the thermal quantities for the parallel and series linkages ( $\dot{Q}_{eva,VCC}$ ,  $\dot{Q}_{eva,ACC}$ , and  $\dot{Q}_{heat,ACC}$ ) are a function of the surrounding temperature  $T_{amb}$ . Hence, increasing the ACC evaporator temperature drives to a reduction in the whole system performance that works in the series linkage and an elevation in the system performance that operates in the parallel linkage, as formerly explained (Figure 4.17) and (Figure 4.18) in this study. The results also show that both system linkages (parallel and series) supply the same value of system performance if they run at specified ACC evaporator temperature. For example, both combine systems (parallel and series) give  $COP_{EXE,H} = 0.209$  at  $T_{eva,ACC} = 15^\circ\text{C}$  if they are worked at  $T_{amb} = 28^\circ\text{C}$ . There is a benefit of mentioning that the same behavior was noticed through the computations if the silica gel-LiCl or RD silica gel 2060 were utilized instead of RD silica gel.

#### 4.4. General remarks

The first part of this PhD dissertation focused on comparing the performance and energy-saving value of the proposed combined cooling system. The system uses silica gel/ water in the adsorption chiller and various refrigerants in the vapor compression chiller (R410A, R152A, R32, R1270, and R1234yf). The mentioned VCC's refrigerants and ACC's working pair with different cycle working conditions were studied and discussed at various VCC evaporator temperatures between  $-40^{\circ}\text{C}$  to  $0^{\circ}\text{C}$ . The general results are summarised as the following:

- All the working fluids in the VCC chiller present similar variations on the  $\text{COP}_{\text{VCC,H}}$  and  $\text{COP}_{\text{H}}$ . Increasing  $T_{\text{eva,VCC}}$  leads to an increase in the  $\text{COP}_{\text{VCC,H}}$  and  $\text{COP}_{\text{H}}$  values and relatively more differences between the coefficient of performances in the VCC alone at the different refrigerants considered.
- Within the range of VCC evaporator temperatures  $T_{\text{eva,VCC}}$  considered in this study R1234yf refrigerant gives the smallest  $\text{COP}_{\text{H}}$  and  $\text{COP}_{\text{VCC,H}}$  values among the working fluids considered that reached to 0.32 and 2.08 at  $T_{\text{eva,VCC}} = -40^{\circ}\text{C}$ , respectively. Furthermore, R1234yf has a  $\text{COP}_{\text{EXE,H}}$  maximum value as 0.324 at  $T_{\text{eva,VCC}} = -15^{\circ}\text{C}$ . On the other hand, the performance increase ratio (IR) increases from 108% to 188% as the VCC evaporator temperature increases from  $-40^{\circ}\text{C}$  to  $0^{\circ}\text{C}$ , respectively. In a similar way, the energy-saving ratio (ES) increases from 51.8% to 65.3% as the VCC evaporator temperature increases from  $-40$  to  $0^{\circ}\text{C}$ , respectively.
- R152A gives the highest  $\text{COP}_{\text{H}}$  and  $\text{COP}_{\text{VCC,H}}$  values reached up to 0.5 and 8.8 at the highest VCC evaporator temperature considered in this study  $T_{\text{eva,VCC}} = 0^{\circ}\text{C}$ , respectively. R152A also gives the highest  $\text{COP}_{\text{EXE,H}}$  value at  $T_{\text{eva,VCC}} = -15^{\circ}\text{C}$  reached up to 0.334. On the other hand, the performance increase ratio (IR) increases from 74% to 162% according to the increase in VCC evaporator

temperature  $T_{\text{eva,VCC}}$  from  $-40$  to  $0^{\circ}\text{C}$ , respectively. Similarly, the energy-saving ratio (ES) increases from 42% to 62% as the evaporation temperature rises.

- The results reveal that there is a peak value of  $\text{COP}_{\text{EXE,H}}$  for all the working fluids considered in the vapor compression chiller according to the VCC evaporator temperature  $T_{\text{eva,VCC}}$  reached to  $-15^{\circ}\text{C}$ .
- The amount of adsorbent mass required to the adsorbent beds at different ACC cycle times, ACC hot inlet temperatures, and the VCC evaporator temperatures to design the proposed combined chiller are also investigated. The results summarised that raising the VCC's evaporator temperature and the ACC hot inlet temperature reduces the needed adsorbent amount in the ACC unit reached 25% and 30%, respectively. Moreover, reducing the ACC cycle time may allow utilizing a lower adsorbent amount in the ACC chiller reached up to 40%.

The second part of this research presented a comparative analysis of the ACC chiller alone. The beds use different kinds of silica gels (RD silica gel 2060, RD silica gel, silica gel-LiCl, and silica gel-CaCl<sub>2</sub>) as adsorbent with water as a refrigerant at different ACC evaporation temperatures (from  $5^{\circ}\text{C}$  to  $20^{\circ}\text{C}$ ) and hot inlet temperatures (from  $65^{\circ}\text{C}$  to  $95^{\circ}\text{C}$ ). The results are concluded as the following:

- By increasing the ACC evaporation temperature  $T_{\text{eva,ACC}}$ , composite adsorbents provide better  $\text{COP}_{\text{ACC}}$  values than the pure adsorbents considered, where the increasing percentage reached up to 20% compared with pure silica gels, while the rising rate for specific cooling power values reached up 370% compared with the standard silica gel, considering the difference in cycle times among all the adsorbents utilized.
- By rising heating inlet temperature  $T_{\text{h}}$ , composite adsorbents (silica gel-LiCl, and silica gel-CaCl<sub>2</sub>) show higher performance values among the others, where the increasing percentage for  $\text{COP}_{\text{ACC}}$  reached up to 13% compared with the pure silica gel, while the rising rate for specific cooling power values reached up 360%

compared with the standard silica gel, considering the difference in cycle time among all the adsorbents utilized.

The third part of this study concerns the comparative performance evaluation of the integration chiller consisting of the two cooling technologies (adsorption and traditional cooling systems). The assessment focuses on using three different kinds of adsorbent materials (RD silica gel 2060, RD silica gel, and silica gel-LiCl) in the adsorption chiller. While the other chiller (vapor compression cooling system) uses R152A refrigerant as it provides better overall system performance according to the first part of the current study. These different types of adsorbents with the two different system configurations (series and parallel) were investigated at several ACC evaporator temperatures between 10°C to 20°C. The conclusion of the computed results is as the following:

- Silica gel-LiCl provides the best system performance  $COP_{EXE,H}$  values among the adsorbents considered. The highest value reached 0.354 according to the working conditions used. On the contrary, RD silica gel 2060 has fewer performance values, where its value reached 0.3 within the same operating conditions executed in this study.
- In the parallel linkage, The overall combined system performance values ( $COP_{EXE,H}$ ) rise as the adsorption evaporator temperature  $T_{eva,ACC}$  increases. However, these performance values decline in the series linkage as the evaporator temperature in the adsorption chiller elevates.
- Silica gel-LiCl provides the best adsorption system performance  $COP_{ACC}$  values, where its values reached 0.584 according to the running conditions considered in this part of the study. The best adsorption system performance values are achieved considering the series linkage compared to the other one. The findings also demonstrated that boosting the ACC evaporator temperature results in a slight elevation in the coefficient of performance of the adsorption chiller linked in series with the vapor compression chiller, while it drives to a decrease in the

coefficient of performance of adsorption chiller linked in parallel with the vapor compression chiller.

- The outcomes showed that the time for the adsorption cycle also has an effect on the combined chiller  $COP_{EXE,H}$ . The best overall system performance values can be achieved by using higher adsorption cycle time.
- The present findings also clarify the connection between the evaporation heat and the requisite adsorbent mass to design the adsorption chiller. The smaller adsorbent amount provides better  $COP_{ACC}$  values using the same cooling load values. On the contrary, more cooling load values lead to better adsorption system performance values if we applied the same amount of adsorbents. In addition to that, the composite adsorbent (silica gel-LiCl) provides better adsorption system performance  $COP_{ACC}$  values at the same cooling load reached 0.71 at the higher cooling load value using in this study.
- The parallel linkage gives smaller vapor compression system performance  $COP_{VCC}$  values than the other one (series linkage). However, the vapor compression chiller combined with the adsorption cooling unit mostly runs more effectively than operating alone within the same running conditions.
- The results reveal that operating the proposed system at higher ambient temperatures increases the system performance  $COP_{EXE,H}$  reached 0.35 for parallel linkage at 40°C. Moreover, both systems (parallel and series) provide the same overall system performance value at a specific value of the ACC evaporator temperature.

## 5. CONCLUSIONS

This study concentrates on a comparative appraisal of a refrigeration system comprised of integrated two cooling technologies, namely the adsorption cooling system (ACC) and conventional vapor mechanical cooling system (VCC). The adsorption chiller has a thermal compressor (two beds) with three different types of adsorbent separately (RD silica gel, RD silica gel 2060, and silica gel-LiCl) and water as the adsorbate. The beds are driven by heat that comes from outside heat sources with low-grade temperatures  $\leq 100^{\circ}\text{C}$ . Whereas in the bottom section, it has been used different types of refrigerants (R410A, R152a, R1234yf, R1270, and R32) driven by the mechanical compressor. These different ACC adsorbents with two different system configurations (series connection and parallel connection) are studied and discussed at different operating conditions. Performance evaluation analysis focuses on the two main criteria as the coefficient of performance (COP) and energy saving ratio (ES%) in these refrigeration systems. The computed results reveal the following main conclusions:

- R1234yf refrigerant gives the lowest performance values among the working fluids considered in the traditional chiller of the combined cooling system. While it provides the highest energy savings reached up to 65%.
- R152A gives the highest overall system performance values at different evaporator temperatures in the traditional cooling unit. In contrast, it provides the lowest energy-saving values and performance increase ratio among the refrigerant considered.
- A peak values of the overall combined system performance for all working fluids considered in the vapor compression chiller within the VCC evaporator temperatures range considered.
- Utilizing the thermal-mechanical compression (VCC-ACC) combined chiller consumes lower electrical energy in the mechanical compressor and operates the VCC chiller more effectively.

- The adsorbent mass in a bed can be reduced by using a higher hot fluid temperature, higher VCC evaporator temperature, and lower adsorption cycle time. Thus, a smaller thermal compressor size can be considered.
- Among all the adsorbents considered, composite adsorbents provide better adsorption system performance and specific cooling power values than the pure adsorbents considered at different ACC evaporator temperatures and hot inlet temperatures, considering the difference in cycle time between all the adsorbent utilized.
- Silica gel-LiCl provides the best overall combined cooling system performance values among the adsorbents considered. In contrast, RD silica gel 2060 has lower values, considering the same cycle time value between all the adsorbents utilized.
- The overall system performance values in the parallel linkage rise while the adsorption evaporator temperature boosts. However, In the series linkage, the performance values decline by increasing the same parameter.
- The series connection has a superior value in the adsorption cooling system performance than the parallel connection.
- The best overall system performance values can be achieved using a higher adsorption cycle time for series and parallel connections.
- The better adsorption cooling system performance can be acquired by considering lower adsorbent mass in a bed and higher cooling load.
- The parallel linkage gives smaller vapor compression system performance values than series linkage.

- Vapor compression chiller combined with the adsorption cooling unit mostly runs more effectively than operating alone within the same running conditions.
- Operating the combined cooling system at high ambient temperature increases the system performance for series and parallel connections.
- Implementing the parallel connection between the adsorption and conventional cooling system allows utilizing the adsorption system at the normal loads, whereas the traditional cooling system can be added at the peak loads.
- According to the results in this research, it is found that utilizing R152A refrigerant in the VCC unit and silica gel-LiCl adsorbent in the ACC unit provide the best VCC-ACC combined cooling system performance. Additionally, the working variables can also be considered in this research to determine the overall system performance values at different operating conditions.

**Suggestions for the further researches:**

According to the findings obtained in this research study, it is clear that the proposed combined cooling system requires improvements in the design and working conditions to achieve an increase in the entire (ACC-VCC) system performance. The following suggestions may be drawn for further works:

- The thesis presented the comparative performance investigation considering silica gel/water as a primary working pair in the adsorption chiller. Therefore, future research can investigate different working pairs such as ammonia with different adsorbents (activated carbon, zeolite, alumina, silica gel) or activated carbon with different adsorbates (methanol, ethanol, some kind of ferrous). Accordingly, new observations can be achieved in the entire combined cooling system performance.
- This work also investigated the adsorbent amount in the thermal compressor without considering the bed type. Therefore, further work might focus on the bed

type and the number of beds (more than two beds) in the thermal compressor and investigate the connection between the different bed types and the number of beds with the whole combined cooling system performance and determine the best design.

- This research evaluated the (ACC-VCC) combined cooling system thermodynamically. Therefore, upcoming studies can consider the detailed design conditions of the adsorption cooling system in accordance with VCC connection requirements such as (ACC evaporator and condenser design, thermal compressor design) in terms of tube length, size, number, materials, and heat transfer areas. Accordingly, a prototype rig can be constructed and experimented.
- This dissertation presented the two different connections between the adsorption and conventional cooling system (series and parallel) without specifying the energy source type. Therefore, future investigations should be focusing on other connection types between the two chillers and identifying the energy source type such as (thermal engine, thermal plant, and renewable energy) to provide the thermal and electrical powers for both chillers. Thus, a comprehensive investigation can be executed on the (ACC-VCC) combined system performance and energy-saving rate.
- This study presented the connection between the adsorption cooling system and the traditional chiller. System performance and energy-saving rates investigations can be performed in future studies in terms of connecting the absorption cooling system or adsorption cooling system with the vapor compression cooling system at the same operating conditions.

## REFERENCES

- Agarwal, S., Arora, A., Arora, B. B. (2020).** Energy and exergy analysis of vapor compression–triple effect absorption cascade refrigeration system. *Engineering Science and Technology, an International Journal*, 23(3), 625–641. <https://doi.org/10.1016/j.jestch.2019.08.001>
- Akahira, A., Alam, K. C. A., Hamamoto, Y., Akisawa, A., Kashiwagi, T. (2005).** Experimental investigation of mass recovery adsorption refrigeration cycle. *International Journal of Refrigeration*, 28(4), 565–572. <https://doi.org/10.1016/j.ijrefrig.2004.10.001>
- Ali, S. M., Chakraborty, A., Leong, K. C. (2017).** CO<sub>2</sub>-assisted compression-adsorption hybrid for cooling and desalination. *Energy Conversion and Management*, 143, 538–552. <https://doi.org/10.1016/j.enconman.2017.04.009>
- Askalany, A. A., Saha, B. B., Habib, K. (2014).** Adsorption Cooling System Employing Activated Carbon/R32 Adsorption Pair. *MATEC Web of Conferences*, 13, 06001. <https://doi.org/10.1051/mateconf/20141306001>
- Askalany, A. A., Salem, M., Ismael, I. M., Ali, A. H. H., Morsy, M. G., & Saha, B. B. (2013).** An overview on adsorption pairs for cooling. *Renewable and Sustainable Energy Reviews*, 19, 565–572. <https://doi.org/10.1016/j.rser.2012.11.037>
- Babaei, S. M., Razmi, A. R., Soltani, M., Nathwani, J. (2020).** Quantifying the effect of nanoparticles addition to a hybrid absorption/recompression refrigeration cycle. *Journal of Cleaner Production*, 260, 121084. <https://doi.org/10.1016/j.jclepro.2020.121084>
- Banker, N. D., Dutta, P., Prasad, M., Srinivasan, K. (2008).** Performance studies on mechanical + adsorption hybrid compression refrigeration cycles with HFC 134a. *International Journal of Refrigeration*, 31(8), 1398–1406. <https://doi.org/10.1016/j.ijrefrig.2008.03.009>
- Bell, I. H., Wronski, J., Quoilin, S., Lemort, V. (2014).** Pure and pseudo-pure fluid thermophysical property evaluation and the open-source thermophysical property library coolprop. *Industrial and Engineering Chemistry Research*, 53(6), 2498–2508. <https://doi.org/10.1021/ie4033999>
- Bolaji, B. O., & Huan, Z. (2013).** Ozone depletion and global warming : Case for the use of natural refrigerant – a review. *Renewable and Sustainable Energy Reviews*, 18, 49–54. <https://doi.org/10.1016/j.rser.2012.10.008>
- Chekirou, W., Boussehain, R., Feidt, M., Karaali, A., Boukheit, N. (2011).** Numerical results on operating parameters influence for a heat recovery adsorption machine. *Energy Procedia*, 6, 202–216. <https://doi.org/10.1016/j.egypro.2011.05.024>  
<https://doi.org/10.1016/j.applthermaleng.2012.02.035>
- Cyklis, P. 2014.** Two stage ecological hybrid sorption-compression refrigeration cycle. *International Journal of Refrigeration*, 48, 121–131. <https://doi.org/10.1016/j.ijrefrig.2014.08.017>
- Demir, H., Mobedi, M., Ülkü, S. (2009).** Effects of porosity on heat and mass transfer in a granular adsorbent bed. *International Communications in Heat and Mass Transfer*, 36(4), 372–377. <https://doi.org/10.1016/j.icheatmasstransfer.2009.01.008>
- Di, J., Wu, J. Y., Xia, Z. Z., Wang, R. Z. (2007).** Theoretical and experimental study on characteristics of a novel silica gel e water chiller under the conditions of variable heat source temperature ´ orique et expe ´ rimentale sur les caracte ´ ristiques d ´ un Etude the refroidisseur innovant fonctionn. 30. <https://doi.org/10.1016/j.ijrefrig.2006.07.022>

- Do, D. D. (1998).** Adsorption analysis: equilibria and kinetics. Series in chemical engineering, 2. University of Queensland, Australia.
- El-Sharkawy, I. I., Hassan, M., Saha, B. B., Koyama, S., & Nasr, M. M. (2009).** Study on adsorption of methanol onto carbon based adsorbents. *International Journal of Refrigeration*, 32(7), 1579–1586. <https://doi.org/10.1016/j.ijrefrig.2009.06.011>
- El-Sharkawy, I. I., Kuwahara, K., Saha, B. B., Koyama, S., Ng, K. C. (2006).** Experimental investigation of activated carbon fibers/ethanol pairs for adsorption cooling system application. *Applied Thermal Engineering*, 26(8–9), 859–865. <https://doi.org/10.1016/j.applthermaleng.2005.10.010>
- El-Sharkawy, I. I., Saha, B. B., Koyama, S., He, J., Ng, K. C., Yap, C. (2008).** Experimental investigation on activated carbon-ethanol pair for solar powered adsorption cooling applications. *International Journal of Refrigeration*, 31(8), 1407–1413. <https://doi.org/10.1016/j.ijrefrig.2008.03.012>
- Fernández-Seara, J., Sieres, J., Vázquez, M. (2006).** Compression-absorption cascade refrigeration system. *Applied Thermal Engineering*, 26(5–6), 502–512. <https://doi.org/10.1016/j.applthermaleng.2005.07.015>
- Freni, A., Maggio, G., Sapienza, A., Frazzica, A., Restuccia, G., Vasta, S. (2016).** Comparative analysis of promising adsorbent/adsorbate pairs for adsorptive heat pumping, air conditioning and refrigeration. *Applied Thermal Engineering*, 104, 85–95. <https://doi.org/10.1016/j.applthermaleng.2016.05.036>
- Gibelhaus, A., Fidorra, N., Lanzerath, F., Bau, U., Köhler, J., Bardow, A. (2019).** Hybrid refrigeration by CO<sub>2</sub> vapour compression cycle and water-based adsorption chiller: An efficient combination of natural working fluids. *International Journal of Refrigeration*, 103, 204–214. <https://doi.org/10.1016/j.ijrefrig.2019.03.036>
- Glaznev, I. S., Aristov, Y. I. (2010).** The effect of cycle boundary conditions and adsorbent grain size on the water sorption dynamics in adsorption chillers. *International Journal of Heat and Mass Transfer*, 53(9–10), 1893–1898. <https://doi.org/10.1016/j.ijheatmasstransfer.2009.12.069>
- Gong, L. X., Wang, R. Z., Xia, Z. Z., & Chen, C. J. (2011).** Design and performance prediction of a new generation adsorption chiller using composite adsorbent. *Energy Conversion and Management*, 52(6), 2345–2350. <https://doi.org/10.1016/j.enconman.2010.12.036>
- Grisel, R. J., Smeding, S. F., Boer, B. R. de. (2010).** Waste heat driven silica gel/water adsorption cooling in trigeneration. *Applied Thermal Engineering*, 30(8–9), 1039–1046. <https://doi.org/10.1016/j.applthermaleng.2010.01.020>
- He, H., Wang, L., Yuan, J., Wang, Z., Fu, W., Liang, K. (2019).** Performance evaluation of solar absorption-compression cascade refrigeration system with an integrated air-cooled compression cycle. *Energy Conversion and Management*, 201(September), 112153. <https://doi.org/10.1016/j.enconman.2019.112153>
- Hojjat Mohammadi, S. M., Ameri, M. (2014).** Energy and exergy comparison of a cascade air conditioning system using different cooling strategies. *International Journal of Refrigeration*, 41, 14–26. <https://doi.org/10.1016/j.ijrefrig.2013.06.015>
- Khan, M. Z. I., Alam, K. C. A., Saha, B. B., Hamamoto, Y., Akisawa, A., Kashiwagi, T. (2006).** Parametric study of a two-stage adsorption chiller using re-heat - The effect of overall thermal conductance and adsorbent mass on system performance. *International Journal of Thermal Sciences*, 45(5), 511–519. <https://doi.org/10.1016/j.ijthermalsci.2005.08.003>
- Kilic, M., Anjrini, M. (2020).** Comparative performance analysis of a combined cooling

system with mechanical and adsorption cycles. *Energy Conversion and Management*, 221, 113208. <https://doi.org/10.1016/j.enconman.2020.113208>

**Kılıç, M. (2018).** Comparative performance analysis of a two-bed adsorption cooling system with adsorption of different adsorbates on silica gel. *Bulgarian Chemical Communications*, 50, 102–110.

**Kumar, P., Sharma, A. (2014).** Experimental Analysis of Mechanical and Adsorption Hybrid Refrigeration with CO<sub>2</sub> as Refrigerant and Activated Carbon as Absorbent. 3(8), 883–890.

**Li, T. X., Wang, R. Z., Oliveira, R. G., Kiplagat, J. K., Wang, L. W. (2009).** A combined double-way chemisorption refrigeration cycle based on adsorption and desorption processes. *International Journal of Refrigeration*, 32(1), 47–57. <https://doi.org/10.1016/j.ijrefrig.2008.07.007>

**Lijuan, H., Wang, S., Suxia, L., Xuan, W. (2019).** Numerical and experimental evaluation of the performance of a coupled vapour absorption-compression refrigeration configuration. *International Journal of Refrigeration*, 99, 429–439. <https://doi.org/10.1016/j.ijrefrig.2018.11.023>

**Liu, X., Ye, Z., Bai, L., He, M. (2019).** Performance comparison of two absorption-compression hybrid refrigeration systems using R1234yf/ionic liquid as working pair. *Energy Conversion and Management*, 181, 319–330. <https://doi.org/10.1016/j.enconman.2018.12.030>

**Lu, Y. Z., Wang, R. Z., Jianzhou, S., Xu, Y. X., Wu, J. Y. (2004).** Practical experiments on an adsorption air conditioner powered by exhausted heat from a diesel locomotive. *Applied Thermal Engineering*, 24(7), 1051–1059. <https://doi.org/10.1016/j.applthermaleng.2003.10.004>

**Lychnos, G., Tamainot-Telto, Z. (2014).** Performance of hybrid refrigeration system using ammonia. *Applied Thermal Engineering*, 62(2), 560–565. <https://doi.org/10.1016/j.applthermaleng.2013.10.013>

**Lychnos, G., Tamainot-Telto, Z. (2018).** Prototype of hybrid refrigeration system using refrigerant R723. *Applied Thermal Engineering*, 134, 95–106. <https://doi.org/10.1016/j.applthermaleng.2017.12.103>

**Ma, Q., Wang, R. Z., Dai, Y. J., Zhai, X. Q. (2006).** Performance analysis on a hybrid air-conditioning system of a green building. *Energy and Buildings*, 38(5), 447–453. <https://doi.org/10.1016/j.enbuild.2005.08.004>

**Maggio, G., Freni, A., Restuccia, G. (2006).** A dynamic model of heat and mass transfer in a double-bed adsorption machine with internal heat recovery. *International Journal of Refrigeration*, 29(4), 589–600. <https://doi.org/10.1016/j.ijrefrig.2005.10.005>

**Maggio, G., Gordeeva, L. G., Freni, A., Aristov, Y. I., Santori, G., Polonara, F., Restuccia, G. (2009).** Simulation of a solid sorption ice-maker based on the novel composite sorbent “lithium chloride in silica gel pores.” *Applied Thermal Engineering*, 29(8–9), 1714–1720. <https://doi.org/10.1016/j.applthermaleng.2008.07.026>

**Metcalf, S. J., Critoph, R. E., Tamainot-Telto, Z. (2012).** Optimal cycle selection in carbon-ammonia adsorption cycles. *International Journal of Refrigeration*, 35(3), 571–580. <https://doi.org/10.1016/j.ijrefrig.2011.11.006>

**Miyazaki, T., Akisawa, A., Saha, B. B., El-Sharkawy, I. I., Chakraborty, A. (2009).** A new cycle time allocation for enhancing the performance of two-bed adsorption chillers. *International Journal of Refrigeration*, 32(5), 846–853. <https://doi.org/10.1016/j.ijrefrig.2008.12.002>

**Miyazaki, Takahiko, Akisawa, A. (2009).** The influence of heat exchanger parameters

- on the optimum cycle time of adsorption chillers. *Applied Thermal Engineering*, 29(13), 2708–2717. <https://doi.org/10.1016/j.applthermaleng.2009.01.005>
- Miyazaki, Takahiko, Akisawa, A., Saha, B. B. (2010).** The performance analysis of a novel dual evaporator type three-bed adsorption chiller. *International Journal of Refrigeration*, 33(2), 276–285. <https://doi.org/10.1016/j.ijrefrig.2009.10.005>
- Mohammed, R. H. (2019).** Experimental and Numerical Investigation of a Novel Adsorption Bed Design for Cooling Applications (Ph.D. Dissertation). University of Central Florida, United State.
- Mohammed, R. H., Mesalhy, O., Elsayed, M. L., Hou, S., Su, M., Chow, L. C. (2018).** Physical properties and adsorption kinetics of silica-gel/water for adsorption chillers. *Applied Thermal Engineering*, 137, 368–376. <https://doi.org/10.1016/j.applthermaleng.2018.03.088>
- Mousavi, S. A., Mehrpooya, M. (2020).** A comprehensive exergy-based evaluation on cascade absorption-compression refrigeration system for low temperature applications - exergy, exergoeconomic, and exergoenvironmental assessments. *Journal of Cleaner Production*, 246, 119005. <https://doi.org/10.1016/j.jclepro.2019.119005>
- Nikbakhti, R., Wang, X., Hussein, A. K., Iranmanesh, A. (2020).** Absorption cooling systems – Review of various techniques for energy performance enhancement. *Alexandria Engineering Journal*, 59(2), 707–738. <https://doi.org/10.1016/j.aej.2020.01.036>
- Palomba, V., Dino, G. E., Frazzica, A. (2020).** Coupling sorption and compression chillers in hybrid cascade layout for efficient exploitation of renewables: Sizing, design and optimization. *Renewable Energy*, 154, 11–28. <https://doi.org/10.1016/j.renene.2020.02.113>
- Palomba, V., Ferraro, M., Frazzica, A., Vasta, S., Sergi, F., Antonucci, V. (2018).** Experimental and numerical analysis of a SOFC-CHP system with adsorption and hybrid chillers for telecommunication applications. *Applied Energy*, 216, 620–633. <https://doi.org/10.1016/j.apenergy.2018.02.063>
- Palomba, V., Frazzica, A., Kühnert, S., Große, A. (2019).** Experimentally Validated Dynamic Model for a Hybrid Cascade System for Solar Heating and Cooling Applications. 1–8. <https://doi.org/10.18086/eurosun2018.04.01>
- Palomba, V., Varvagiannis, E., Karellas, S., Frazzica, A. (2019).** Hybrid adsorption-compression systems for air conditioning in efficient buildings: Design through validated dynamic models. *Energies*, 12(6), 1–27. <https://doi.org/10.3390/en12061161>
- Palomba, V., Vasta, S., Frazzica, A., Freni, A. (2017).** Analysis and testing of a novel cascaded adsorption-compression chiller for industrial applications. *Proceedings of 12th IEA Heat Pump Conference*, May.
- Rezk, A. (2012).** Theoretical and experimental investigation of silica gel/water adsorption refrigeration systems ( Ph.D. dissertation). University of Birmingham, UK.
- Saha, Bidyut B., Habib, K., El-Sharkawy, I. I., Koyama, S. (2009).** Adsorption characteristics and heat of adsorption measurements of R-134a on activated carbon. *International Journal of Refrigeration*, 32(7), 1563–1569. <https://doi.org/10.1016/j.ijrefrig.2009.03.010>
- Saha, Bidyut B., Koyama, S., El-Sharkawy, I. I., Habib, K., Srinivasan, K., Dutta, P. (2007).** Evaluation of adsorption parameters and heats of adsorption through desorption measurements. *Journal of Chemical and Engineering Data*, 52(6), 2419–2424. <https://doi.org/10.1021/jc700369j>
- Saha, Bidyut B, Boelman, E. c, Kashiwagi, T. (1995).** Computational analysis of an

advanced adsorption refrigeration cycles. 20(10), 983–994.

**Saha, Bidyut Baran, Chakraborty, A., Koyama, S., Aristov, Y. I. (2009).** A new generation cooling device employing CaCl<sub>2</sub>-in-silica gel-water system. *International Journal of Heat and Mass Transfer*, 52(1–2), 516–524. <https://doi.org/10.1016/j.ijheatmasstransfer.2008.06.018>

**Saha, Bidyut Barana, El-Sharkawy, I. I., Koyama, S., Lee, J. B., Kuwahara, K. (2006).** Waste heat driven multi-bed adsorption chiller: Heat exchangers overall thermal conductance on chiller performance. *Heat Transfer Engineering*, 27(5), 80–87. <https://doi.org/10.1080/01457630600560742>

**Sharafian, A., Bahrami, M. (2014).** Assessment of adsorber bed designs in waste-heat driven adsorption cooling systems for vehicle air conditioning and refrigeration. *Renewable and Sustainable Energy Reviews*, 30, 440–451. <https://doi.org/10.1016/j.rser.2013.10.031>

**Sharafian, A., Bahrami, M. (2015).** Critical analysis of thermodynamic cycle modeling of adsorption cooling systems for light-duty vehicle air conditioning applications. *Renewable and Sustainable Energy Reviews*, 48, 857–869. <https://doi.org/10.1016/j.rser.2015.04.055>

**Song, M., Wang, L., Yuan, J., Wang, Z., Li, X., Liang, K. (2020).** Proposal and parametric study of solar absorption/dual compression hybrid refrigeration system for temperature and humidity independent control application. *Energy Conversion and Management*, 220(April), 113107. <https://doi.org/10.1016/j.enconman.2020.113107>

**Srivastava, N. C., Eames, I. W. (1998).** A review of adsorbents and adsorbates in solid-vapour adsorption heat pump systems. *Applied Thermal Engineering*, 18(9–10), 707–714. [https://doi.org/10.1016/S1359-4311\(97\)00106-3](https://doi.org/10.1016/S1359-4311(97)00106-3)

**Suzuki, M. (1991).** Adsorption engineering. In *Reactive Polymers*, 14(3), 269–270. [https://doi.org/10.1016/0923-1137\(91\)90043-n](https://doi.org/10.1016/0923-1137(91)90043-n)

**Uddin, K., Miyazaki, T., Koyama, S., Saha, B. B. (2013).** Performance Investigation of Adsorption–Compression Hybrid Refrigeration Systems. *International Journal of Air-Conditioning and Refrigeration*, 21(04), 1350024. <https://doi.org/10.1142/s2010132513500247>

**Ustaoglu, A. (2020).** Parametric study of absorption refrigeration with vapor compression refrigeration cycle using wet, isentropic and azeotropic working fluids: Conventional and advanced exergy approach. *Energy*, 201, 117491. <https://doi.org/10.1016/j.energy.2020.117491>

**Van Der Pal, M., Wemmers, A., Smeding, S., De Boer, R. (2013).** Technical and economical feasibility of the hybrid adsorption compression heat pump concept for industrial applications. *Applied Thermal Engineering*, 61(2), 837–840. <https://doi.org/10.1016/j.applthermaleng.2013.04.048>

**Vasta, S., Freni, A., Sapienza, A., Costa, F., Restuccia, G. (2012).** Development and lab-test of a mobile adsorption air-conditioner. *International Journal of Refrigeration*, 35(3), 701–708. <https://doi.org/10.1016/j.ijrefrig.2011.03.013>

**Vasta, S., Palomba, V., La Rosa, D., Mittelbach, W. (2018).** Adsorption-compression cascade cycles: An experimental study. *Energy Conversion and Management*, 156, 365–375. <https://doi.org/10.1016/j.enconman.2017.11.061>

**Vodianitskaia, P. J., Soares, J. J., Melo, H., Gurgel, J. M. (2017).** Experimental chiller with silica gel: Adsorption kinetics analysis and performance evaluation. *Energy Conversion and Management*, 132, 172–179. <https://doi.org/10.1016/j.enconman.2016.11.028>

- Wang, D. C., Li, Y. H., Li, D., Xia, Y. Z., Zhang, J. P. (2010).** A review on adsorption refrigeration technology and adsorption deterioration in physical adsorption systems. *Renewable and Sustainable Energy Reviews*, 14(1), 344–353. <https://doi.org/10.1016/j.rser.2009.08.001>
- Wang, D. C., Xia, Z. Z., Wu, J. Y. (2006).** Design and performance prediction of a novel zeolite-water adsorption air conditioner. *Energy Conversion and Management*, 47(5), 590–610. <https://doi.org/10.1016/j.enconman.2005.05.011>
- Wang, J., Wang, B., Wu, W., Li, X., Shi, W. (2016).** Performance analysis of an absorption-compression hybrid refrigeration system recovering condensation heat for generation. *Applied Thermal Engineering*, 108, 54–65. <https://doi.org/10.1016/j.applthermaleng.2016.07.100>
- Wang, L. W., Wang, R. Z., Oliveira, R. G. (2009).** A review on adsorption working pairs for refrigeration. *Renewable and Sustainable Energy Reviews*, 13(3), 518–534. <https://doi.org/10.1016/j.rser.2007.12.002>
- Wang, L. W., Wang, R. Z., Wu, J. Y., Xu, Y. X., Wang, S. G. (2006).** Design, simulation and performance of a waste heat driven adsorption ice maker for fishing boat. *Energy*, 31(2–3), 244–259. <https://doi.org/10.1016/j.energy.2005.03.006>
- Wang, X., Chua, H. T. (2007a).** A comparative evaluation of two different heat-recovery schemes as applied to a two-bed adsorption chiller. *International Journal of Heat and Mass Transfer*, 50(3–4), 433–443. <https://doi.org/10.1016/j.ijheatmasstransfer.2006.08.003>
- Wang, X., Chua, H. T. (2007b).** Two bed silica gel-water adsorption chillers: An effectual lumped parameter model. *International Journal of Refrigeration*, 30(8), 1417–1426. <https://doi.org/10.1016/j.ijrefrig.2007.03.010>
- Wittstadt, U., Kröhnert, C., Lubryka, E. (2018).** WP3 System Integration High Performance Solar Heat Pumps Components. Report Hycool, 792073. [www.hycool-project.eu](http://www.hycool-project.eu)
- Wu, J. W., Chen, L., Hu, E. J. (2016).** Performance estimation of adsorption cooling cycle with sorption hysteresis. *Applied Thermal Engineering*, 105, 159–162. <https://doi.org/10.1016/j.applthermaleng.2016.05.154>
- Younes, M. M., El-Sharkawy, I. I., Kabeel, A. E., Saha, B. B. (2017).** A review on adsorbent-adsorbate pairs for cooling applications. *Applied Thermal Engineering*, 114, 394–414. <https://doi.org/10.1016/j.applthermaleng.2016.11.138>

## **APPENDIXES**

- APPX 1** Mathematical codes and software environments for VCC and ACC modeling (the first and third parts of calculations).
- APPX 2** Mathematical codes and software environments for ACC modeling (the second part of calculations).

**APPX 1:** Mathematical codes and software environments for VCC and ACC modeling (the first and third parts of calculations).

### **Input Variables**

```
//T_Con=[ ] [K]
//T_Eva=[ ] [K]
//Q_Eva_dot=[ ] [kW]
//R$='[ ]'
//eta_is=[ ]
//eta_ele= [ ]
```

### **Thermodynamic parameters calculations**

```
T[0]=T_Eva
x[0]=1
p[0]=Pressure(R$,T=T[0], x=x[0]([
s[0]=Entropy(R$,T=T[0], x=x[0]([
h[0]=Enthalpy(R$,T=T[1], x=x[0]([
```

```
T[1]=T_Eva+5
p[1]=p[0]
s[1]=Entropy(R$,T=T[1], p=p[1])
h[1]=Enthalpy(R$,T=T[1], p=p[1])
```

```
T[3]=T_Con
x[3]=0
s[3]=Entropy(R$,T=T[3], x=x[3])
p[3]=Pressure(R$,T=T[3], x=x[3])
h[3]=Enthalpy(R$,T=T[3], x=x[3])
```

```
s_s[2]=s[1]
```

$p[2]=p[3]$   
 $h\_s[2]=\text{Enthalpy}(R\$,s=s\_s[2], p=p[2])$   
 $T\_s[2]=\text{Temperature}(R\$,s=s\_s[2], p=p[2])$   
 $h[2]= (h\_s[2]-h[1])/eta\_is +h[1]$   
 $T[2]= (T\_s[2]-T[1])/eta\_is +T[1]$   
 $s[2]=\text{Entropy}(R\$,p=p[2], h=h[2])$

$T[4]=T\_Con - 4$   
 $p[4]=p[3]$   
 $s[4]=\text{Entropy}(R\$,T=T[4], p=p[4])$   
 $h[4]=\text{Enthalpy}(R\$,T=T[4], p=p[4])$

$h[5]=h[4]$   
 $p[5]=p[0]$   
 $s[5]=\text{Entropy}(R\$,h=h[5], p=p[5])$   
 $T[5]=\text{Temperature}(R\$,h=h[5], p=p[5])$

### **Output Variables**

$m\_dot=Q\_Eva\_dot/(h[1]-h[5])$   
 $Q\_dot\_con= m\_dot*(h[2]-h[4])$   
 $W\_dot\_com= m\_dot*(h[2]-h[1])$   
 $W\_dot\_elec= m\_dot*(h[2]-h[1])/eta\_ele$   
 $COP=Q\_Eva\_dot/W\_dot\_elec$



**APPX 2:** Mathematical codes and software environments for ACC modeling (the second part of calculations).

%% Calculation of the coefficient of performance for the adsorption unit part (RD silica gel/water)

% Calculation of the maximum adsorbate uptake.

T\_eva=10+273.15 % K

P\_eva= py.CoolProp.CoolProp.PropsSI('P','T',T\_eva,'Q',1,'water');% pa

T\_cool\_in=30+273.15;% K

T\_A=T\_cool\_in + 2; % K

P\_A= py.CoolProp.CoolProp.PropsSI('P','T',T\_A,'Q',1,'water');% pa

v\_bo=0.001043; % m<sup>3</sup>/kg

v\_o=0.000875;% m<sup>3</sup>/kg

T\_bo=100+273.15;% K

ohm=0.001764;

v\_a=v\_bo\*exp(ohm\*(T\_A-T\_b));% m<sup>3</sup>/kg

X\_0=0.48; % kg/kg

W\_0=X\_0\*v\_o; % m<sup>3</sup>/kg

R= 0.4615; % Kj/Kg.K

E= 192.29; % kJ/kg

A =R/E;

n=1.35,

W\_max=W\_0\*exp(-(A\*T\_A\*log(P\_A/P\_eva))^n); % m<sup>3</sup>/kg

X\_max=W\_max/v\_a; % Kg\_adsorbate/ kg\_silica

% Calculation of the minimum adsorbate uptake

T\_con=32 +273.15;% K

P\_con= py.CoolProp.CoolProp.PropsSI('P','T',T\_con,'Q',0,'water');% pa

T\_heat\_in=65+273.15;% K

T\_D=T\_heat\_in -2;% K

P\_D= py.CoolProp.CoolProp.PropsSI('P','T',T\_D,'Q',0,'water');% pa

```

T_bo=100+273.15; % k
v_a2=v_b*exp(ohm*(T_D-T_bo)); % m^3/kg
v_b=0.001043;% m^3/kg
W_min=W_0*exp(-(A*T_D*log(P_D/P_con))^n);% m^3/kg
X_min=W_min/v_a2; % Kg_adsorbate/ kg_silica

% Calculation coefficient of performance

% Input physical parameters
m_adsorber = 47;% kg Silica gel
CP_ads = 0.92; % KJ/kg.K
CP_ref=4.18;% kJ/kg.K
E=192.29; % KJ/kg
MC=78; % (M_bm*C_bm) KJ/K
m_water_max=X_max*m_adsorber; % kg_water
deltX = X_max - X_min;
T_B= 50 +273.15; % K
H_B_L=py.CoolProp.CoolProp.PropsSI('H','T',T_B,'Q',0,'water'); % J/kg
H_B_v=py.CoolProp.CoolProp.PropsSI('H','T',T_B,'Q',1,'water'); % J/kg
H_fg_B= (H_B_v- H_B_L)*0.001;% kJ/kg
H_ev_L=py.CoolProp.CoolProp.PropsSI('H','T',T_eva,'Q',0,'water'); % J/kg
H_ev_v=py.CoolProp.CoolProp.PropsSI('H','T',T_eva,'Q',1,'water'); % J/kg
H_fg_ev= (H_ev_v- H_ev_L)*0.001;% Kj/Kg
deltaH_des = H_fg_B + (E)*(log (W_0/W_max))^1/n + (E*T_B*ohm/n)*(log
(W_0/W_max))^((1-n)/n); % kJ/kg

% Calculate the thermal amounts in the bed during the adsorption period [KJ]
Q_ish = (m_adsorber*CP_ads+m_water_max*CP_ref +MC)*(T_B-T_A);
Q_des = (m_adsorber*CP_ads + m_water_max*CP_ref +MC)*(T_D-T_B) +
(m_adsorber *deltaH_des)*deltX;
Q_adsH_tot = Q_ish + Q_des;

```

```
% Calculate the thermal amount in the evaporator of the adsorption part [KJ]
```

```
Q_eva = (deltX*H_fg_ev - CP_ref*deltX*(T_con-T_eva))*m_adsorber;
```

```
% Calculate the coefficient of performance of the adsorption part.
```

```
COP_ad = Q_eva/(Q_ish+Q_des);
```

```
%% Adsorbate uptake rate modeling at T_eva= 5 °C
```

```
X_eq=0.0352 % Kg_adsorbate/ kg_silica
```

```
D_so=0.00029 % m^2/s
```

```
E_a=41500 % J/mol
```

```
R_u= 8.314 % J/mol.k
```

```
D_e=0.75*10^-3 % m
```

```
K_1 = 60*D_so/D_e^2; % 1/s
```

```
K_2= E_a/R_u % K
```

```
T_b=(56+90)/2; % K
```

```
T_ads1= T_b +273.15; % K
```

```
dwdt=@(t,X_2) K_1*exp(-K_2/T_ads1)*(X_eq-X_2)
```

```
[t1 X_2]=ode45(dwdt,[0:500],0.1275);
```

```
%% plotting
```

```
plot(t1,X_2)
```

```
xlabel('Time (second)')
```

```
ylabel('Adsorbate Uptake Rate(kg/kg)')
```

```
legend('T_e=5^0C')
```

```
title('RD Silica gel')
```

## RESUME

Name Surname : Mustafa ANJRINI  
Place and Date of Birth : Aleppo/Syria 01/01/1988  
Foreign Languages : Arabic, English

Education Status  
High School : Al-mamoun high school/2002-2005  
Bachelor's : Aleppo Uni. Mechanical Engineering./2005-2010  
Master's : Aleppo Uni. Mechanical Engineering./2010-2014

Work Experience : Lecturer – Aleppo Uni. /2011-2013  
Mechanical Engineer - Directorate of Engineering  
and Services – Aleppo Uni. /2011-2015  
Internship – Turkish airlines /2019

Contact (e-mail) : [Mustafa.anjrini@hotmail.com](mailto:Mustafa.anjrini@hotmail.com)  
511510010@org.uludag.edu.tr

Publications :

**Anjrini, M., Kilic, M. (2019).** Comparative performance analysis of two-bed adsorption cooling system using water vapor adsorption on different types of silica gel. Book of Full-text proceedings Turkish physical society 35<sup>th</sup> international physics congress (TPS35), 01, No.05, 355-363.

**Kilic, M., Anjrini, M. (2020).** Comparative performance analysis of a combined cooling system with mechanical and adsorption cycles. Energy Conversion and Management, 221, 113208. <https://doi.org/10.1016/j.enconman.2020.113208>

**Anjrini, M., Kilic, M. (2020).** Thermal investigations on the intermediate heat exchanger of the combined refrigeration system. Alternative Energy Sources, Materials and Technology (AESMT'20), 02, 55-56.

